Earth-Science Reviews 114 (2012) 325–368

Contents lists available at SciVerse ScienceDirect

Earth-Science Reviews

journal homepage: www.elsevier.com/locate/earscirev

Phanerozoic polar wander, palaeogeography and dynamics

Trond H. Torsvik [a,b,c,d,*], Rob Van der Voo [a,e], Ulla Preeden [f], Conall Mac Niocaill [g], Bernhard Steinberger [h,a,b], Pavel V. Doubrovine [a,b], Douwe J.J. van Hinsbergen [a,b], Mathew Domeier [e,b], Carmen Gaina [a,b], Eric Tohver [i], Joseph G. Meert [j], Phil J.A. McCausland [k], L. Robin M. Cocks [l]

[a] Center for Advanced Study, Norwegian Academy of Science and Letters, Drammensveien 78, 0271 Oslo, Norway
[b] Center for Physics of Geological Processes (PGP), University of Oslo, Sem Sælands vei 24, NO-0316 Oslo, Norway
[c] Geodynamics, Geological Survey of Norway, Leiv Eirikssons vei 39, 7491Trondheim, Norway
[d] School of Geosciences, University of the Witwatersrand, WITS 2050 Johannesburg, South Africa
[e] Department of Earth and Environmental Sciences, University of Michigan, Ann Arbor, MI 48109-1005, USA
[f] Department of Geology, University of Tartu, Ravila 14A, 50411 Tartu, Estonia
[g] Department of Earth Sciences, South Parks Road, Oxford OX1 3AN, UK
[h] Helmholtz Centre Potsdam, GFZ German Research Centre for Geosciences, Section 2.5, Geodynamic Modelling, Helmholtzstrasse 6, H6 117, 14467 Potsdam, Germany
[i] School of Earth and Environment, University of Western Australia, 35 Stirling Highway, Crawley, WA 6009, Australia
[j] Department of Geological Sciences, 355 Williamson Hall, University of Florida, Gainesville, FL 32611, USA
[k] Department of Earth Sciences, University of Western Ontario, London, ON, Canada N6A 5B7
[l] Department of Earth Sciences, The Natural History Museum, London SW7 5BD, UK

ARTICLE INFO

Article history:
Received 19 October 2011
Accepted 21 June 2012
Available online 9 July 2012

Keywords:
Phanerozoic
Palaeomagnetism
Apparent Polar Wander
Palaeogeography
True Polar Wander

ABSTRACT

A significant number of new palaeomagnetic poles have become available since the last time a compilation was made (assembled in 2005, published in 2008) to indicate to us that a new and significantly expanded set of tables with palaeomagnetic results would be valuable, with results coming from the Gondwana cratonic elements, Laurentia, Baltica/Europe, and Siberia. Following the Silurian Caledonian Orogeny, Laurentia's and Baltica's Apparent Polar Wander Paths (APWPs) can be merged into a Laurussia path, followed in turn by a merger of the Laurussia and Siberia data from latest Permian time onward into a Laurasian combined path. Meanwhile, after about 320 Ma, Gondwana's and Laurussia/Laurasia's path can be combined into what comes steadily closer to the ideal of a Global Apparent Polar Wander Path (GAPWaP) for late Palaeozoic and younger times. Tests for True Polar Wander (TPW) episodes are now feasible since Pangaea fusion and we identify four important episodes of Mesozoic TPW between 250 and 100 Ma. TPW rates are in the order of 0.45–0.8°/M.y. but cumulative TPW is nearly zero since the Late Carboniferous. With the exception of a few intervals where data are truly scarce (e.g., 390–340 Ma), the palaeomagnetic database is robust and allows us to make a series of new palaeogeographic reconstructions from the Late Cambrian to the Palaeogene.

Contents

1. Introduction . . . 326
2. From Laurentia to Laurussia and Laurasia: overview . . . 330
   2.1. Laurentia (North America and Greenland) . . . 330
   2.2. Baltica and Stable or Extra-Alpine Europe . . . 332
   2.3. Laurussia/Laurasia . . . 333
3. Gondwana: overview . . . 334
4. Siberia: Palaeozoic update . . . 334
5. Global polar wander: overview . . . 335

* Corresponding author at: PGP, University of Oslo, P.O. Box 1048, N-0316 Oslo, Norway.
E-mail addresses: t.h.torsvik@geo.uio.no (T.H. Torsvik), voo@umich.edu (R. Van der Voo), ulla.preeden@ut.ee (U. Preeden), conallm@earth.ox.ac.uk (C. Mac Niocaill), bstein@gfz-potsdam.de (B. Steinberger), paveld@fys.uio.no (P.V. Doubrovine), d.v.hinsbergen@fys.uio.no (D.J.J. van Hinsbergen), domeier@umich.edu (M. Domeier), carmen.gaina@geo.uio.no (C. Gaina), etohver@cyllene.uwa.edu.au (E. Tohver), jmeert@ufl.edu (J.G. Meert), pmccausl@uwo.ca (P.J.A. McCausland), r.cocks@nhm.ac.uk (L.R.M. Cocks).

0012-8252/$ – see front matter © 2012 Elsevier B.V. All rights reserved.
doi:10.1016/j.earscirev.2012.06.007

6. Palaeogeography and plate speeds . . . 336
6.1. Early Palaeozoic (Cambrian to Silurian) . . . 336
6.2. Late Palaeozoic (Devonian to Permian) . . . 338
6.3. Mesozoic and Early Cenozoic (Triassic to Palaeogene) . . . 340
7. True Polar Wander (TPW) . . . 343
7.1. TPW since Pangaea assembly . . . 343
7.2. TPW: influence on APW rates and net lithosphere rotation . . . 345
8. Conclusions and future outlook . . . 358
Acknowledgements . . . 363
Appendix 1. Computing TPW in the absence of hotspot tracks . . . 363
References . . . 363

1. Introduction

Since the advent of the understanding of plate tectonics, Earth scientists have wanted to know where the continents lay in past ages, partly from curiosity, but partly so as to understand biodiversity, climate change and where best to search for natural resources. The chief tool in deciphering palaeogeography has been and remains palaeomagnetism, the study of the Earth's magnetic field preserved in rocks. The Earth's ancient magnetic field has provided one of the most fundamental markers used to document the motion of the continents and evolution of the Earth. Changes in ancient magnetic polarity at irregular intervals are recorded in the surface rock record, and over some fifty years, palaeomagnetic data have been used to create the geomagnetic time scale, to firmly document seafloor spreading, to validate plate tectonics, and to reconstruct vanished supercontinents.

Palaeomagnetic results can conveniently be expressed in terms of palaeopoles that are calculated using the geocentric axial dipole field model. In turn, those palaeopoles can be used to construct Apparent Polar Wander Paths (APWPs). This way, instead of plotting the motion of a continent while holding the rotation axis fixed, the motion of the polar axis relative to the continent is visualised (Fig. 1). The motion of continents relative to the Earth's spin axis may be either due to the drift of individual continents or due to a rotation of the entire Earth relative to its spin axis — the latter is called True Polar Wander (TPW). Creer, Irving and Runcorn were the first to publish an APWP for 'Europe' as early as 1954 (Creer et al., 1954), based on late Precambrian to Eocene palaeomagnetic poles from Britain. Those poles all differed markedly from the present-day pole and were interpreted at first as due to a slow change in the axis of rotation of the Earth with respect to its surface, i.e. TPW. Two years later, however, Runcorn (1956) published an APWP for North America and this allowed him to compare the European and North American paths. He noted that they were broadly similar in shape, but some 30° apart in longitude, which he interpreted as caused by the opening of the modern Atlantic. This was the first independent geophysical evidence for 'continental drift' (sensu Wegener, 1912).

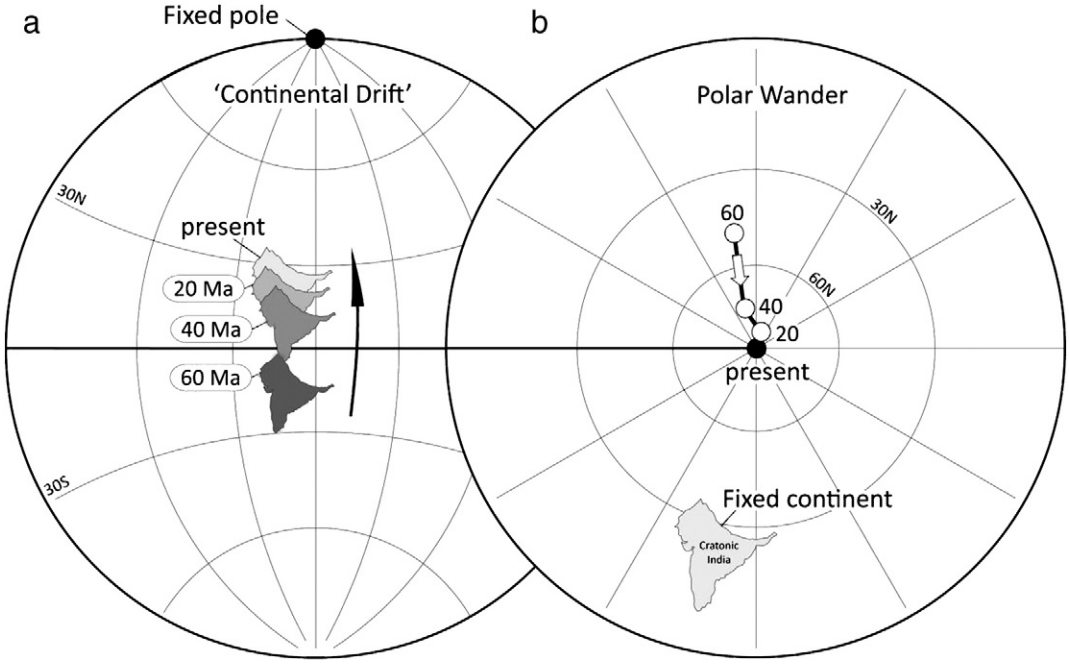

Fig. 1. In (a) the situation depicted is that of a moving continent and a fixed polar axis; this used to be called "continental drift" before the term "plate tectonics" took over. As the continent drifts steadily northward during the last 60 million years, the magnetic field direction at a site in the continent gets recorded by rocks, which then retain a memory of these changing directions (declination and inclination) as a function of time. In (b) the situation is that the continent stays fixed, but that the polar axis is left to wander while following a path called Apparent Polar Wander Path. The word "apparent" denotes the caution that this wandering may or may not be real and that in reality the situation could be as in (a). The sequential locations of the poles are calculated from the declinations and inclinations in the Indian rocks. If all continents show the same Apparent Polar Wander Path, then they shared the same coherent motion with respect to the pole. In that case, it is warranted to call the path a True Polar Wander Path. Figure is based on Tauxe (2009) but here we show palaeomagnetic poles (60, 40 and 20 Ma) and reconstructions of India based on the global APWP developed in this paper. Stereographic (Wulff) projection.

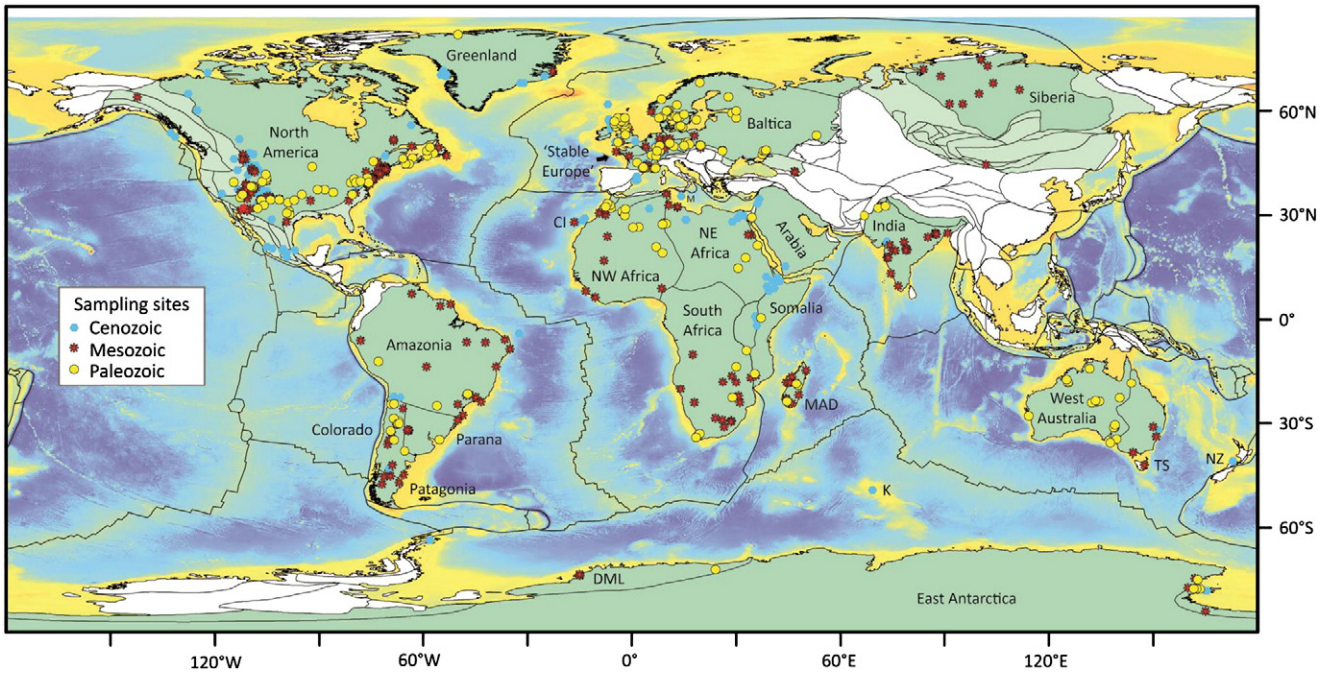

Fig. 2. World map with palaeomagnetic sampling sites for palaeomagnetic poles used in the present data compilation (Table 1). Their symbols and colours are differentiated by geological eras. Thin black lines are old terrane boundaries. Palaeomagnetic data are excluded from white areas. The oceanic areas show present day plate boundaries draped on satellite bathymetry (Smith and Sandwell, 1997). MAD = Madagascar, DML = Dronning Maud Land, NZ = New Zealand, TS = Tasmania, K = Kerguelen.

If the relative positions of a number of continents are reasonably well known, all being defined in the same plate circuit, then palaeomagnetic data from these continents can be combined into a Global APWP (GAPWaP). Widely used GAPWaP's have been published by Besse and Courtillot (2002) covering the last 200 M.y. and by Torsvik et al. (2008a) starting at 320 Ma when the supercontinent Pangaea began to be assembled. Conventional palaeomagnetic reconstructions constrain ancient latitudes and orientations (rotations) of continents, but not their palaeolongitudes. This allows a degree of freedom in making palaeogeographic models unless additional information is available that constrains palaeolongitude. Such information can sometimes be provided by choosing a reference plate that has remained stationary (or quasi-stationary) with respect to longitude. In other words, if there is a reason to suppose that a specific continent has moved little in an east–west sense since the time represented by the reconstruction, that continent can be used as the reference plate. Other continents, partnering in the same plate circuit, will then be seen to occupy their own palaeo-longitudinal positions relative to the deep mantle. Because Africa meets the criteria required of a reference plate, at least since Pangaea breakup (Burke and Torsvik, 2004; Torsvik et al., 2008a,b), we can tie all other continental motions to a 'fixed' African plate. This is important for estimating TPW (Section 7) and to develop semi-absolute reference frames from palaeomagnetic data.

Building on the GAPWaP of Torsvik et al. (2008a) we present two different GAPWaP's for the past 320 million years (M.y.): (1) One without TPW correction to be used in classical palaeo-geographic/-climatic reconstructions and as reference frame for new palaeomagnetic data, where the true relation to the spin-axis is imperative, and (2) one with TPW correction that leads to a smoother plate model that only describes 'continental drift', and that *must* be used, for example, to calculate net lithosphere rotation (Section 7) or to compare surface processes with heterogeneities in the deepest mantle (Torsvik et al., 2010a).

In addition to the construction of a new and more robust GAPWaP, back to the time when Pangaea assembled, we also construct new Palaeozoic APWPs for Gondwana, Laurentia, Baltica and Siberia back to the dawn of the Phanerozoic. After the Silurian Caledonian Orogeny we can combine palaeomagnetic data from Laurentia and Baltica to produce a joint APWP for Laurussia.

Asian blocks such as North and South China, the Tibetan blocks, Tarim, Annamia (Indochina), Kolyma–Omolon, Kazakhstania elements, Sunda blocks, and Tethyan (Cimmerian) terranes are not represented and are left white in Fig. 2, because tectonic activity, such as local rotation and intense deformation, introduces too much noise in the construction of their APWPs.

Palaeomagnetic data (Figs. 2–3; Table 1) were compiled and graded according to Van der Voo's classification system (Van der Voo, 1990, 1993), and rotated with a given continent to its reconstructed position; rotation parameters (e.g., Table 2) for most of the relative fits follow Torsvik et al. (2008a) unless noted in the text. Only palaeomagnetic data with a quality factor Q≥3 (Van der Voo, 1990)

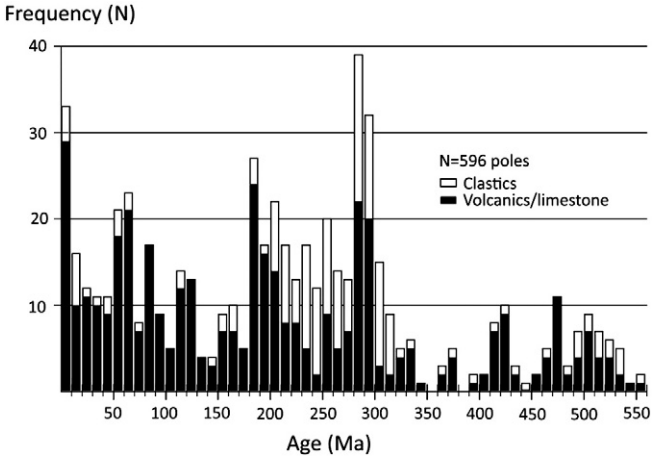

Fig. 3. Age frequency histogram (10 Myr bins) of palaeomagnetic poles (Table 1) compiled in this study. Poles are subdivided into those obtained from detrital sedimentary rocks (labelled "clastics") and those of volcanic rocks/limestone. Note the near-total absence of reliable palaeomagnetic poles for Early Carboniferous (350–360 Ma) and Mid-Devonian (380–390 Ma) times.

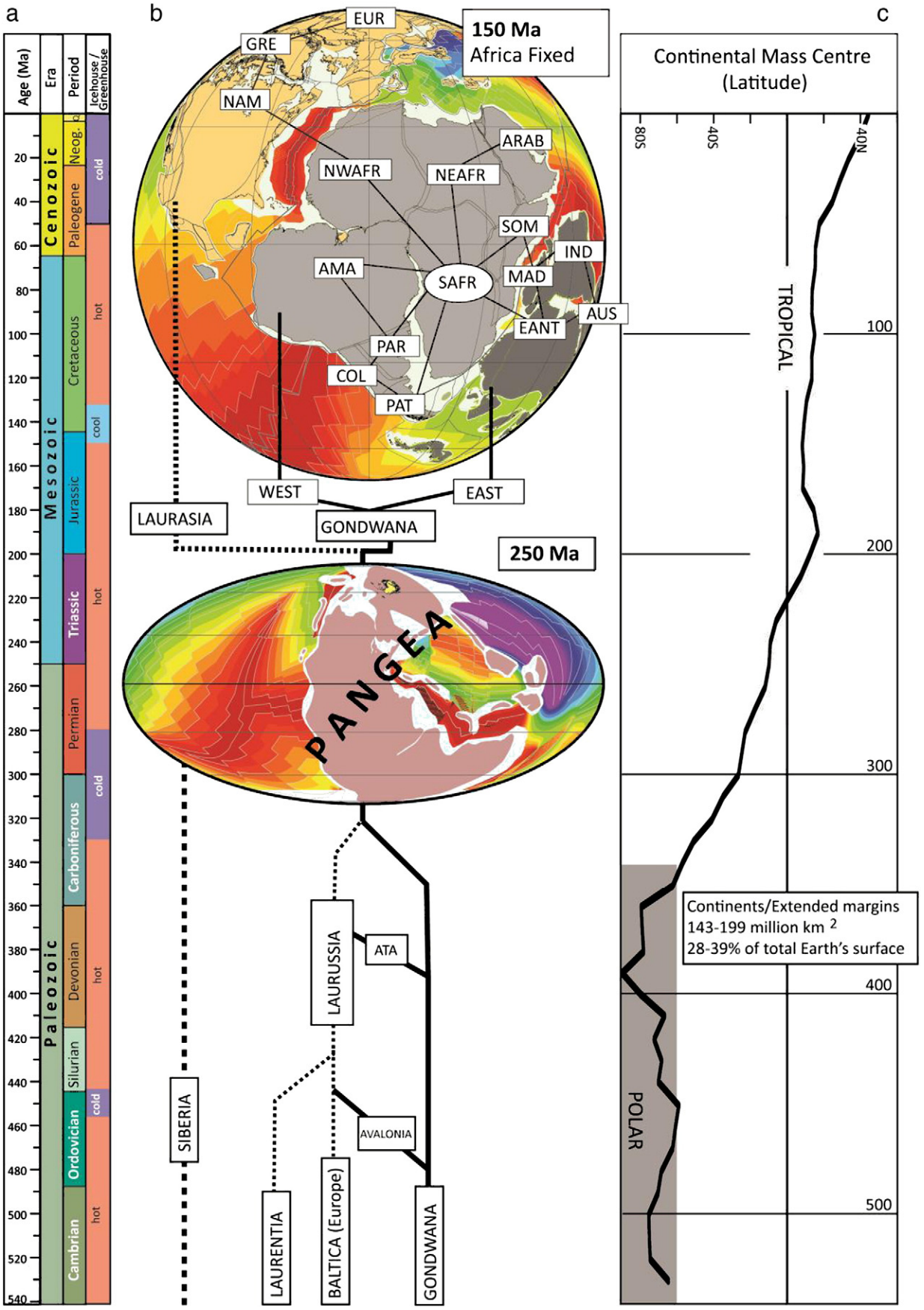
a
b
c
Age (Ma)
Era
Period
Icehouse / Greenhouse
Cenozoic
Mesozoic
Paleozoic
Neog.
Paleogene
Cretaceous
Jurassic
Triassic
Permian
Carboniferous
Devonian
Silurian
Ordovician
Cambrian
cold
hot
cool
150 Ma
Africa Fixed
EUR
GRE
NAM
ARAB
NWAFR
NEAFR
SOM
IND
AMA
SAFR
MAD
AUS
EANT
PAR
COL
PAT
WEST
EAST
LAURASIA
GONDWANA
250 Ma
PANGEA
LAURUSSIA
ATA
SIBERIA
AVALONIA
LAURENTIA
BALTICA (Europe)
GONDWANA
Continental Mass Centre
(Latitude)
80S
40S
40N
TROPICAL
POLAR
100
200
300
400
500
Continents/Extended margins
143-199 million km 2
28-39% of total Earth's surface

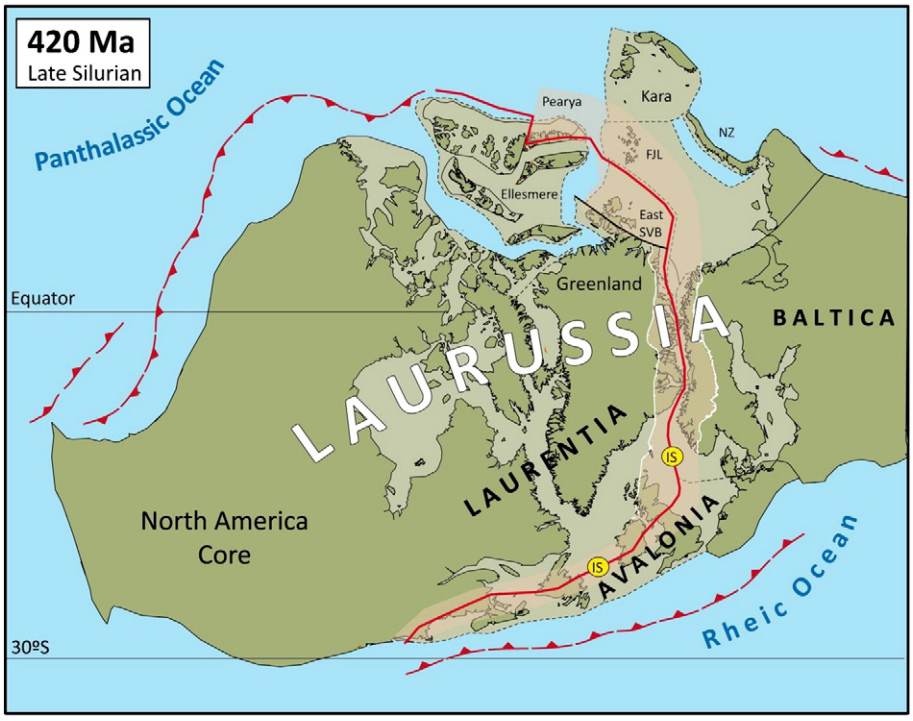

Fig. 5. The outline of Laurussia, plotted on a ca. 420 Ma reconstruction. Area of Caledonide orogenic deformation is tinted light brown, and the white lines from east Greenland to Scotland and in Norway represent the Caledonide Nappe Front. FJL, Franz Josef Land; IS, Iapetus Suture; NZ, Novaya Zemlya; SVB, Svalbard; WI, Wrangel Island. Simplified from Cocks and Torsvik (2011).

are used, but palaeomagnetic poles that knowingly fail the assumption that the magnetisation age equals the actual rock age are not included in our analysis. Our procedures to generate APWPs (either running mean or spherical spline paths; Jupp and Kent, 1987) are detailed in Torsvik et al. (1992, 1996, 2008a). Running mean paths are non-weighted whereas input poles in all spherical spline paths were weighted by Van der Voo's (1990) quality factor Q (Table 1). Instead of weighting the data by 95% confidence ovals (α_{95}, "criterion 2" in Van der Voo's classification system) we weighted by 7/Q. This causes the smooth path to pass close to the data which score "7" (full-marks).

Van der Voo and Torsvik (2004) analysed the APWP of Baltica/Stable Europe for Permian times, paying particular attention to aspects that could introduce a systematic bias. They identified three problems: (1) palaeopoles from some (but not all) detrital sedimentary rocks exhibited a palaeolatitudinal offset when compared to latitudes calculated from coeval igneous rocks (e.g., Estérel results, Zijderveld, 1975), (2) palaeopoles based on outmoded demagnetisation methodologies revealed a minor bias with respect to results obtained by principal component analysis (e.g., Kirschvink, 1980; Kent et al., 1983), and (3) palaeopoles associated with dubious or no radiometric age dating revealed a bias of some 10° on average with respect to results based on $^{40}Ar/^{39}Ar$ or U/Pb methods. Importantly, observation (3) produced the most substantial bias. It is not (yet) feasible to remedy the bias of items (2) and (3) by omission of potentially flawed data, because too many gaps would occur in the temporal sequences of the APWPs. We can (and do here) remedy the situation of bias (1) by correcting for (inferred) inclination errors in all results obtained from detrital sedimentary rocks. Similar efforts have begun to be applied in other studies (e.g., Tauxe and Kent, 2004; Kent and Tauxe, 2005; Yan et al., 2005; Kodama, 2009; Bilardello and Kodama, 2010a; Kent and Irving, 2010; Domeier et al., 2011a), and are likely to become standard in the very near future.

Inclination (I) error in sediments is latitude dependent and anti-symmetric. This bias closely mimics errors produced by octupole fields of the same sign as the dipole field (Rochette and Vandamme, 2001; Torsvik and Van der Voo, 2002; Tauxe, 2005; Domeier et al., 2012). The degree of inclination shallowing depends on rock type and remanence acquisition/shallowing mode. Inclination shallowing is commonly predicted from:

$$\tan(\mathrm{INC}_{\mathrm{Observed}}) = f \tan(\mathrm{INC}_{\mathrm{Field}}),$$

where INC is the inclination and f is the degree of inclination error (King, 1955) — *In this paper all detrital sedimentary poles have been corrected for inclination shallowing using a commonly observed f value of 0.6, unless inclination shallowing was corrected for by the original authors using the* Tauxe and Kent (2004) *E/I method or the magnetic fabric method of* Kodama (2009) — this is a little more conservative than f values derived from laboratory experiments (0.4–0.55; King, 1955, Løvlie and Torsvik, 1984; Tauxe and Kent, 1984). Correcting detrital

Fig. 4. (a) Phanerozoic time scale and icehouse (cold) vs. greenhouse (hot) conditions. (b) Schematic evolution for the formation and break-up of Pangaea (main continental players): The bulk of Pangaea formed by collision of Gondwana and Laurussia (Laurentia and Baltica/Avalonia that fused in the Mid Silurian) in the Late Carboniferous followed by Siberia in Late Permian–Triassic times. First major break-up was witnessed by the Early Jurassic opening of the Central Atlantic and separation of Gondwana and Laurasia. The Pangaea 250 Ma reconstruction is an 'absolute' reconstruction with land, shelf and a modelled oceanic age grid (red is young, blue is old oceanic crust). Distribution of Siberian Trap rocks shown in yellow. The top reconstruction is for 150 Ma (relative to SAFR, southern Africa, held fixed) and is also shown with an oceanic age grid. SAFR serves as the reference continent relative to which the motion of all other plates is determined since Pangaea formation (ca. 320 Ma). Laurasia, West- and East-Gondwana continental elements shown with light brown, grey and dark grey shading. Abbreviations: EUR, stable Europe; GRE, Greenland; NAM, North America; NWAFR, northwest Africa; NEAFR, northeast Africa; ARAB, Arabia; SOM, Somalia; AMA, Amazonia (South America); PAR, Parana; COL, Colorado; PAT, Patagonia; IND, India; MAD, Madagascar; EANT, East Antarctica; AUS, Australia; ATA, Armorican Terrane Assemblage. (c) Continental (latitude) mass centre calculated from our plate polygon model. Mass centre calculation also includes the areas of submerged continental crust between coastlines and the continent–ocean boundary [e.g., light grey areas in 150 Ma reconstruction in (b)].

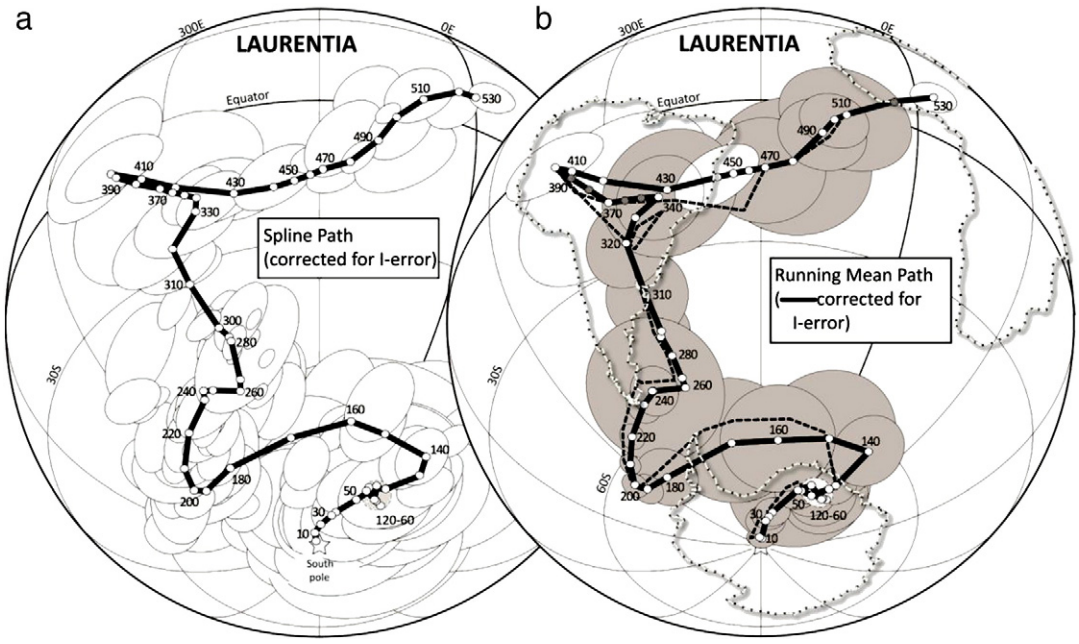

Fig. 6. (a) 95% confidence ovals for Laurentian input poles (white shading) and a fitted spherical spline path. The spline path is moderately smoothed (smoothing factor = 300) and input poles have been weighted by their Q-factor (see Torsvik et al., 1992, 1996 for procedure). Detrital sedimentary input poles and spline path are shown after correction for potential I-errors (flattening factor *f* of 0.6). (b) Running Mean path (20 M.y. window) shown with A95 ovals (grey shading) after I-error correction (black thick lines with ages in million years) and a running mean path without correction for inclination shallowing (black stippled line with no A95's). A95 or dp/dm ovals are white about a given palaeomagnetic pole if it is the only entry for its bin. Dark grey dots (black curve) are purely interpolated mean poles. *The recommended APWP is the spline path in* (*a*). Orthogonal projection.

sediments with an *f* value of 0.6 amounts to a maximum latitude correction of 14.5° (1600 km) at around 50° N/S. This is comparable to the effects of octupole contributions as high as 22%. All detrital sedimentary sequences used in the spline fits in our paper are corrected for inclination shallowing.

In total, our Phanerozoic palaeomagnetic data compilation includes 626 poles (Table 1). For analysis and visualisation we primarily used the GMAP software (Torsvik and Smethurst, 1999) in addition to GMT (Wessel and Smith, 1991). A new and improved version of GMAP will be made available in 2012 (work in progress) along with all our palaeomagnetic data in digital GMAP and GPlates (www.gplates.org; Boyden et al., 2011) format.

2. From Laurentia to Laurussia and Laurasia: overview

The Palaeozoic continent Laurentia is represented largely by cratonic North America, but also includes Greenland, Ellesmere and parts of present-day Europe (e.g., Scotland, NW Ireland and Svalbard). It was drifting independently until collision with Baltica and Avalonia produced the Caledonian Orogeny at 430–420 Ma (Figs. 3–4). Laurentia then became the western portion of Laurussia, which in turn became part of the Pangaea Supercontinent during the Late Carboniferous (Cocks and Torsvik, 2011). By Late Permian times, Siberia had essentially joined Baltica, and along with other European and Asian elements, the combined continent is referred to as Laurasia.

2.1. Laurentia (North America and Greenland)

Due to a steadily growing palaeomagnetic database, many updated APWPs have been published in the past 50 years for North America (e.g., Irving, 1964, 1979; Runcorn, 1965; Hospers and Van Andel, 1968; McElhinny, 1973; Van der Voo and French, 1974; Van der Voo, 1981, 1990; Irving and Irving, 1982; Mac Niocaill and Smethurst, 1994). Compared to earlier compilations for the Palaeozoic by Torsvik et al. (1996) and for late Palaeozoic (<320 M.y.) and younger times (Torsvik et al., 2008a), we have included 64 additional poles in the present compilation. Most are based on new studies but some are 'old' sedimentary poles corrected for I-error using the inclination–elongation method of Tauxe and Kent (2004) or the anisotropy of magnetic susceptibility information (Kodama, 2009).

Our pole collection from the Phanerozoic of Laurentia (North America and Greenland) includes 195 poles ranging in age from 0.5 to 532 Ma (Table 1). Poles from Greenland have been rotated to account for seafloor spreading in the Labrador Sea/Baffin Bay (67→33 Ma) as well as pre-drift extension back to Cretaceous (Barremian) times (Table 2). Most poles from North America are from the cratonic core (Figs. 2 and 5) except for a few poles derived from young rocks that accreted to North America during the Mesozoic/Cenozoic (Table 1).

A moderately smoothed spherical spline path in 10 M.y. intervals, with results from detrital sedimentary rocks corrected for I-error along with their associated 95% confidence ovals (based on α_{95}) or A95 (rare; see Table 1) for the input poles is shown in Fig. 6a (Table 3). We also show a running mean path (Fig. 6b) with or without correction for I-error (thick black line with 95 ovals, or black stippled line in Fig. 6b, respectively). The different APW paths show gross similarities: keeping North America fixed, and using the present-day distribution of continents as a descriptive reference, the South Pole was located in NW Africa in the Cambrian, it had moved to South America (Brazil–Ecuador) by the Early Devonian, followed by southward movement and arrival to the east of Patagonia (southernmost South America) by Permian and early Mesozoic times. The South Pole has stayed close to Antarctica since the Late Triassic, but with a pronounced easterly trend during the Jurassic (~200–140 Ma), followed by the well-known Cretaceous still-stand (120–60 Ma, marked by white oval). The Jurassic trend is dominated by a TPW signal (Steinberger and Torsvik, 2008 and Section 7).

Data-coverage is notably poor for Laurentia between 340 and 400 Ma, implying that the running mean poles for 350–360 Ma and 380–390 Ma (dark grey dots in Fig. 6b) are all interpolated; this is the so-called Siluro-Devonian cusp that has previously been

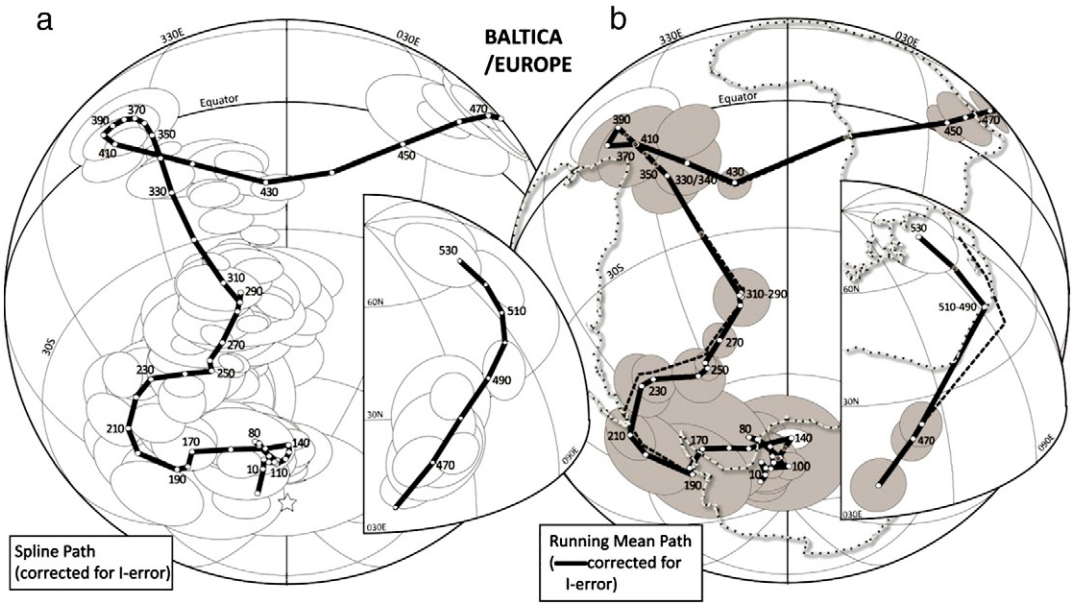

Fig. 7. (a) 95% confidence ovals for Baltica/Stable Europe input poles (white shading) and a fitted spherical spline path. The spline path is moderately smoothed (smoothing factor = 300) and input poles have been weighted by their Q-factor. Detrital sedimentary input poles and spline path shown after correction for potential inclination shallowing. Inset map shows Cambrian and Early Ordovician path segments based on spline fitting. (b) Running Mean path shown with A95 ovals (grey shading) after sedimentary inclination correction (black thick lines with ages in million years) and a running mean path without correction for inclination shallowing (black stippled line with no A95's). A95 or dp/dm ovals are white about a given palaeomagnetic pole if it is the only entry for its bin. Dark grey dots (black thick curve) are purely interpolated mean poles. *The recommended APWP is the spline path in* (*a*). Orthogonal projection.

interpreted as TPW (Van der Voo, 1994). The paucity of data in this section of the APWP results in markedly different 'fits' between the spline-fitted and running mean methods. The effect of correcting detrital sedimentary rock results for I-error can also be seen in Fig. 6b: On average the great-circle difference (GCD) between a pair of coeval poles from each of the two paths is small (2.8 ± 2.9°; mean and standard deviation), but the Late Jurassic–Early Cretaceous (140–160 Ma) and Late Devonian (360–370 Ma) APWP segments show larger and more systematic differences of as much as 8–11°. Although the GCD is always greater than or equal to

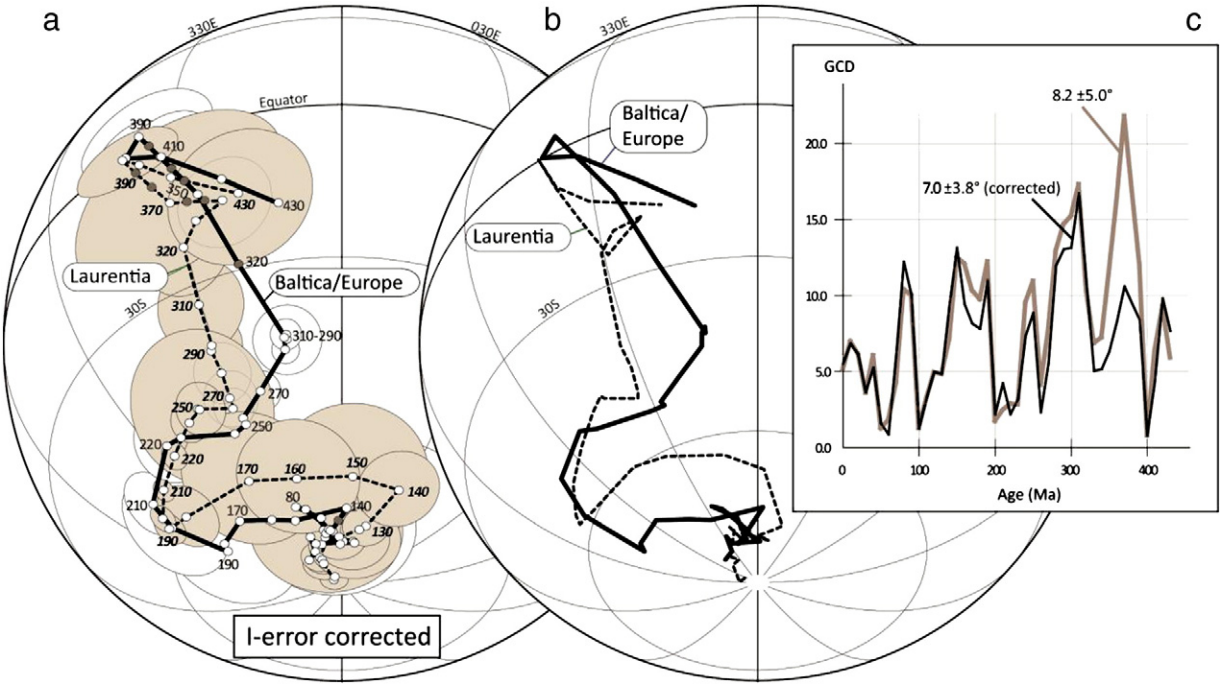

Fig. 8. (a) Running Mean paths for Baltica/Stable Europe and Laurentia (rotated to European co-ordinates), shown with A95 ovals. Dark grey dots are purely interpolated mean poles. Both paths are corrected for inclination shallowing in detrital sedimentary rocks (b) Same as (a) but not corrected for inclination shallowing and shown without A95s. (c) Great-circle distance (GCD) between poles of the same age from Baltica/Stable Europe and Laurentia with (black line) and without (grey thick line) correction for potential inclination shallowing.

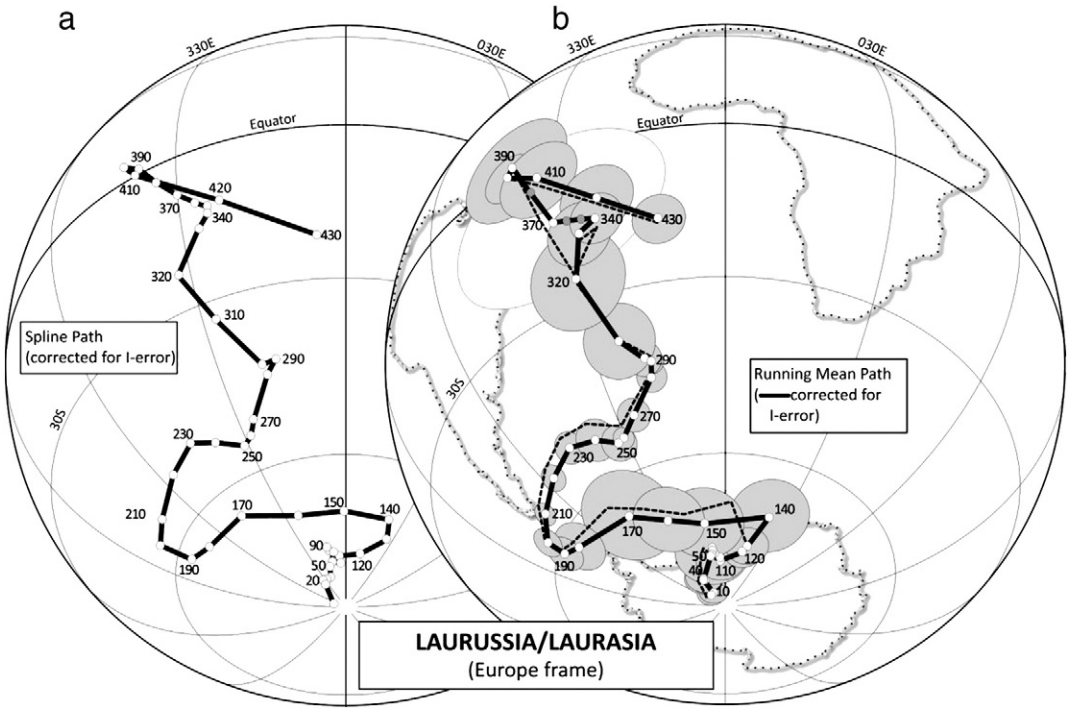

Fig. 9. (a) Combined spline path (smoothing 300, Q-factor weighted) for Laurussia and Laurasia (after 250 Ma). (b) Running Mean paths for Laurussia/Laurasia shown with (black line with grey A95s) and without (black stippled line) correction for inclination shallowing. Dark grey dots are purely interpolated mean poles. White oval represent a single dp/dm oval (Catskill Formation South pole, Table 1). *The recommended APWP is the spline path in* (*a*).

zero, and hence its distribution is not truly Gaussian, we nevertheless use the normal definition of standard deviation as a simple means of describing the variance.

Statistically (in this case) there is no significant change in A95's but the inclination-corrected path is considerably smoother than the non-corrected one. More importantly, the systematically higher corrected-pole latitudes during the Jurassic become important when comparing the Laurentia APWP with Europe/Baltica and Gondwana (Sections 2.3, 3). The spline and running mean paths (both I-error corrected) differ on average by $1.9 \pm 1.4°$ with a peak difference of 6.2° during the Middle Cambrian (Table 3).

2.2. Baltica and Stable or Extra-Alpine Europe

Numerous APW paths have been published for Baltica and its younger incarnations (e.g., Stable or Extra-Alpine Europe) over the past decades. Our present compilation includes 167 palaeomagnetic poles (0.5–535 Ma), 44 more than in our previous 2005 compilation (Torsvik et al., 2008a), but nine of these poles are from stable Siberia and one Early Cretaceous pole is from peri-Siberia (Mongolia). Siberia was quasi-stable in its position relative to Baltica/Laurussia between Late Triassic and Early Jurassic times, but the estimated correction is so small (a few degrees around an Euler pole of 77°N and 144.6°E; Buiter and Torsvik, 2007) that we include the few Siberian poles (mostly Siberian Traps, ~251 Ma poles) from the Permo–Triassic boundary and onwards in our compilation. Cambrian and Ordovician poles are exclusively from Baltica but for Silurian (~430 Ma) and younger times we progressively include more and more poles from areas that can be characterised as having become part of Stable Europe. The oldest of these 'Stable' Europe poles are from Scotland and were derived from undeformed Silurian granites ('Newer' Granites) and Lower Devonian volcanics that postdate Iapetus closure across the British Caledonide sector. Poles from these rocks also compare well with similar-aged poles from the core of Baltica (Torsvik et al., 1996).

The Baltica/Europe APWP (Fig. 7, 355° in GCD length) is considerably longer than the Laurentian APWP (269°), owing to widely separated Cambrian and Ordovician palaeopoles from Baltica/Europe (the cumulate APW is measured here from the respective spline paths). With respect to a fixed Baltica/Europe, the mean South Poles for the Cambrian (Fig. 7b) are located in Arctic Siberia, followed by a drift of the pole over Arabia and Central Africa in the Ordovician to the

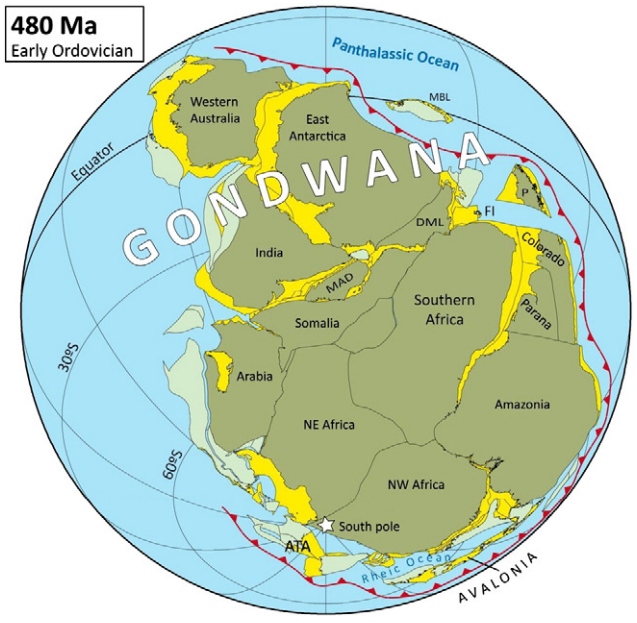

Fig. 10. Outline of Gondwana and peri-Gondwana, plotted on a 480 Ma reconstruction. Black lines are old terrane boundaries. Our palaeomagnetic compilation is only derived from areas shaded in dark green and does not include Ordovician data from peri-Gondwana terranes (e.g. Avalonia and ATA). ATA = Amorican Terrane Assemblage; MBL = Marie Bird Land; FI = Falkland Islands; DML = Dronning Maud Land; MAD = Madagascar.
After Torsvik and Cocks (2011).

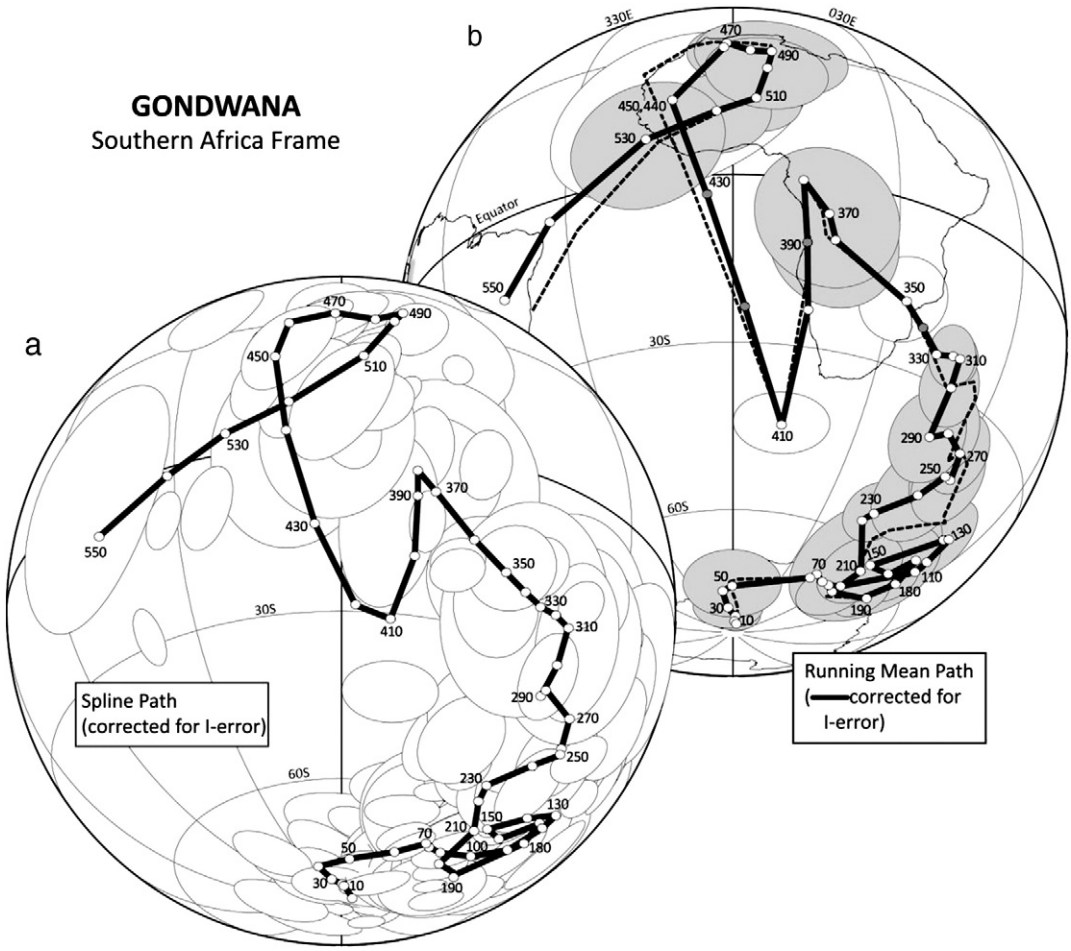

Fig. 11. (a) 95% confidence ovals for Gondwana input poles in Southern Africa co-ordinates (white shading) and a fitted spherical spline path. The spline path uses a smoothing factor of 500 and input poles are weighted by their Q-factor. Spline path shown after correction for potential inclination shallowing. (b) Running Mean path (20 Myr window) shown with A95 ovals (grey shading) after sedimentary inclination correction (black thick lines with ages in million years) and a running mean path without correction for inclination shallowing (black stippled line with no A95s). White A95 ovals are dp/dm ovals from a single palaeomagnetic pole. Dark grey dots (black curve) are purely interpolated mean poles. *The recommended APWP is the spline path in* (*a*). Orthogonal projection.

Atlantic off the NE corner of Brazil in the Siluro-Devonian cusp. We recall that this cusp was also seen in Laurentia's APWP. Subsequent southward movement brought the South Pole near Patagonia in the Triassic, after which the pole remained close to Antarctica in the Jurassic.

Spline and running mean APWPs are grossly similar ($3.5 \pm 3.5°$) but differences can be as much as ~19° in the Early Ordovician (Table 4), given the rapid and significant shift of the mean poles between 510 and 430 Ma. Running mean paths, corrected as well as uncorrected for I-error differ on average by $1.4 \pm 2.8°$ but this reaches values between 7 and 14° in Cambrian–Early Ordovician times. As was the case for Laurentia, there are very few poles between 400 and 310 Ma and the Mid-Devonian to Late Carboniferous APW segment is thus largely interpolated.

2.3. Laurussia/Laurasia

Laurentia (including Scotland and Greenland) collided with Baltica and Avalonia at ~430 Ma (Figs. 4–5) and from then on we can combine Laurentia and Baltica/Stable Europe poles into one APWP with the correction for younger pre-drift extension and the opening of the North Atlantic Ocean in early Palaeogene time. Avalonia's results from Lower and Middle Palaeozoic rocks, possibly having suffered local or regional rotations (Torsvik et al., 1993), are not included in our current analysis. From 251 Ma onwards we also include poles from Siberia as part of the larger Laurasian continent.

A fit published by Bullard et al. (1965) is typically preferred for rotation of North American poles into European coordinate (or vice versa); this fit (Euler pole latitude = 88.5°N, longitude = 27.7°E, angle = −38.0°) matches poles quite well, but leads to a rather loose fit between the opposing continental edges in the NE Atlantic. Torsvik et al. (2001, 2008a) have therefore proposed more geologically plausible (and tighter) fits that can account for the pre-drift extension history along the opposing Norwegian and Greenland margins. In this paper we use a tight mid–late Palaeozoic–early Mesozoic fit of Torsvik et al. (2006), elaborated in Alvey (2009 and manuscript in preparation) and Domeier et al. (2012), and tested/confirmed by estimates of lithosphere stretching based on gravity inversion and seismic refraction data (Alvey, 2009). This 'tighter' fit (seen in Fig. 5) is broadly similar to that used by Torsvik et al. (2008a), which was based on a 2005 plate-circuit compilation. Reconstruction parameters for Europe vs. North America and Greenland are listed in 5 Myr intervals in Table 2. The Cenozoic spreading history for both the NE Atlantic and the Labrador Sea follows that of Gaina et al. (2002) and Gaina's unpublished data (listed in Torsvik et al., 2008a).

After adjusting for seafloor spreading and pre-drift extension in the North Atlantic realm, the APWPs for Laurentia and Baltica/Europe resemble each other quite well, except for (1) the Late Carboniferous–Early Permian (note discordant 310–290 mean poles in Fig. 8a)

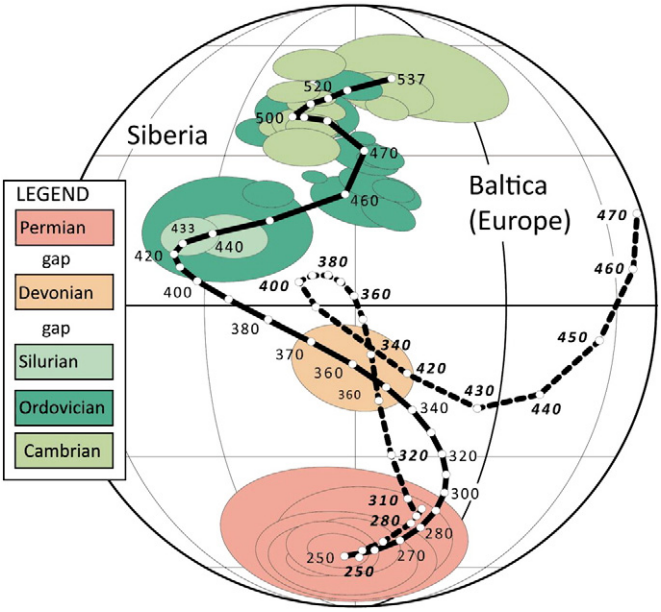

Fig. 12. (a) Revised APWP for Siberia (after Cocks and Torsvik, 2007). Spline path with smoothing parameter of 300 and Q-factor weighted input poles. This path is based on one new Silurian pole (433 Ma; Shatsillo et al., 2007) and elimination of two similar-aged and less reliable poles from Siberia (see text). The Siberian spline path (black thick line) is compared with the spline path for Baltica (Fig. 7a).

and (2) the Jurassic–Early Cretaceous. In the latter case, Laurentian poles systematically plot at lower latitudes, a problem noted in numerous papers (e.g., Van der Voo, 1992; Courtillot et al., 1994). We note that correcting clastics for I-error leads to smoother APWPs and better agreement between pairs of coeval poles from each of the two paths (GCD reduced from 8.2 ± 5.0° to 7.0 ± 3.8° after correction; Fig. 8c).

336 poles are included in our Laurussia (from 430 Ma) and Laurasia (from 251 Ma) APWP (Table 5) and are represented both in a spherical spline path (Fig. 9a) and in running mean path segments (Fig. 9b). The running mean path is based on an average of 17 poles for each mean pole with A95 averaging to 4.7 ± 2.8° (corrected for I-error) and 4.9 ± 3.0° (uncorrected). The average difference between coeval points on the uncorrected and corrected running mean paths is 2.1 ± 2.4°. A95 errors are slightly reduced when correcting for I-error and the path becomes notably smoother.

The difference between coeval poles from the spline and running mean paths is 2.0 ± 1.7° with peak values of 6–7° in the Late Devonian (370 Ma) and Silurian (410, 430 Ma) segments. The 390 to 340 Ma segment; however, is based on a single pole from the Catskill Formation (370 Ma) and renders this segment less reliable and dominated by interpolation (see grey dots in Fig. 9b and Table 5). Middle Devonian to Early Carboniferous palaeomagnetic poles are *urgently* needed for Laurussia. The combined running mean and spline paths are broadly similar (Fig. 9).

3. Gondwana: overview

Published APWPs for the combined Gondwana continents (e.g., Morel and Irving, 1978; Hurley and Van der Voo, 1987; Bachtadse and Briden, 1990; Schmidt and Embleton, 1990; Chen et al., 1994) differ widely and depend critically on data selection/rejection criteria employed by the authors resulting in a large variety of shapes/loops (e.g., portrayed in Van der Voo, 1993, *Fig. 5.15*; see also Kent and Van der Voo, 1990). Our syn- to post-Pangaea data selection (<320 Ma) follows Torsvik et al. (2008a), whilst pre-Pangaea data are updated from the compilation of Torsvik and Van der Voo (2002). Gondwana (Fig. 10) was mostly assembled at around 550 Ma (Meert and Van der Voo, 1997) although the fusion of some cratonic elements (Amazonia, West Africa) with the central Gondwanan elements may have occurred during Mid to Late Cambrian times (Tohver et al., 2006, 2010, 2012; Trindade et al., 2006). Relative fits for Gondwana are listed in Table 6 for the reconstructions with respect to Southern Africa of the following cratons: Western Australia, East Antarctica, the Indian subcontinent, Madagascar, South America (Amazonia, Parana, Colorado and Patagonia), NW and NE Africa, Somalia, and Arabia. Compared with the Torsvik et al. (2008a) plate circuit compilation, the relative fits within the Indian Ocean (e.g., for India; Cande et al., 2010) and internal fits for Africa (e.g., for Somalia; Horner-Johnson et al., 2007) and South America (e.g., Patagonia; Torsvik et al., 2009) have been updated. In our compilation we have not included results from transient peri-Gondwana elements (Fig. 4) such as Avalonia and the Armorican/Cadomian Terrane Assemblage (e.g., Spain, France), that rifted from Gondwana during the Early Ordovician (opening of the Rheic Ocean; Fig. 10) or the Early Devonian (opening of the Palaeotethys) respectively (Torsvik and Cocks, 2011).

Our selection (Fig. 11) from the former Gondwana continents contains 229 poles (including 49 'new' poles and 59 sedimentary poles corrected for potential I-errors). Two poles are included from volcanic provinces in Kerguelen (27 Ma) and West Antarctica (5 Ma) (Table 1) that were part of East Antarctica at their time of eruption. For cratonic Australia we exclude all poles within the Tasman Fold-belt or east of the Tasman Line, following Torsvik and Van der Voo (2002). Here we also exclude three Cambrian poles from Pakistan (listed in Torsvik and Van der Voo, 2002) due to possible structural corrections owing to oroclinal bending in the Himalayas (Klootwijk, 1996). However, exclusion/inclusion of these poles produces only minor changes (<5°) in the Gondwana 540 and 530 Ma mean poles.

The new APWP for Gondwana (Table 7) shows gross similarities to that of Torsvik and Van der Voo (2002): Keeping Southern Africa fixed, the APW of the South Pole tracks from near Brazil's coast in the latest Precambrian (550 Ma), thence to NW Africa during most of the Late Cambrian and Ordovician, followed by a rapid cusp during Silurian to Early Devonian times. During the Late Devonian, the South Pole was located in equatorial Africa and then migrated southeastward during the Carboniferous. Since the Triassic (~230 Ma), the south-pole has remained close to East Antarctica (Fig. 11b). Thus, this Palaeozoic APWP for Gondwana can be summarised by a simple SE-ward track from NW Africa to Antarctica (Path X of Morel and Irving, 1978), with superimposed a back-and-forth loop (path Y of Morel and Irving, 1978) between 430 and 380 Ma. The variety in Gondwana APWP shapes published by different authors, and referred to above, is related to acceptance or rejection of one or both of these superimposed loops.

The spline and the running mean path resulting from our selection of palaeopoles show gross similarities except for the Early Devonian where a single pole causes the deviation. The effect of correcting poles from detrital sediments for I-error is most notable in the Carboniferous–Triassic section of the path (Fig. 11b), with implications for Pangaea fits (e.g., Rochette and Vandamme, 2001; Domeier et al., 2011b, 2012). The difference between the spline (Fig. 11a) and running mean path (Fig. 11b) is 3.4 ± 3.0° with peak values of 11–14° in the Silurian and Early Devonian. The Silurian segments, however, are entirely interpolated due to the scarcity of palaeomagnetic data for that interval.

4. Siberia: Palaeozoic update

The Siberian palaeocontinent includes political Siberia and adjacent areas of Mongolia, eastern Kazakhstan, and NW China (Cocks and Torsvik, 2007). Siberia was essentially an independent continent

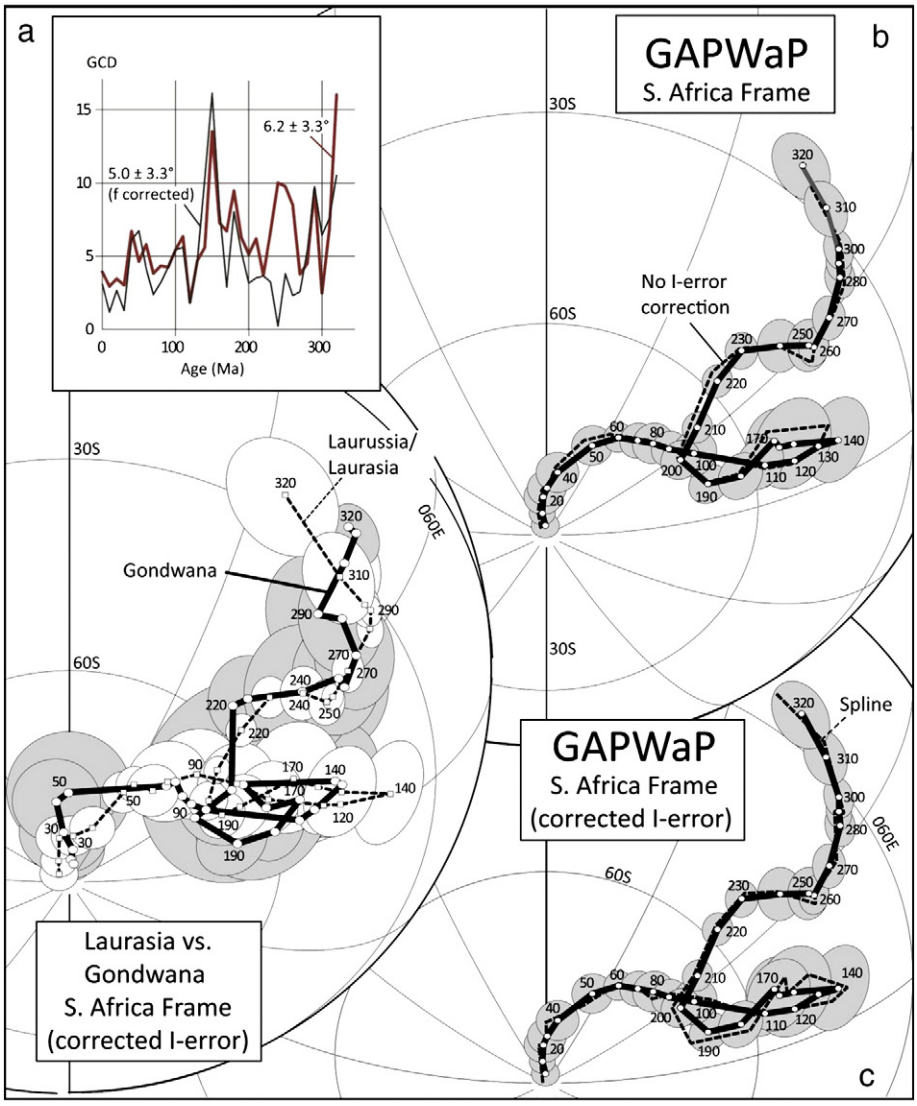

Fig. 13. (a) Bottom: Running Mean paths for Gondwana (thick black curve) and Laurussia/Laurasia (rotated to Southern Africa co-ordinates) shown with A95 ovals. Both paths are corrected for inclination shallowing. Top: Great-circle distance (GCD) between poles of the same age from Gondwana and Laurentia with (black thin line) and without (grey thick line) correction for inclination shallowing. (b) Global running mean APWP (GAPWaP), corrected (black line with A95s) and uncorrected (stippled line) for inclination shallowing. (**c**) Global spline path (smoothing parameter of 300 and Q-factor weighted input poles) compared with the running mean path in (b). Both are corrected for potential I-error. *The recommended APWP is the running mean path in* (*c*). (For interpretation of the references to colour in this figure legend, the reader is referred to the web version of this article.)

during late Precambrian and Palaeozoic times and became part of Pangaea during the early Mesozoic. Palaeozoic palaeomagnetic data were reviewed by Cocks and Torsvik in 2007 but due to a newly published Silurian pole from Siberia (Shatsillo et al., 2007) that supersedes two less reliable poles (435 and 439 Ma Lena River Sediments poles in Table 1a of Cocks and Torsvik, 2007) we have here substantially modified the APWP for Siberia for Silurian and Early Devonian times (Fig. 12). In essence, our revised APWP and implied reconstructions place Siberia at lower and mostly tropical latitudes during Silurian and Early Devonian times. There is only one reliable palaeomagnetic pole between Silurian and Permo-Triassic times (360 Ma pole in Fig. 12) and thus the late Palaeozoic APWP is essentially interpolated, albeit showing convergence with the Baltica/Stable Europe APWP in Permian time (Bazhenov et al., 2008). Our revised Siberia APWP (Table 8) is a spline path and is shown in South Siberian co-ordinates where Cambrian to Silurian palaeomagnetic poles from the southern and northern parts of Siberia are fitted with an Euler pole of 60°N, 120°E and a rotation angle of 13° (see Cocks and Torsvik, 2007).

5. Global polar wander: overview

Gondwana and the intervening terranes collided with Laurussia during the Late Carboniferous (~320 Ma), and from then on we combine all palaeomagnetic data into a Global Apparent Polar Wander Path (GAPWaP). A Pangaea-A type fit is our preferred configuration (Dominguez et al., 2011; Domeier et al., 2012) but other alternatives exist (e.g., Irving, 1977, 2004; Muttoni et al., 2003). Relative fits between Gondwana (NW Africa) and Laurussia/Laurasia (North America) are given in Table 9 and the closure fit follows that of Labails et al. (2010), which slightly modifies the fit of Torsvik et al. (2008a).

Fig. 13 shows a comparison of Laurussia/Laurasia and Gondwana running mean APWPs in a Pangaea-A type fit. Poles from detrital sedimentary rocks are corrected for I-error and for the bulk of the Phanerozoic, the two paths overlap at the 95% confidence interval. In particular, we note the very good fit of Carboniferous to Triassic mean poles in the Pangaea-A type configuration. On average the

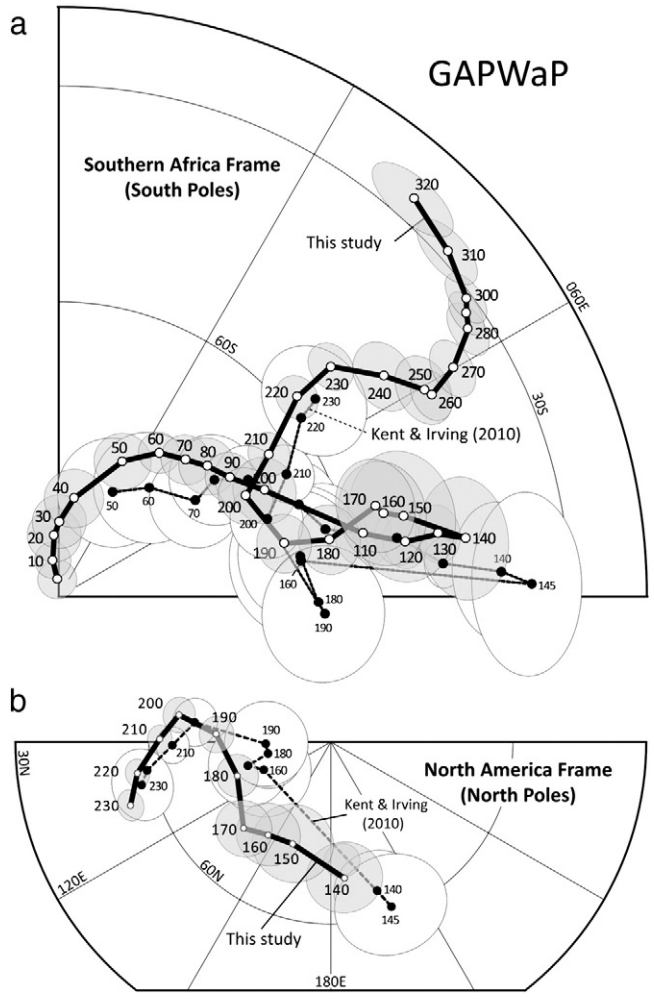

Fig. 14. (a) Comparison of our new running mean GAPWaP (Fig. 13c) with that of Kent and Irving (2010) for the 50–230 Ma range. Mean South Poles are shown in Southern African co-ordinates as previous diagrams. (b) Same as (a) but shown as north poles in North American co-ordinates in the 320–140 Ma range (compare with Fig. 4 in Kent and Irving, 2010).

GCD between a pair of coeval poles from each of the two paths is $5.0 \pm 3.3°$ with the largest differences during Late Jurassic times (~16°). Correction for I-error leads to a markedly improved correlation of the two APWPs (Fig. 13a, inset diagram), most notably for the Permian section of the APWPs (see also Domeier et al., 2012).

Our new GAPWaP, combining *five hundred* Laurussia/Laurasia and Gondwana poles, is shown in Fig. 13b. This is a running mean path that is also compared with the same path using uncorrected poles from detrital sediments (stippled line). We also compare our new running mean GAPWaP with a moderately smoothed spline path (Fig. 13c). Owing to the now large number of input poles (and no large age gaps), the running mean and spline paths are almost identical (GCD = $1.5 \pm 1.1°$). We therefore use the running mean GAPWaP in our further analysis because it can be easily reproduced by other workers. Conversely, when data-coverage is poor we prefer to use spline-derived APWPs. Our new running mean GAPWaP is also listed in North America, Europe, India, Australia and East Antarctica co-ordinates in Table 11.

In comparison to previously published GAPWaP's [Torsvik et al. (2008a) back to 320 Ma; Besse and Courtillot (2002) back to 200 Ma] our new compilation differs on average from those compilations by 3.9° (Torsvik et al., 2008a) and 2.6° (Besse and Courtillot, 2002). In Fig. 14 we compare our GAPWaP with a 230 to 50 Ma running mean path of Kent and Irving (2010). The Kent and Irving (2010) path (hereafter K&I) is constructed from volcanic rocks, and detrital sedimentary rocks, but the latter only when individual poles were corrected for I-errors using the E/I method of Tauxe and Kent (2004). The Triassic section (230–200 Ma) of the K&I GAPWaP compares well with our GAPWaP but the Jurassic 'spike' (Fig. 14a; note 190–140 Ma poles) seen in the K&I path differs strongly from our and all other published paths (e.g. Besse and Courtillot, 2002). The K&I GAPWaP differs on average $4.1 \pm 2.6°$ from ours with a peak deviation of 10.4° at 160 Ma. In Fig. 14b we also compare these two paths in North American co-ordinates and all mean poles between 230 and 140 Ma are also plotted as North poles (as in Fig. 6 in Kent and Irving, 2010). In the K&I path there is 12° of APW between 200 and 190 Ma (1.2°/M.y.) and 30° of APW between 160 and 145 Ma that amounts to 2°/M.y. The 190–160 Ma section of the K&I GAPWaP is also characterised by a near still-stand in APW (Fig. 14b). In contrast, our GAPWaP's show a smooth path from 200 to 140 Ma. These differences arise mainly from the low number of input poles used by K&I. As an example, their 160 Ma mean pole is based on only four poles, one from North America, one from Australia and two Patagonian poles. Conversely, our mean pole is derived from 19 poles (including the four input poles used by K&I) from six different continents (Table 1). We also use different reconstruction parameters (most notably for Patagonia).

6. Palaeogeography and plate speeds

In this section we calculate latitudinal drift-velocities and angular rotation rates (Figs. 15–16) and present ten new reconstructions in 50 million year intervals from 500 to 50 Ma. We focus on the location and evolution of Gondwana, Laurentia and Baltica and their joint fusions into Laurussia, Laurasia and Pangaea. Palaeozoic reconstructions (Figs. 17–19) largely follow Torsvik et al. (1992, 1996), Torsvik (1998), McKerrow et al. (2000a,b), Cocks and Torsvik (2002, 2005, 2007, 2011), and Torsvik and Cocks (2004, 2009, 2011b, in press), but are refined and modified in accordance with our new APWPs. Pre-Pangaean maps and plate velocities are based on I-error corrected spherical spline paths from the various continental blocks, whilst maps for 300 Ma and younger are based on the running mean GAPWaP.

Our reconstructed maps are based on more than 300 time-dependent plate polygons (terrane boundaries), e.g. Cocks and Torsvik (2005, 2007, 2011) and seen in our Figs. 2, 4, 5 and 10, currently summarised in industry reports (e.g. Labails et al., 2009), but soon to be made public in digital form. The maps were generated with the open-source GPlates software (www.gplates.org; Boyden et al., 2011). They include some spreading centres and subduction zones, but for the Palaeozoic the geometry and even the polarity of subduction can be disputed. These tentative features should therefore be treated with caution.

6.1. Early Palaeozoic (Cambrian to Silurian)

The Palaeozoic was extraordinary in Earth history for several reasons, not only for the blossoming of complex life forms (Cambrian), dispersion of major taxa (Ordovician) and the catastrophic extinction at the end of the Palaeozoic, but also in terms of unique palaeogeographic conditions. The continents covered the globe from the tropics to southern polar latitudes. Greenhouse climates prevailed but were punctuated by Icehouse periods in the Late Ordovician (short-lived) and in the Permo-Carboniferous (Figs. 4, 15, and 16). Latitudinal mean mass-centres (independent of absolute or relative palaeolongitude) were calculated from our global maps (reconstructed polygons) at 10 M.y. intervals. The latitudinal continental mean mass-centre was located in polar latitudes throughout the early Palaeozoic (Fig. 4). Reconstructed polygons comprise the

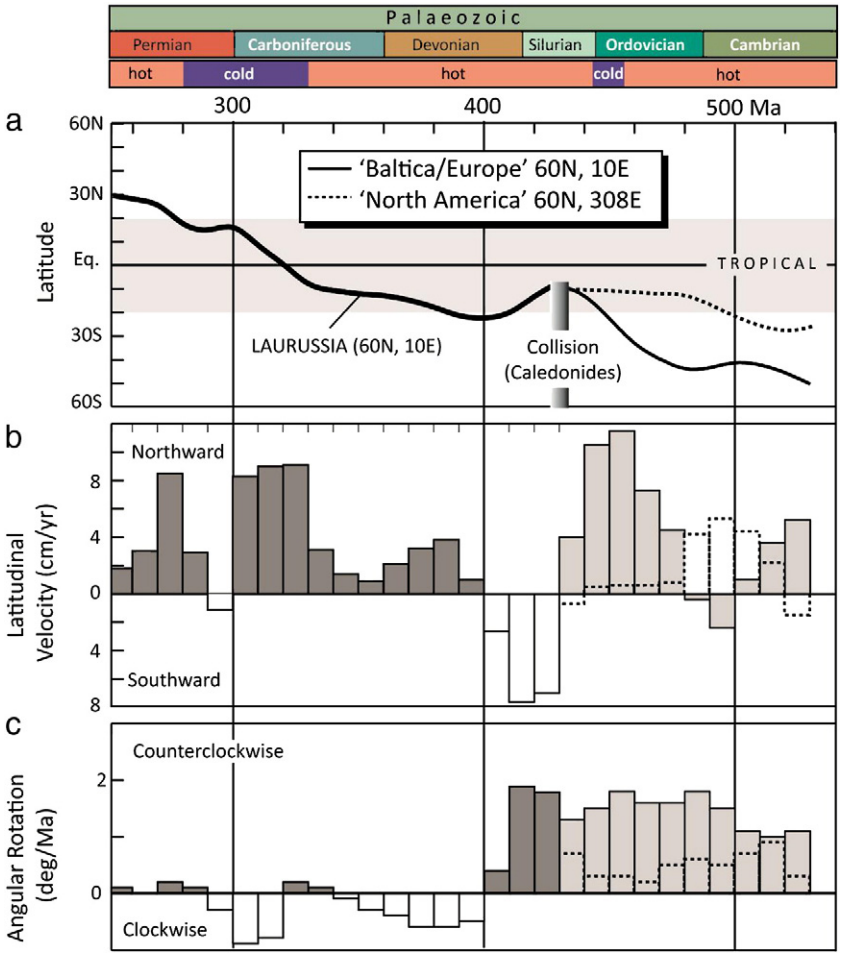

Fig. 15. (a) Palaeozoic latitudinal drift for a location in Europe (black curve, 60°N, 10°E) and North America (black stippled, 60°N, 308°E) based on Baltica/Stable Europe and Laurentia spline paths. (b) Latitudinal velocities for Europe (light grey shaded histograms) and North America (black stippled curve) separated into northward and southward (minimum velocities, because palaeo-longitude is 'unknown'). After 430 Ma, Baltica/Laurentia have been combined into Laurussia and calculations were based on 60°N, 10°E (in European reference frame), and histograms are shaded dark grey for northward motion and white for southward motion. (**c**) Angle of rotation of Europe, North America and Laurussia; colours in analogy to (b). Laurentia curves are rotated to European frame before calculations.

areal extent of continental lithosphere and their stretched continental margins through time. For the Phanerozoic, our global model of continents/extended margins amounts to 143–199×10^6 km^2 or ~28–39% of the Earth's total surface area.

Gondwana was the largest amalgamation, almost 100 million km^2 in size during the early Palaeozoic covering ~20% of the Earth's surface (see also Torsvik and Cocks, 2009; 2012, in press). In the Late Cambrian and Early Ordovician (Fig. 17), Gondwana stretched from the South Pole (northern Africa) to the equator (Australia). The pole-facing margin was fringed with peri-Gondwanan elements such as Avalonia, the Armorican Terrane Assemblage (ATA, e.g. Iberia and France) and many others that rifted from Gondwana at various times, and in the process generated vast Palaeozoic Oceans such as the Rheic (Fig. 17) and the Palaeotethys (Fig. 18). Fig. 16 shows the palaeo-latitude development, latitudinal drift-rates and rotations for a location in Central Africa. During the Cambrian, Central Africa drifted rapidly southward at rates as high as 10 cm/yr or more, which was associated with counterclockwise rotations as high as 2°/M.y. These values are significantly higher than those seen in the same time period for Baltica and Laurentia (Fig. 15). Central Africa remained at latitudes at around 40°S during most of Ordovician and Silurian times.

The Palaeozoic latitudinal drift and rotational history for Baltica (Stable Europe) and Laurentia (North America) for the given geographic location are shown in Fig. 15. Baltica was at intermediate to high southerly latitudes in the Late Cambrian, and almost geographically inverted. Between the Early Ordovician and Mid-Silurian, Baltica drifted towards the tropics, followed by southward drift after collision with Laurentia (Caledonian Orogeny and formation of Laurussia; Fig. 5). Latitudinal drift-rates are within plate tectonic 'speed limits' and always lower than 10 cm/yr. Baltica rotated counterclockwise (1–2°/M.y.) from Cambrian to Early Devonian times (~160° in total from 500 to 400 Ma); the destruction of the Iapetus Ocean (Harland and Gayer, 1972) was dominated by N–S closure and the long-lasting rotation of Baltica was probably accommodated by low-latitude Euler pole geometries (Torsvik, 1998, Fig. 8) that brought Baltica from high Cambrian/Early Ordovician latitudes to near equatorial latitudes by the Late Silurian (compare Figs. 17 and 5). After the Caledonian Orogeny there is a distinct decrease in the rate of rotation and the Devonian to Permian interval is characterised by minor, but systematic clockwise rotations, in the order of 0.5°/M.y. (Fig. 15).

Laurentia was located in equatorial to low southerly latitudes during most of the early Palaeozoic, and was separated from Baltica by the Iapetus Ocean. The Iapetus Ocean between Laurentia and Baltica (up to 3000 km wide) and the Avalonian sector of Gondwana (up to 5000 km wide) was at its widest in the Early Ordovician. Avalonia rifted from Gondwana in the Early Ordovician (Tremadocian), opening the Rheic Ocean in its wake (Cocks and Fortey, 2009), which reached a maximum width of 5000–5500 km during Late Ordovician to Mid-Silurian

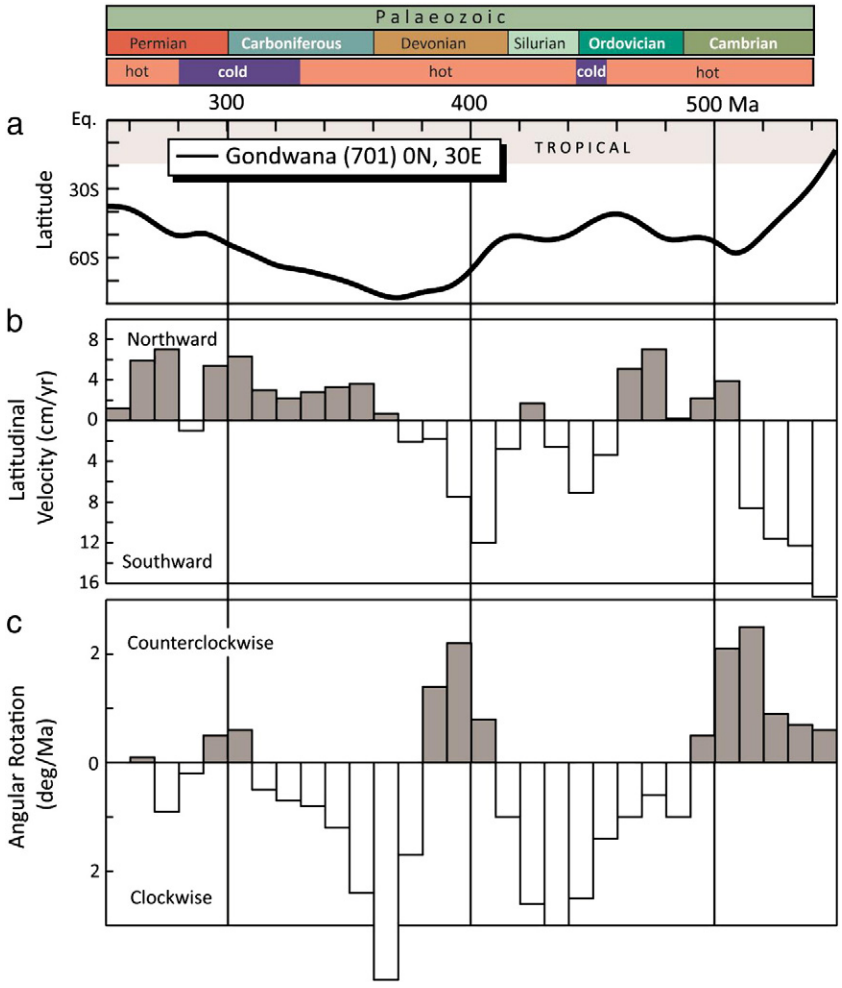

Fig. 16. (a) Gondwana Palaeozoic latitudinal drift for a location in Africa (0°, 30°E) based on the Gondwana spherical spline path in Fig. 11a (b) Latitudinal velocities separated into northward and southward. (c) Angle of rotation separated into clockwise and counter-clockwise rotations.

time. Avalonia and Baltica merged obliquely in a relatively soft docking near the Ordovician–Silurian boundary (~ 443 Ma), and thus Avalonia was only an independent terrane during Ordovician time (Torsvik and Rehnström, 2003). The end of the Ordovician was also marked by the short, but nevertheless intense Hirnantian glaciation (Fig. 17).

During the closure of the Iapetus Ocean, the rotating and northward moving Baltica (together with Avalonia) collided with a quasi-stationary Laurentia. Subsequently all these continents (Laurussia) drifted southward until ~400 Ma followed by systematic northward drift. Compared with our early to mid 1990s compilations (Torsvik et al., 1992, 1996; Gurnis and Torsvik, 1994), a previously noted velocity burst in the Late Silurian (as high as 20 cm/yr. for Laurentia), is no longer recognised in our improved data-sets (below 8 cm/yr in Fig. 15). Laurussia, including the loosely connected high Arctic, Ellesmere, Svalbard and Kara Terranes, covered a surface area of 37 million km^2.

6.2. Late Palaeozoic (Devonian to Permian)

The Rheic Ocean started to close during the Middle Silurian and by the Early Devonian (Fig. 17) the Amazonia–Laurussia segment of the Rheic was reduced to 750–1500 km (McKerrow et al., 2000a). Laurussia drifted to more southerly latitudes (Fig. 15) with plate speeds and rotations peaking at 10 cm/yr and 2°/M.y. respectively. By the Early Devonian, Laurussia stretched from the equator to almost 60°S whilst Gondwana was nearly centred on the South Pole. From Late Devonian times, Gondwana systematically drifted northward, accompanied by large clockwise rotations that peaked at ~360 Ma (>4°/M.y.).

The exact timing of separation between the Armorican Terrane Assemblage (ATA) and Gondwana during the opening of the Palaeotethys Ocean is poorly constrained. In our reconstruction at 400 Ma, we show a developing Palaeotethys Ocean and consider the initial onset of spreading to be of earliest Devonian age (Fig. 18). If the ATA is to reach a proximal Laurussian position by the Early Carboniferous, the opening of the Palaeotethys must have proceeded rapidly and was accompanied by sinistral displacement along the NW Gondwana margin. In this context, the Variscan Orogeny (particularly in the Sudetes area of Perunica) shows a tectono-metamorphic peak in the Early Carboniferous (~340 Ma; Lange et al., 2005). The Rheic Ocean was about 5000 km wide between ATA and Laurussia in the Early Devonian and reduced to near zero by the Early Carboniferous — this would require convergence rates in the order of 10 cm/yr.

By the Early Carboniferous, the entire segment of the Rheic Ocean was narrow. Laurussia rotated slowly clockwise and Siberia and Kazakh terranes were approaching each other (Fig. 18). The Variscan Orogeny waned in Late Carboniferous (end-Westphalian) times, when crustal shortening ceased after the amalgamation of Laurussia and Gondwana. By then, the bulk of Pangaea was already formed, centred on the equator and stretching from pole-to-pole by

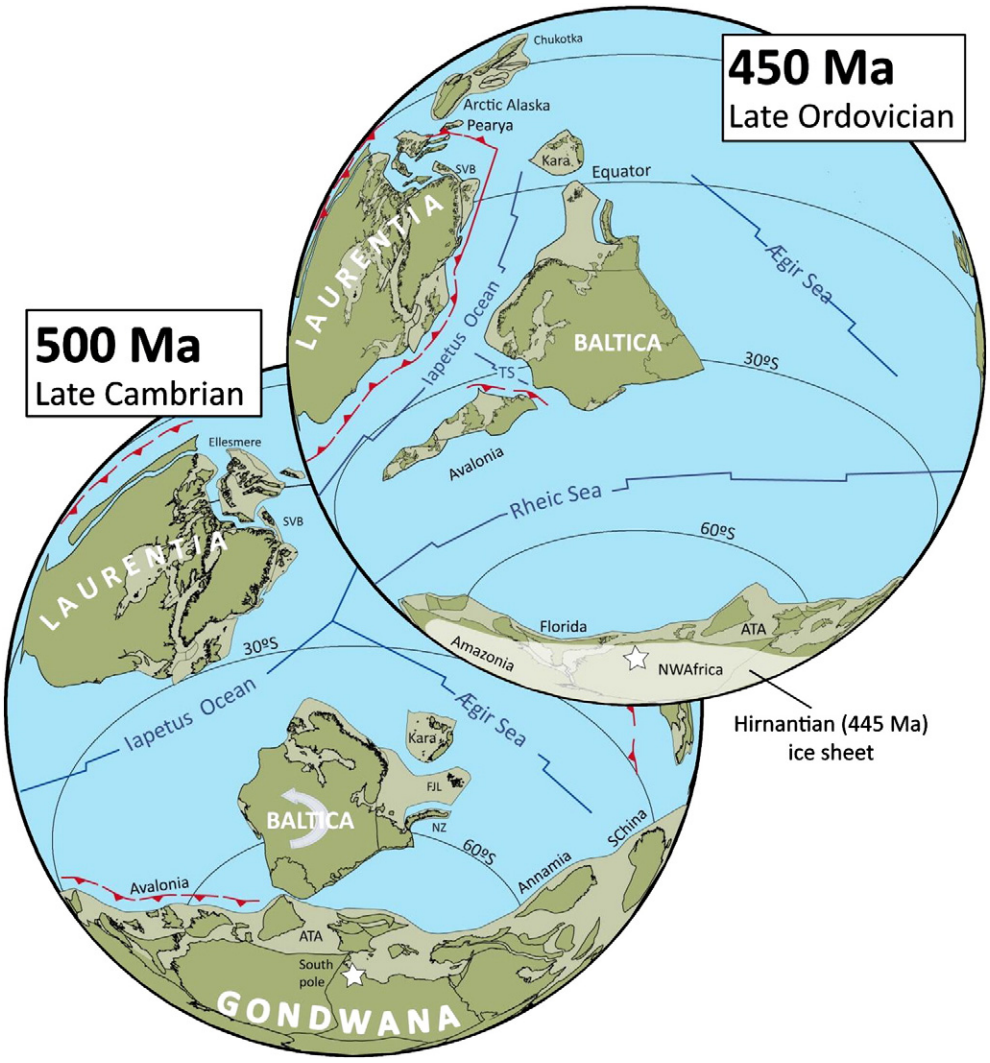

Fig. 17. Late Cambrian and Late Ordovician reconstructions in orthogonal projection. The major continents are described in the main text but on our Palaeozoic maps we also tentatively show Arctic Alaska. Our present tectonic model takes into account results of new studies (e.g., Oakey and Damaske, 2006; Dawes, 2009) that postulate minor to moderate strike–slip motion along the Nares Strait (between Greenland and the southernmost Ellesmere Island) during the opening of the Labrador Sea and Baffin Bay. SW Ellesmere, including Devon Island, is semi-locked to the Greenland plate, and the other Ellesmerian Terranes (four in total in our model) are kept semi-locked to North America, until the Early Tertiary Eurekan Orogenesis (that continued until 33 Ma) caused compression within the combined 'Greenland–SW Ellesmere–Arctic Canada' plate. Svalbard was composed of three or possibly four different terranes, here portrayed as two principal terranes, both of Laurentia affinity, which were later juxtaposed by sinistral strike–slip faulting and subsequently transferred to the European plate (Cocks and Torsvik, 2011).

the Late Permian (Fig. 19). Since the Late Devonian, Laurussia and Gondwana (Figs. 15–16) and later their fusion into Pangaea (from 320 Ma; Fig 20) have drifted almost systematically northward (Fig. 4). During the fairly long-lived and extensive Permo-Carboniferous glaciations in Gondwana (Fig. 19), the South Pole was located in southern Africa. We note that the Permo-Carboniferous glaciations are contemporaneous with Pangaea formation and the destruction of intervening gateways for oceanic circulation (such as the Rheic Ocean).

It should be emphasised that the paucity of Devonian and Early Carboniferous palaeomagnetic data is a global phenomena (Fig. 3; Table 1) and thus the initial phases of Pangaea formation are uncertain. The available data suggest an Early Carboniferous Pangaea B–C type configuration (Gondwana located 'east' of Laurussia; see Fig. 18) evolving into a Pangaea-A configuration during the Late Carboniferous (Domeier et al., 2012).

Siberia was already close to Laurussia by the Early Carboniferous (Fig. 18) along with many of the Kazakh terranes. The latter had mostly fused with Baltica/Laurussia by the Late Carboniferous (Uralides) but Siberia (Buiter and Torsvik, 2007; Cocks and Torsvik, 2007) and many smaller terranes such as Tarim were still evolving in terms of their relative position to Laurussia until the early Mesozoic (Van der Voo, 1993; Van der Voo et al., 2006; Abrajevitch et al., 2008).

Pangaea ('All Land') did not truly include all continental crust. For example, the North and South China Blocks were not part of Pangaea at any given time. Also during the Early Permian phase of Pangaea assembly, the Neotethys opened (Fig. 19), and Cimmerian terranes (Şengör et al., 1984) such as Lut, Helmand, Qiangtang (N Tibet) and Sibumasu drifted away from the northeast Gondwana margin. Pangaea achieved its maximum size during late Palaeozoic and early Mesozoic times, but the most important growth phase occurred during the Late Carboniferous when Gondwana, Laurussia and intervening terranes collided, and in the process produced the Hercynian Orogenic Belt in Western Europe (Matte, 2001; Torsvik and Cocks, 2004). We calculate a Pangaea size of 160 million km^2 at 250 Ma, i.e. 93% of all continental material (Siberia included) and ~30% of the Earth's surface.

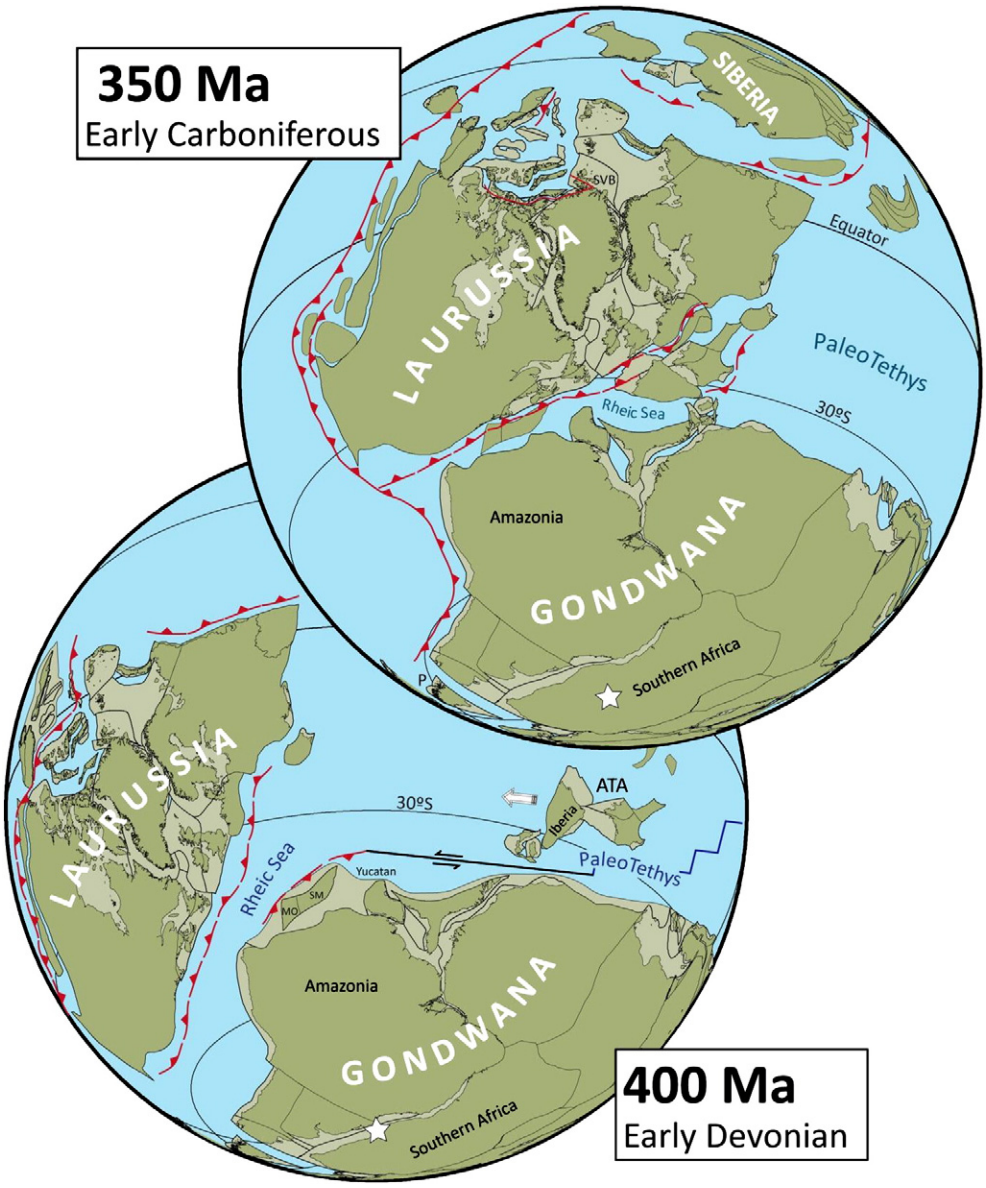

Fig. 18. Early Devonian and Early Carboniferous (poor data coverage, see Fig. 3) reconstructions. Orthogonal Projection.

6.3. Mesozoic and Early Cenozoic (Triassic to Palaeogene)

The Mesozoic is a remarkable story about Pangaea dispersal, and in fact Pangaea is the only supercontinent in Earth's history that can be modelled with some, if any, confidence. In this section all of our analysis is based on the GAPWaP, southern Africa is the reference plate and all other continents are modelled according to their position in the plate circuit hierarchy. Pangaea and post-Pangaea (i.e. Africa) evolution (modelled for a Central African location in Fig. 20) is mostly characterised by northward drift (typically around 2–4 cm/yr) and slow angular rotations (typically less than 1°/M.y.). Pangaea's (= ~Africa's) northward drift, however, appears to be almost 8 cm/yr between 210 and 220 Ma, some of which (~2 cm/yr) can be related to TPW (Section 7). Throughout the Mesozoic, the latitudinal continental mean mass-centre was located in tropical latitudes (Fig. 4). In Palaeogene times, however, at around 50 Ma, there is a marked transition with the mean mass-centre migrating towards northern latitudes; this pronounced global shift is associated with a global transition to Icehouse climate conditions (Fig. 4).

Perhaps the most dynamic phase of Pangaea break-up occurred during (and shortly after) the emplacement of the Central Atlantic Magmatic Province (CAMP) (200 Ma, e.g. Deenen et al., 2010) and the subsequent opening of the Central Atlantic Ocean at ~195 Ma (Labails et al., 2010). The emplacement of CAMP probably resulted in the break-up of Pangaea, manifested as the separation of Laurasia and Gondwana and accompanied by the initial fragmentation of long-lived Gondwana (Figs. 4 and 21).

The most important step after initial Pangaea rifting is the Jurassic separation of West (e.g. Africa and South America) and East Gondwana (e.g. Madagascar, India, East Antarctica and Australia). The exact timing of seafloor spreading initiation is uncertain, prolonged extension took place in late Palaeozoic and early Mesozoic times, break-up may have occurred as early as 180–177 Ma, with the first identifiable magnetic anomaly M25 (~155 Ma) in the oceanic crust of the Somali (Eagles and König, 2008) and Mozambique Basins (König and Jokat, 2010) (Fig. 21). The Mesozoic evolution of the Neo- and Palaeotethys is not detailed here, but the China blocks probably fused with Asia (Laurasia) in Late Jurassic to Early Cretaceous time and thus *after* the initial rifting of Pangaea.

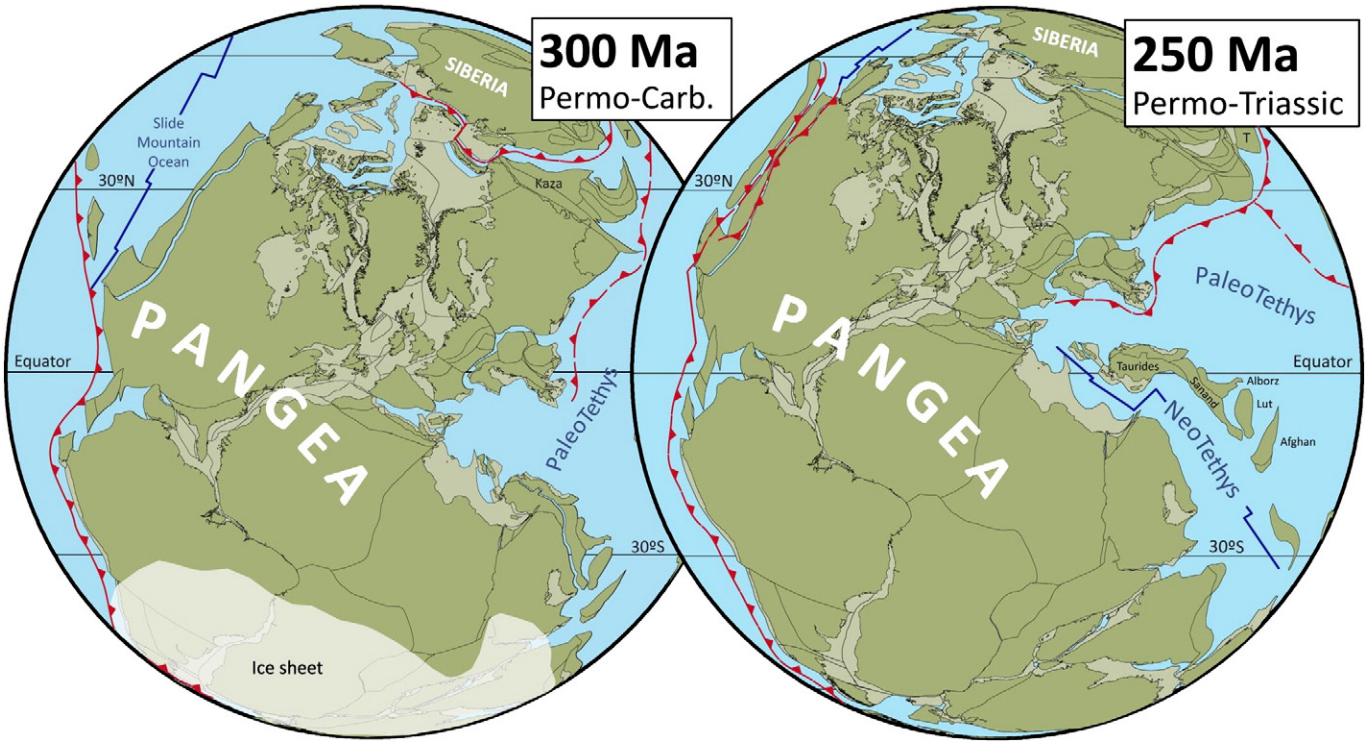

Fig. 19. Late Carboniferous/Early Permian and Late Permian/Early Triassic reconstructions. Orthogonal Projection. Permo-Carboniferous ice-sheet after Torsvik and Cocks (2004).

In West Gondwana, the South Atlantic opened at around 130 Ma, starting in the south and at 100 Ma (Fig. 22) there was a full oceanic connection with the Central Atlantic (Torsvik et al., 2009). During the earliest opening of the South Atlantic, seafloor spreading between Madagascar and Africa (Somalia) ceased (Eagles and König, 2008). At ~130 Ma, seafloor spreading was initiated between East Antarctica and India (Gaina et al., 2007), and at the same time, India broke off from Australia (Mihut and Müller, 1998; Heine et al., 2004; Torsvik et al., 2008c). At around 85 Ma, India and the Seychelles drifted off Madagascar following thermal upwelling associated with the Marion hotspot (e.g. Storey et al., 1995; Torsvik et al., 2000; Meert and Tamrat, 2006).

Fifty million years ago (Fig. 22), the promontory of India (extended continental crust separated from the Indian subcontinent by oceanic basins; van Hinsbergen et al., 2012) collided with Eurasia. India had separated from the Seychelles at ~62 Ma (Ganerød et al., 2011) shortly after the Deccan magmatic event (65 Ma). During break-up India attained velocities of up to 18 cm/yr. This is the highest velocity

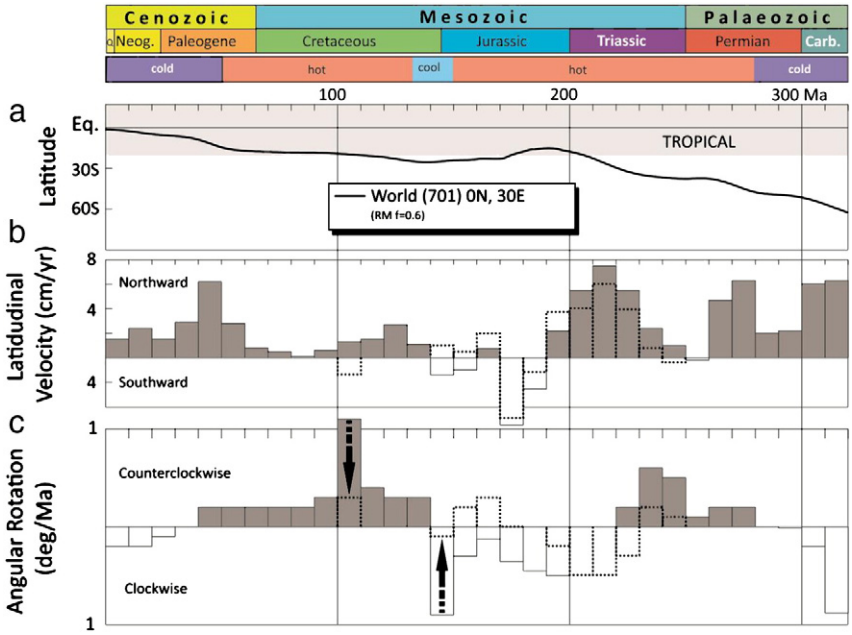

Fig. 20. (a) Latitudinal drift for a location in Africa (0°, 30°E) based on the GAPWaP (running mean path with I-error correction, Fig. 14a. (b) Latitudinal velocities separated into northward and southward drift. (c) Angle of rotation separated into clockwise (CW) and counterclockwise (CCW) rotations. Stippled lines in (b, c) between 250 and 100 Ma after correction for TPW with two black arrows demonstrating the large reduction in angular rotation after TPW correction.

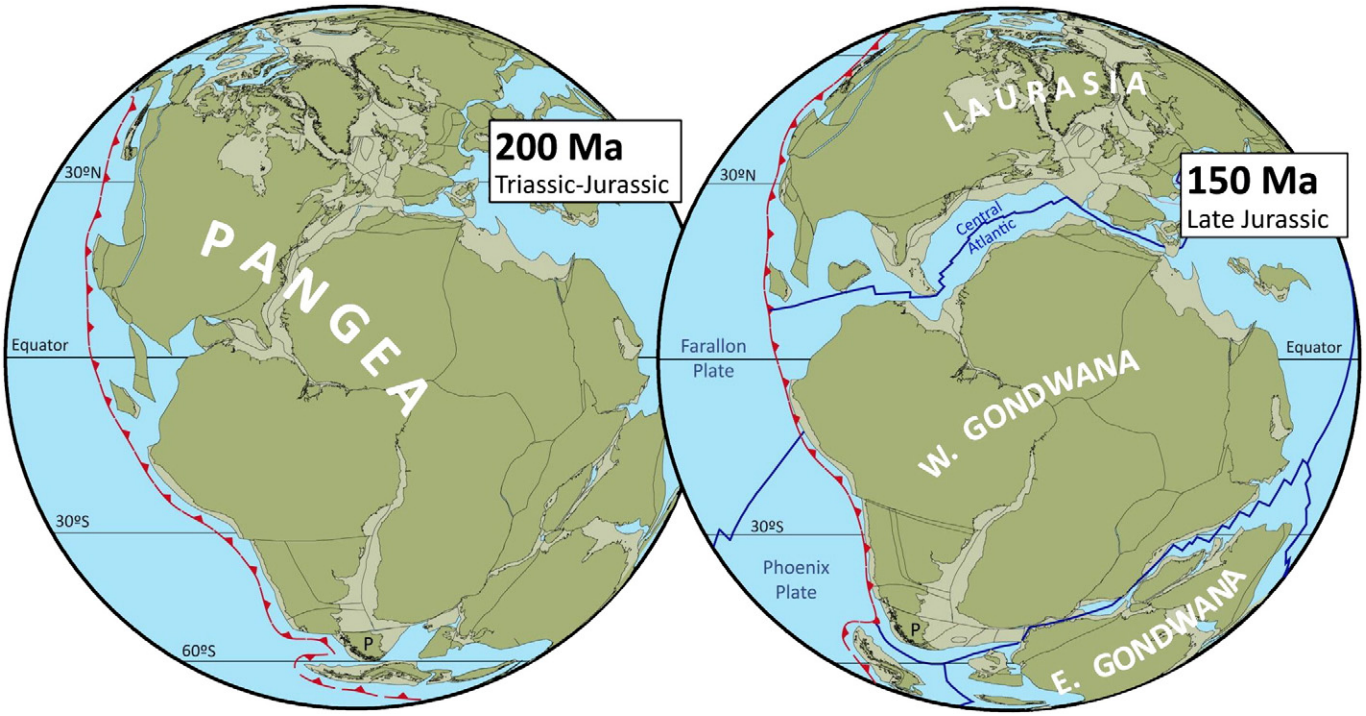

Fig. 21. Late Triassic/Early Jurassic and Late Jurassic reconstructions in orthogonal projection.

recorded for any continental plate in Mesozoic and Cenozoic times, and was propelled by thermal buoyancy of the Reunion hot spot (Cande and Stegman, 2011; van Hinsbergen et al., 2011).

In the North Atlantic, seafloor spreading was underway in the Labrador Sea (starting at ~67 Ma and stopping at ~33 Ma), the Norwegian–Greenland Sea (started at ~54 Ma;) and the Eurasian Basin in the Arctic (started at ~55 Ma) (Chalmers and Laursen, 1995; Gaina et al., 2002, 2009; Mosar et al., 2002). Seafloor spreading between Greenland and Europe was associated with vast Large Igneous Province (LIP) activity, the North Atlantic Igneous Province (e.g., Ganerød et al., 2010). Gateways from pole-to-pole across the central part of the former Pangaean continent from ~50 Ma may have paved the way for the cold global climate (Fig. 4) since then, and the first known bipolar glaciations in Earth history (e.g., Tripati et al., 2005).

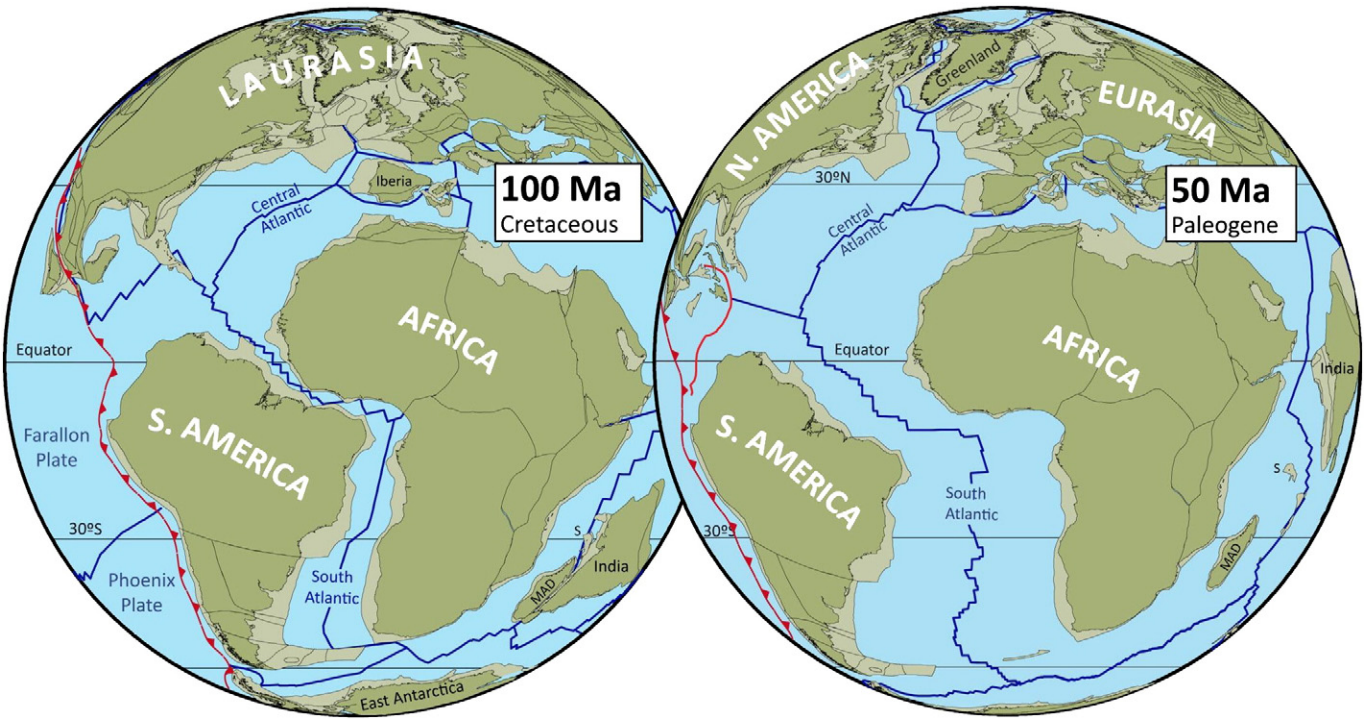

Fig. 22. Cretaceous and Palaeogene reconstructions in orthogonal projection.

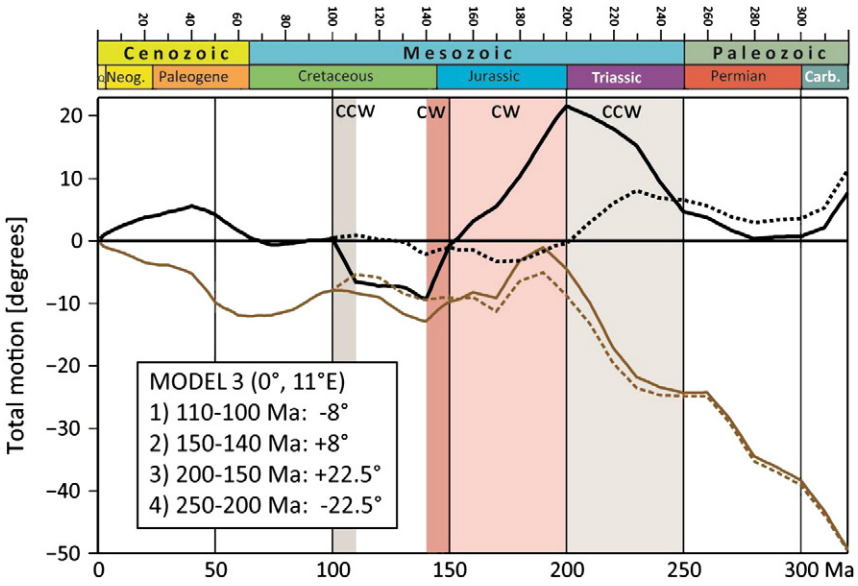

Fig. 23. Cumulative rotation and north–south motion averaged for 'all' continents based on the GAPWaP. Solid black line shows rotation around an equatorial axis at the same longitude as the centre of mass of 'all' continents (green dots in Fig. 24), and positive values for a given time correspond to clockwise (CW) rotation since that time. Solid brown line shows rotation around an equatorial axis orthogonal to the first axis; negative values for a given time correspond to northward motion of continents since that time. Stippled lines are in a new reference frame, similar to the palaeomagnetic one, except that rotations (listed in the inset box) around an equatorial axis (0°, 11°E) at constant rate have been subtracted from the African plate motion.

7. True Polar Wander (TPW)

APWPs record a combined signal from the two sources of absolute motion: motion of lithospheric plates relative to the Earth's mantle ("continental drift") and the rotation of the entire solid Earth with respect to the spin axis. The latter component, commonly referred to as TPW, arises from the gradual redistribution of density heterogeneities within the mantle and corresponding changes in the planetary moment of inertia (Goldreich and Toomre, 1969; Steinberger and Torsvik, 2010). To establish the magnitude of TPW with confidence, the absolute velocity field and the plate geometry for both continental and oceanic lithosphere are required as well as a robust set of palaeomagnetic data. This is difficult for pre-Cretaceous time because no useful connection exists for reconstructing the motion of oceanic plates in the Pacific domain prior to ~84 Ma (e.g., Doubrovine and Tarduno, 2008a,b). Furthermore, APWPs for the Pacific plate are not considered reliable given the limited quality of Pacific palaeomagnetic poles (see Torsvik et al., 2002; Cottrell and Tarduno, 2003; Tarduno, 2007 for discussion). Estimates of the relative magnitude of TPW should therefore rely on continental palaeomagnetic data.

In spite of these difficulties, we attempt to determine the magnitude of TPW by extracting the coherent (mean) rotation of all the continents around their common centre of mass in the palaeomagnetic reference frame, an approach taken and tested by Marcano et al. (1999) for Pangaea in Permian and Triassic time. The rationale for this approach is that a common rotation of all continents is more easily explained, if it occurs *jointly* with the underlying mantle (TPW) rather than *relative to* it. A rotation of all continents corresponds to a large toroidal component of plate motion, and it has been suggested that convection with surface plates tends towards a state that minimises the toroidal (strike–slip and plate spin)-poloidal (convergence and divergence) ratio (O'Connell et al., 1991). Hence episodes of large toroidal power are not expected to be associated with 'continental drift', and we therefore argue that coherent rotations of very large plates are more likely due to TPW.

The motion of the centre of mass of all continents could be either due to TPW or plate motion relative to the mantle. Northward and southward motion can be determined in the palaeomagnetic frame. In order to assign the eastward or westward component of motion an additional assumption is made that the axis of finite rotation for the *African* plate in the palaeomagnetic reference frame always remains on the equator. We can refer to this as the quasi-stationary African assumption whereby Africa does not substantially move eastward or westward. While this choice of the African plate as a "reference plate" is somewhat arbitrary, we argue that this assumption is reasonable (Torsvik et al., 2008b). Based on the quasi-stationary African assumption, it is found that the longitude of the centre of mass of all continents, as well as its antipode, remained close to the longitudes of the centre of masses of the African and Pacific Large Low Shear-wave Velocity Provinces (LLSVPs), respectively. These LLSVPs are associated with large-scale geoid highs, dominated by degree two terms of the spherical harmonic expansion of the Earth's gravity potential (Hager, 1984; Burke et al., 2008). Both the LLSVP's and their inherently associated geoid highs are expected to have remained stable for at least 300 M.y. (Burke and Torsvik, 2004; Torsvik et al., 2006, 2010a). This is based on the observation that most reconstructed LIPs and kimberlites since Pangaea assembly are sourced by plumes from the edges of the LLSVPs, and thus these must have remained stationary since then. TPW is by definition a rotation about an equatorial axis. Additionally, because the maximum of the degree two geoid corresponds to the axis of minimum moment of inertia it should remain at the equator during TPW. Given that the centre of mass of continents and the African LLSVP (and corresponding geoid highs) are at similar longitudes, we regard it as unlikely that northward or southward motions of the centre of mass of all continents are due to TPW and therefore interpret all such motion as continental drift relative to the mantle. In contrast, a rotation of all continents around their common centre of mass (located on the equator) corresponds to a large toroidal component of plate motion and most likely represents TPW.

7.1. TPW since Pangaea assembly

To define the magnitude of TPW, we follow the method developed by Steinberger and Torsvik (2008) (see Appendix 1 for details). Based on the motion of continents in the palaeomagnetic frame, evaluated on a 1° grid, both the coherent rotation of all continents

around an equatorial axis at the same longitude as their centre of mass (interpreted as largely due to TPW) and around an equatorial axis at 90° from the first one (interpreted as mostly continental drift) are determined. Episodes of CW and CCW TPW thus determined (from the brown continuous line in Fig. 23) are similar to those presented by Steinberger and Torsvik (2008). Differences are due to updates in (1) the African absolute plate motion in the palaeomagnetic reference frame, i.e. the African APWP, (2) relative plate motions and (3) plate geometry.

Interpretation of the cumulative rotation of all continents about their centre of mass (Fig. 23) suggests four episodes of TPW: (1) a CCW rotation in the time interval 250–200 Ma followed by (2) the same amount of CW rotation between 200 and 150 Ma, (3) a CW rotation during the 150–140 Ma interval, and (4) a rotation with a similar magnitude but in opposite sense (CCW) between 110 and 100 Ma. The latter rotation is consistent with the Early Cretaceous episode of TPW suggested by a comparison of the motion of Africa in palaeomagnetic and hotspot reference frames (e.g., Besse and

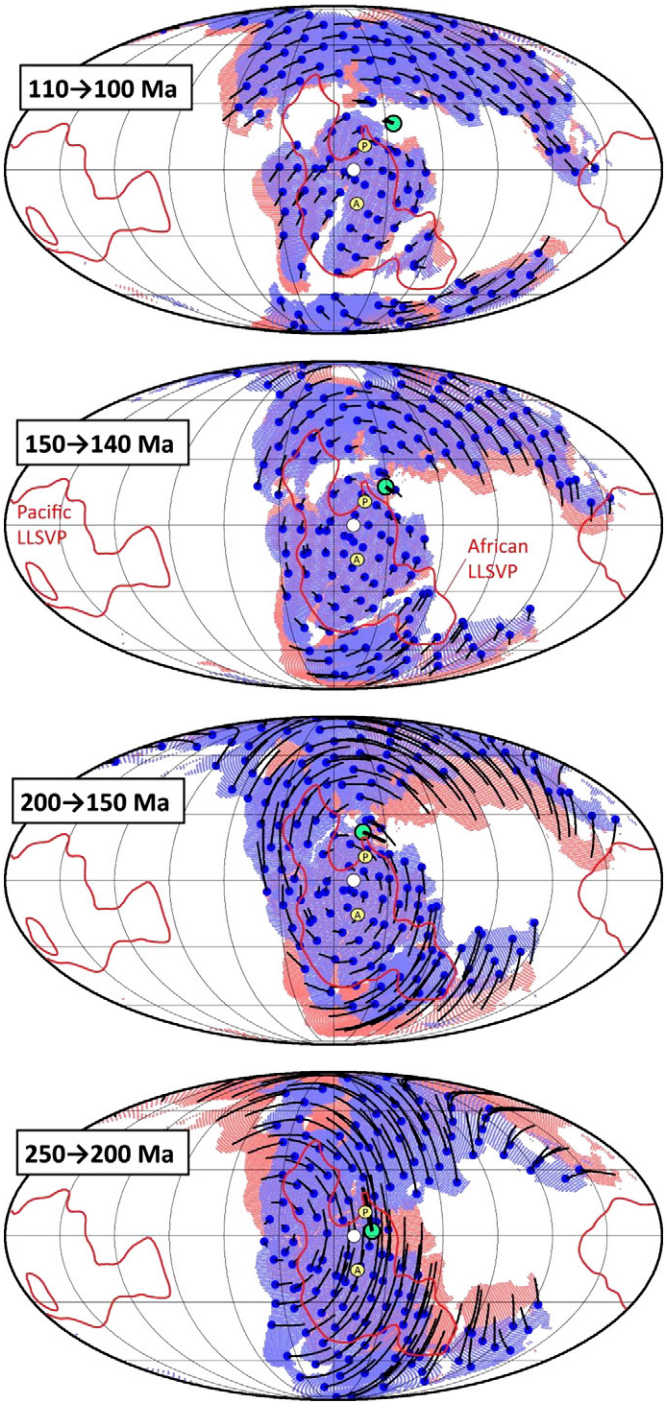

Fig. 24. Motions of continents reconstructed in the palaeomagnetic reference frame during four time intervals. Total motions are shown as black lines, connected to blue dots (locations at the beginning of the time intervals). Large green dots with thick black lines indicate location and motion of the centre of mass of 'all' continents. Eurasia is here shown for reasons of simplicity as a coherent plate, but at the time of the lowermost diagram, for example, north and south China were in reality not part of Eurasia/Pangaea. Yellow dots marked A and P are the centres of mass for the African and the near antipodal Pacific LLSVPs (outlines above core–mantle boundary shown in red, based on the SMEAN tomography model of Becker and Boschi (2002)) (see text). Open white circle is the preferred centre for TPW. Blue and pink shading represent reconstruction at the start and at the end of the TPW episode.

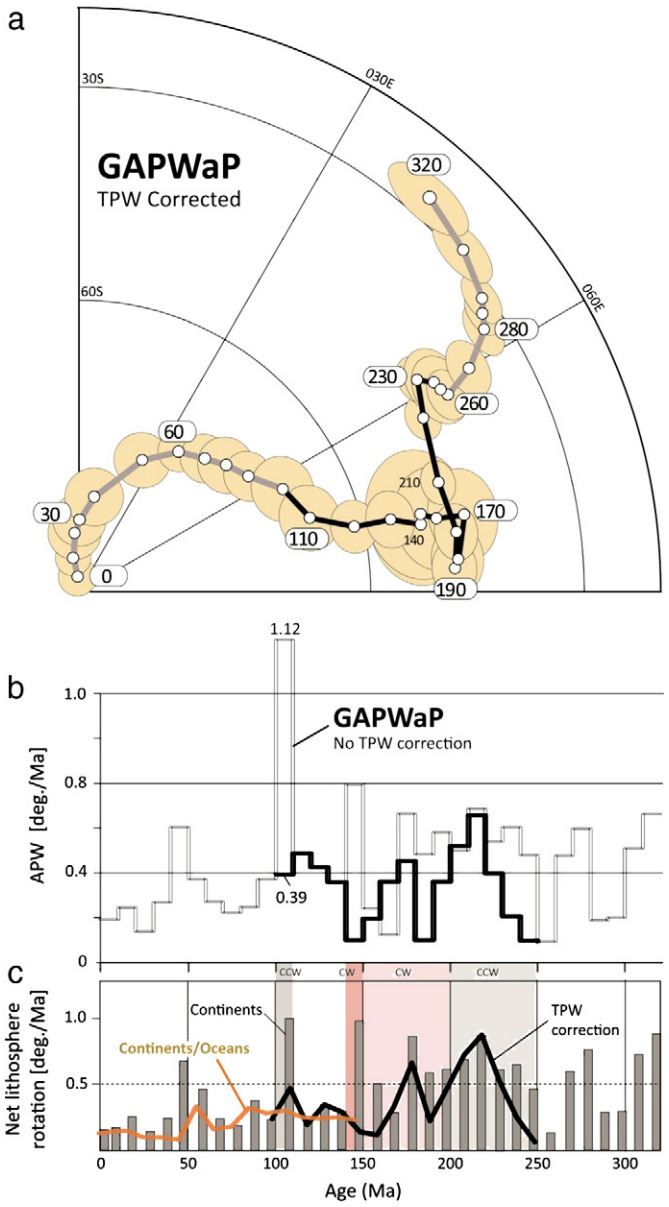

Fig. 25. (a) Southern Africa GAPWaP (Fig. 14a) corrected for TPW 250–100 Ma (black line). (b) APW (10 Myr bins) before (black double line) and after TPW correction (black thick line). The most dramatic change occurs between 110 and 100 Ma although this segment is not seen as a cusp/bend in the APWP in (a). (c) Net lithosphere rotation (NR) for continents before (dark grey bars) and after TPW correction (thick black line). A more appropriate treatment of NR, calculated from both continental and oceanic lithosphere for the past 150 Myr (Torsvik et al., 2010a), is shown as thick brown line. Episodes of clockwise (CW) and counter-clockwise (CCW) TPW are shaded.

Courtillot, 2002; Torsvik et al., 2008a; Steinberger and Torsvik, 2010).

Fig. 24 shows that the continental motion in these time intervals is indeed largely a coherent rotation around an equatorial axis: (1) 250–200 Ma at longitude 32.3°W, (2) 200–150 Ma at longitude 5.1°E, (3) 150–140 Ma at longitude 11.3°E, and (4) 110–100 Ma at longitude 17.1°E. In the last three time intervals (after 200 Ma), the axis of this coherent rotation is at a longitude similar to the centre of mass of all continents, which is also at a similar longitude as the centre of mass of the African LLSVP and the antipode of the Pacific LLSVP. Longitudes of the centre of mass of continents and the axis of coherent rotation depend on the reference frame used. In a hotspot reference frame (Steinberger et al., 2004; O'Neill et al., 2005) they would be 5 to 9° further west, in a slab-fitting reference frame (van der Meer et al., 2010) they would be placed 8 to 18° further west. Nonetheless, they would remain close to the LLSVP (antipodal) centres of mass. The one exception is for the time interval from 250 to 200 Ma where the axis of rotation is displaced substantially further west. This may indicate a distinct TPW axis, but it may also represent a superposition of (1) a rotation around a similar axis as for the later episodes, that we consider to be due to TPW, and (2) a northward motion of the continents, at that time still assembled in Pangaea, relative to the mantle. This northward motion would be at similar speeds as during the time interval 320–250 Ma, for which no TPW was inferred. Here we prefer the second interpretation, and leave the axis of TPW rotation at a constant equatorial location of 11°E (Table 12), close to the centre of mass of the African LLSVP (15.6°S, 13°E) as well as its antipode at the Pacific LLSVP (11°S, 197.1°E) (Burke et al., 2008). This corresponds to the minimum moment of inertia axis for both LLSVPs at 2.7°S, 11.9°E (Steinberger and Torsvik, 2010) and the long-term geoid high and the geotectonic bipolarity axis at 0°N, 10°E (Pavoni, 1985). This conceptually simple model should be regarded as an approximation. The orientation of the minimum moment of inertia axis of the Earth (and hence TPW) is mainly controlled by LLSVPs, but its position may change through time due to mass variations from subducted slabs and rising plume heads. As an example, the present-day minimum moment of inertia for the geoid is located at 15°W (Steinberger and Torsvik, 2010).

As a consequence of the above, we modify our plate motion model by subtracting the inferred TPW from the African plate motion relative to the spin axis (i.e. the motion in the palaeomagnetic reference frame). In our simple model, we apply four subsequent stage rotations about the equatorial axis at 11°E, with the magnitudes (rotation angles) listed in Table 12. If the assumption of the zero longitude motion for Africa is valid, the resulting TPW-corrected rotations describe the motion of Africa in an absolute reference frame fixed with respect to the entire solid Earth (i.e., relative to the Earth's mantle). We then re-calculate the stage and finite rotations of all plates with the same relative plate motions and recompute the mean continental coherent rotations in the TPW-corrected reference frame. The results are shown by the dotted lines in Fig. 23. As expected, coherent rotations around the centre of mass of the continents were substantially reduced. What remains is a strong northward motion of all the continents prior to about 190 Ma. If we had adopted an axis of TPW rotation further west in the initial time interval, the resulting northward motion would be much less and the coherent rotation would remain small. It will require further study and geodynamic modelling to determine whether such a rapid northward motion of Pangaea (~6 cm/yr) is geodynamically reasonable, or whether there are reasons to assume that the degree-two geoid high and TPW axis of rotation were located further west.

7.2. TPW: influence on APW rates and net lithosphere rotation

TPW rates are on the order of 0.45–0.8°/M.y. but cumulative TPW since the Late Carboniferous is close to zero. Fig. 25a (Table 13) shows the TPW-corrected GAPWaP by simply adding the Euler rotations listed in Table 12 (but with opposite sign of rotation). Cumulative APW before correction amounts to 139° for the past 320 M.y. with a mean APW rate of 0.44 ± 0.23°/M.y. (Fig. 25b). This is reduced to 110° and 0.34 ± 0.18°/M.y. after TPW correction (Fig. 25b), i.e. ~20% reduction for the past 320 million years but 37% over the time range (250–100 Ma) actually adjusted for TPW. TPW correction reduces APW rates, and most notably between 110 and 100 Ma where the APW rate is reduced from 1.2 to 0.39°/M.y. This is also readily observed in angular rotations for a Central African location (Fig. 20c), which for the past 310 M.y. never exceeded 0.5°/M.y. after TPW correction (see reduction in peaks between 100–110 Ma and 140–

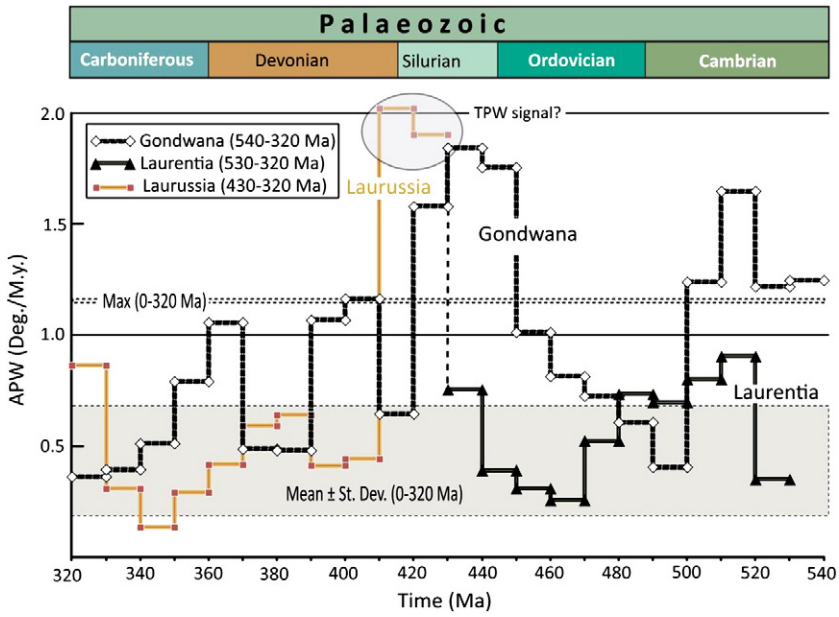

Fig. 26. APW rates for Gondwana and Laurussia from 320 Ma and older. Laurussia from 320 to 430 Ma and before that is only based on Laurentia. Typical rates since Pangaea assembly are shown as grey shading (mean and standard deviation) and a black stippled double line (maximum). St.Dev., standard deviation.

Table 1
Global palaeomagnetic compilation. Q = Quality Factor (Van der Voo, 1990, 1993); α_{95} = 95% confidence oval (or A95 if bold and underlined); Com = Comments: I = Inclination corrected using the inclination–elongation (I/E) method of Tauxe and Kent (2004) or the anisotropy of magnetic susceptibility information (Kodama, 2009) [I**, I/E corrected]; # = corrected for counterclockwise Colorado Plateau rotation of 5.4° (Bryan and Gordon, 1990). Lat/Lon = Pole Latitude/Longitude; CLat/CLon = Pole Latitude/Longitude corrected for inclination shallowing with f = 0.6 (only for clastic sediments); Rlat/Rlon = Pole rotated to Southern Africa frame; EULER = Rotation latitude, longitude and angle; Age in Ma; GPDB RefNo/Reference = T = Listed in Torsvik et al. (2008a); TV = Listed in Torsvik and Van der Voo (2002); T96 = Listed in Torsvik et al. (1996). Note that numerically assigned pole ages can differ substantially from original sources or the GPDB due to different time-scales (if stratigraphically dated; in this paper we use Gradstein et al., 2004) or new isotopic ages.

Q	α_{95}	Com	Formation	Lat	Lon	CLat	CLon	RLat	RLon	EULER	Age	GPDB RefNo/Reference
			Laurussia									
			North America (101)									
5	4.8		USGS SW North America composite	−86.3	5.7						0.5	Mankinen (2008)
5	9.1		Michoacan Guanajuato volcanic field	−86.4	8.4			−86.4	9.2	(79.2/23/.2)	0.8	Maciel Peña et al. (2009)
5	7.1		Tequila volcanic fields	−85.3	265.9			−85.3	−94.1	(79.9/22.7/.3)	1	Ceja et al. (2006)
5	**8.7**		Meseta Lago Buenos Aires	−88.4	225.5			−88.4	−135.7	(79.9/22.7/.3)	1	Brown et al. (2004)
5	4.3		Trans Mexican Volcanic Belt	−88.9	285			−88.9	−75.1	(79.9/22.7/.3)	1	Ruiz-Martínez et al., 2010
3	4.9		Katherine Creek sediments	−77.9	303.7	−80	3.5	−80	4.2	(80.8/22.8/.4)	1.5	3060, T
3	7		Banks Island deposits	−85.7	122.7	−81.2	73.9	−81.1	74.5	(80.8/22.8/.4)	1.5	3206, T
5	5.7		USGS SW North America composite	−84.5	241			−84.5	−119.1	(80.8/22.8/.4)	1.5	Mankinen (2008)
5	6.2		Trans-Mexican Volcanic Belt	−89.5	214.8			−89.5	−157.9	(80.8/22.9/.8)	3	Mejia et al. (2005)
5	4.1		Trans Mexican Volcanic Belt	−84.6	332.3			−84.8	−25.6	(80.9/22.8/1)	4	Ruiz-Martínez et al. (2010)
5	6.7		Eastern Alkaline Province	−87.9	275.9			−88	−84.4	(80.9/22.8/1)	4	Goguitchaichvili et al. (2007)
5	5		Snake River Plain	−85.5	197.4			−85.5	−163.9	(80.9/22.8/1.3)	5	Tauxe et al. (2004)
5	5		USGS SW North America composite	−85.3	262.1			−85.5	−97.9	(80.9/22.8/1.8)	7	Mankinen (2008)
5	6.9		Trans Mexican Volcanic Belt	−85.9	357.7			−86	3.9	(80.9/22.8/2)	8	Ruiz-Martínez et al. (2010)
5	7.8		USGS SW North America composite	−82.9	309.1			−83.3	−47.3	(80.9/22.9/2.6)	10	Mankinen (2008)
3	12.9		Hepburn's Mesa Formation	−81.1	225.3	−83.1	93.2	−82.4	98.8	(80.9/23.2/4.2)	15.5	2288, T
5	3.7		Stoddard Mountain laccolith	−82.9	346.2			−83.5	−1.3	(80.3/25.4/5.8)	21	Petronis et al. (2004)
5	9.8		Dinan Bay lavas	−82.7	301.7			−83.7	−51	(80.2/26/6)	21.7	Irving et al. (2000)
4	6.7		Younger plutons	−87.1	189.5			−86.7	177.4	(80/26.6/6.2)	22.5	1402, T
3	8.4		Lake City Caldera	−76.4	30.3			−76.2	41	(79.9/26.9/6.3)	23	1300, T
4	5.2		Latir volcanics	−80.9	331.2			−81.8	−17.8	(79.8/27.3/6.4)	23.5	1299, T
4	6.8		Conejos and Hinsdale Formation	−79.7	342.8			−80.5	−4.3	(79.3/27.5/7.1)	26	3130, T
4	5.4		Latir extrusives, sediments	−80.2	315.4			−81.4	−32.9	(78.8/22.7/7.5)	27	1299, T
3	5		Mongollon–Datil volcanics	−82.8	316.2			−84.2	−24	(77.4/12.5/8.6)	30	2631, T
4	4.4		Mongollon–Datil volcanics	−81.9	323.6			−83.1	−16.9	(77.4/12.5/8.6)	30	1315, T
6	6.2		Tuzantlán–Copalillo basin	−80.6	22.1			−79.5	43.5	(76/6.1/9.7)	33	Molina-Garza and Ortega-Rivera (2006)
4	4.3		Mariscal Mountain Gabbro	−79.8	5.9			−78.9	31.9	(74.9/1.4/11.4)	37	2943, T
5	7		Ramsay Island lavas	−78.2	297.5			−80.7	−40.3	(74.5/.1/12)	38.5	Irving et al. (2000)
3	2.4		Mistastin Lake Impact	−85.2	296.6			−87.2	−9.1	(74.5/−1.1/12.6)	40	562, T
6	3		Beaver River alkalic complex	−79.2	326.4			−80.1	−1.7	(74.4/−2.5/13.4)	42	Symons et al. (2003)
5	7.7		East Fork Washakia Basin	−83.7	323.7	−76.7	50.4	−73.2	70.3	(74.3/−3.7/14.2)	44	1632, T
5	8		Absaroka flows	−82.7	333.6			−82.6	19.8	(74.2/−4.9/15)	46	1117, T
4	**9.6**		Rattlesnake Hills volcanics	−79.3	324.3			−80.2	0.8	(74.2/−4.9/15)	46	1712, T
4	10.1		Monterey intrusives	−85.2	62			−81.2	84	(74.5/−4.8/15.3)	47	1865, T
6	5.6		Bitterroot Dome dike swarm	−72	343.4			−71.9	10.7	(74.5/−4.8/15.3)	47	2560, T
5	4		Robinson Anticline intrusives	−77.1	325.8			−78.1	−0.9	(75.9/−3.5/16.2)	50	1348, T
6	6.2		Absorako volcanics	−83.1	326.3			−83.5	15.9	(75.9/−3.5/16.2)	50	Harlan and Morgan (2010)
6	4.9		Wasatch and Green River Formation	−77.6	309.1	−78.3	22.7	−75.8	51.7	(76.5/−2.8/16.5)	51	3150, T
6	2.6		Combined Eocene intrusives	−82.7	347.2			−81.8	31.2	(76.5/−2.8/16.5)	51	1270, T
6	4.4		Bighorn Basin	−81.4	347.7	−73.9	48.8	−71.3	71.7	(79.8/4.1/17.6)	55	Clyde et al. (2007)
5	14		Rhyolite intrusion and contact	−68.1	9.4			−67.3	34.2	(80.9/6.2/18.2)	57	504, T
6	3		Nacimiento formation	−75.9	326.4	−74.9	24.7	−73.4	52	(81.8/4.8/19.4)	61	1033, T
4	1.1		Gringo Gulch volcanics	−77.1	21.3			−75.6	50.6	(82.2/4/20)	63	1710, T
4	6.6		Edmonton Group, Alberta	−72	5.3	−68	38.1	−66.1	62.3	(82.2/4/20)	63	1914, T
6	3.7		Combined Palaeocene intrusions	−81.9	350.6			−81.7	29.2	(82.2/4/20)	63	1270, T
5	3.9		Alkalic intrusives	−80.5	359.4			−79.9	34.6	(82.4/3.6/20.4)	64	1711, T
5	5.8	#	Tombstone volcanics and intrusions	−71.8	28.3			−69.2	56.8	(81.4/−8.2/22.7)	71	2806, T
5	6.2	#	Roskruge volcanics	−69.8	354.9			−68.6	26.4	(81.3/−9.2/23.1)	72	1240, T
6	4.6		Adel Mountain volcanics	−83.7	15.4			−80.7	58.1	(80.7/−12.3/24.3)	74.5	2370, T
6	9		Doherty Mountain sills	−80.8	358.1			−78	43.4	(79.5/−15.9/25.7)	77	Harlan et al. (2008)
5	9.6		Niobrara Formation	−59.8	17.7	−57.8	41.8	−52.8	70.3	(78.7/−18.1/26.9)	79	Shive and Frerichs (1974)
6	6.2		Maudlow Formation welded tuffs	−70.5	27.6			−65.5	60.8	(78.2/−18.8/27.5)	80	2397, T
7	6.6		Elkhorn Mountains	−81.8	7.8			−77.2	55.4	(77.8/−19.4/28.1)	81	2382, T

5	4.4		Magnet Cove and other intrusions	−73.6	11.1			−61.2	65.2	(69.4/−23.5/40.5)	100	1322, T	
5	8.3		Cuttingsville	−72.4	20.7			−59.3	70	(69.4/−23.5/40.5)	100	3087, T	
5	4		Randall Mountain	−76.4	319.4			−69.4	45.2	(68.8/−23.1/42.6)	103	3087, T	
5	4.4		Little Rattlesnake Complex	−71.5	2.4			−56	67.6	(67.3/−22/48.2)	111	3087, T	
5	6.5		Pleasant Mountain	−77.4	5.9			−60.7	74.5	(67.2/−21.8/48.9)	112	3087, T	
5	5.6		Burnt Meadow Mountains	−75.7	29.1			−57.1	84.1	(67/−21.7/49.6)	113	3087, T	
5	3.6		Alfred Complex	−74.2	30.3			−53.1	88.2	(66/−20.6/54.2)	120	3036, T	
5	5.3		Cape Neddick	−74.8	354.8			−56.5	73.9	(65.8/−20.2/54.8)	121	3036, T	
5	4.6		Tatnic Complex	−65.9	27.8			−44.4	86.2	(65.7/−19.8/55.3)	122	3036, T	
6	2.4		Monteregian Hills intrusives	−72	11.2			−51.7	79.7	(65.7/−19.8/55.3)	122	1853, T	
5	3.3		White Mountains igneous complex	−71.3	7.5			−51.5	77.6	(65.7/−19.8/55.3)	122	2644, T	
5	7.5		Lebanon diorite	−71	16.9			−49.4	83.7	(65.4/−18.9/56.8)	125	3036, T	
5	3.6		Notre Dame Bay dikes	−67.2	30.8			−43.6	91.6	(64.9/−17.7/58.7)	129	1854, T	
7	2.6		Kimberlite dikes	−58	23.1			−33.4	89.2	(64.9/−16.7/63.2)	144	2717, T	
6	4.1	#	Morrison Formation, Brushy Basin Member	−64.2	338.8	−65.5	12.5	−41.3	86.4	(64.8/−16.8/64.4)	148	2870, T	
5	3.6	#	Upper Morrison Formation	−63.4	344.8	−64	17.5	−39.3	89.3	(65.1/−16.1/64.9)	150	787, T	
6	7	#	Canelo Hills volcanics	−58.7	315.1			−49.8	50.8	(65.3/−15.7/65.2)	151	1256, T	
5	5.3	#	Lower Morrison Formation	−57.4	327.5	−62.5	351	−42.6	76.4	(65.8/−14.2/66.8)	156	787, T	
6	6	#	Summerville Formation, Trujillo	−56.8	328.1	−58.1	350.6	−37.8	76.3	(65.8/−13.5/69.6)	163	Steiner (2003)	
6	7.4	#	Summerville Formation	−52.6	318.2	−58.6	334.6	−42	69.4	(65.9/−13/71.5)	168	2419, T	
5	4.3	#	Summerville sandstone	−64	299	−71.4	321.9	−54.9	77	(65.9/−13/71.5)	168	1121, T	
4	7.4		Moat volcanics	−78.7	270.3			−68.5	87.8	(65.9/−12.9/71.9)	169	Van Fossen and Kent (1990)	
5	7.8	#	Corral Canyon rocks	−58	303.8			−51.9	53	(65.6/−12.9/72.9)	172	1294, T	
4	**1.4**		Newark volcanics II	−63.2	283.2			−61.7	54.7	(64.8/−13.4/75)	180	1702, T	
3	1		Anticosti dikes	−75.7	264.7			−67.6	85	(64.4/−13.6/75.7)	183	Larochelle (1971)	
6	3.3	#	Kayenta Formation	−58.8	256.4	−62	257.2	−72	47.8	(64.1/−13.8/76.5)	186	2380, T	
5	7	#	Kayenta Formation	−61.3	264.8	−67.8	268.3	−67.4	64.9	(64.1/−13.8/76.5)	186	Steiner and Helsley (1974)	
4	9.8	#	Kayenta Formation	−58.7	277.8	−64.4	283	−61	59.4	(64.1/−13.8/76.5)	186	Johnson and Nairn (1972)	
3	7.2	#	Sil Nakya Formation	−73.1	275.4			−64.1	78.6	(63.8/−14/77.3)	189	T, Kluger-Cohen et al. (1986)	
5	3.1		Combined dikes	−72.8	268.1			−66.1	79.2	(63.7/−14/77.6)	190	1932, T	
5	8.9		Piedmont dikes	−66	266			−66.7	63.8	(63.3/−14.2/78.6)	194	1796, T	
4	2.3		Newark volcanics I	−63	263.1			−67.6	56.7	(63.2/−14.2/79)	197	1702, T	
4	11.1		Connecticut Valley volcanics	−65.5	267.5			−65.9	63.2	(63.2/−14.2/79)	197	477, T	
6	2.8	#,I	Moenave Formation	−62.5	251			−73.2	55.4	(63.2/−14.2/79)	197	Donohoo-Hurley et al. (2010)	
5	4		Hartford Newark basalts and volcanics	−68	268.5			−65.4	69.2	(63.2/−14.2/79)	197	2278, T	
5	6.2		Watchung basalts	−63.6	268.7			−65.2	58.6	(63.2/−14.2/79)	197	1339, T	
5	6		Hettangian Newark red beds	−55.6	274.6	−59.8	273.3	−62.2	51.5	(63.2/−14.2/79.1)	198	2312, T	
5	7.9		Piedmont dikes	−61.5	234			−81	61.6	(63.2/−14.2/79.2)	199	1809, T	
6	10.7		North Mountain basalt	−66.4	252			−71.9	68.2	(63.2/−14.1/79.2)	200	1932, T	
7	3.2	I	Hartford basin	−66.6	268.2			−65.5	66.3	(63.2/−14.1/79.3)	201	Kent and Olsen (2008)	
6	5	I	Newark Martinsville core	−67.8	275.8			−62.5	69.5	(63.2/−14/79.5)	204	Kent and Tauxe (2005)	
5	8		Chinle Group, Redonda Formation	−58.5	256.9	−61.2	257.1	−70.3	51.8	(63.2/−14/79.5)	204	2979, T	
6	10.7	#	Chinle Formation	−58.7	250.9	−62.8	251.2	−73	57.3	(63.2/−14/79.5)	204	2800, T	
6	4.2		Chinle Formation, Redonda Member	−57.8	259.3	−59.6	259.5	−68.9	47.8	(63.2/−14/79.5)	204	152, T	
6	6.5	I	Newark Martinsville core	−64.9	276.6			−61.9	63.3	(63.2/−14/79.5)	204	Tan et al. (2007)	
6	2.5	I	Newark Weston core	−58.1	271.8			−62.3	48.4	(63.2/−13.9/79.7)	207	Tan et al. (2007)	
6	5	I	Newark Westonville	−66.9	267.2			−65.8	67.6	(63.2/−13.9/79.7)	207	Kent and Tauxe (2005)	
6	4.7		Passaic Formation, baked sediments	−65.5	255.1			−70.7	65.7	(63.2/−13.9/79.9)	211	2791, T	
7	5.6		Passaic Formation, C component	−55.6	274.6	−59.9	273.3	−62.1	52.8	(63.2/−13.9/79.9)	211	2312, T	
6	3.4	#	Chinle Formation	−56.6	255.9	−58.6	256.2	−70.3	45	(63.2/−13.9/79.9)	211	2380, T	
6	4	I	Newark Somerset core	−61.7	274.7			−61.9	57	(63.2/−13.9/79.9)	211	Kent and Tauxe (2005)	
5	3		Newark Basin both polarities	−57.6	269.6	−63.3	266.9	−65.7	59	(63.2/−13.9/79.9)	211	1339, T	
4	**5.2**		Taylor Mountain batholith	−61.4	282.2			−58.4	58.5	(63.2/−13.9/79.9)	212	Symons et al. (2009)	
6	3.1	I	Newark Rutgers core	−60.1	277.1			−60.3	54.5	(63.2/−13.9/79.9)	214	Kent and Tauxe (2005)	
4	7		Manicouagan Stucture, Quebec	−60.1	271.8			−62.9	52.7	(63.2/−13.9/79.9)	215	434, T	
3	10		Manicouagan Stucture, Quebec	−59	267.6			−64.6	49	(63.2/−13.9/79.9)	215	443, T	
3	14		Popo Agie Formation, Chugwater	−56.1	276	−62.4	280.5	−59.5	59.9	(63.2/−13.9/79.9)	215	1134, T	
7	7.8		Ankareh Formation	−50.5	267.6	−53.4	268.7	−62.1	37.9	(63.2/−13.9/79.9)	215	Weil et al. (2010)	
6	5.6		Chinle Formation, Bull Canyon Member	−57.4	267.7	−59.3	268.4	−64.3	50	(63.2/−13.9/79.9)	216	2380, T	
6	3.2	I	Newark Titusville core	−59.9	279.4			−59.2	54.9	(63.2/−13.9/79.9)	217	Kent and Tauxe (2005)	
6	5.1	#	Chinle, Sangre de Cristo	−52.9	282	−53.5	282.5	−54.9	45.6	(63.2/−13.9/79.9)	218	2979, T	
6	7.7		Dockum Group, Trujillo and Tecovas Formations	−56.4	276.8	−58	277.6	−59.4	50.7	(63.2/−13.9/79.9)	218	2944, T	
7	5	#	Shinarump Member, Chinle Formation	−59.6	277.5	−63.5	280.6	−59.7	61.9	(63.2/−13.9/79.9)	220	2489, T	

(continued on next page)

Table 1 (*continued*)

Q	α_{95}	Com	Formation	Lat	Lon	CLat	CLon	RLat	RLon	EULER	Age	GPDB RefNo/Reference
6	5		Newark Basin, Lower redbeds	−53.4	281.7	−55.9	281.5	−56.6	48.9	(63.2/−13.9/79.9)	220	2331, T
6	2	I	Dan River–Danville Basin	−58.5	279.5			−58.6	52.4	(63.2/−13.9/79.9)	221	Kent and Tauxe (2005)
5	5	I	Newark Nursery core	−60.5	281.6			−58.4	56.7	(63.2/−13.9/79.9)	221	Kent and Tauxe (2005)
4	3.9		Abbott Pluton	−48.3	272.3			−57.6	31.5	(63.2/−13.9/79.9)	221	1831, T
6	5		Upper Red Peak Formation	−49.1	285.1	−52.7	287.8	−51.7	47.3	(63.2/−13.9/79.9)	225	1134, T
6	4	I	Newark Princeton core	−54.1	285.2			−53.8	47.9	(63.2/−13.9/79.9)	227	Kent and Tauxe (2005)
6	3.2		Agamenticus Pluton	−48.4	278.5			−54.2	35.8	(63.2/−13.9/79.9)	228	1831, T
5	2.5	#	Upper Moenkopi drillcore	−54.1	288.3	−58.6	293.1	−52.3	58	(63.2/−13.9/79.9)	230	160, T
6	4		Chugwater Formation	−45.2	295.4	−49.1	299	−44	49.4	(63.2/−13.9/79.9)	230	1266, T
5	3.1	#	Upper Moenkopi Formation	−52.5	290.7	−56.6	295	−50.4	56.1	(63.2/−13.9/79.9)	230	159, T
6	4.5	#	Moenkopi Formation (upper)	−56.5	283.2	−59.8	286.6	−55.8	57.3	(63.2/−13.9/79.9)	230	2808, T
6	3.3		Chugwater Formation	−46.1	293.6	−49.8	296.9	−45.5	48.9	(63.2/−13.9/79.9)	230	1271, T
7	3.4	#	Moenkopi Formation	−55.5	287.9	−58.2	290.7	−53.2	56.5	(63.2/−13.9/79.9)	234	2489, T
7	5	#	Moenkopi Formation (Gray Mountain)	−54.6	284.5	−57.8	287.8	−54.4	54.5	(63.2/−13.9/79.9)	234	1221, T
6	4.9	#	Moenkopi Formation, Anton Chico Member	−44.7	301.4	−44.9	301.7	−39.8	46.9	(63.2/−13.9/79.9)	234	2979, T
5	4.9	#	Moenkopi Formation	−55.6	285.8	−60.5	290.9	−54.2	59.9	(63.2/−13.9/79.9)	234	2489, T
4	5.3	#	Moenkopi Formation	−41.1	305.6	−40.8	305.2	−35	45.7	(63.2/−13.9/79.9)	234	2632, T
5	7		Lower Red Peak Formation	−46.1	301	−50.6	306.1	−41.5	55.1	(63.2/−13.9/79.9)	235	1134, T
6	7.2		Lower Fundy Group	−44.3	271.6	−45.5	271.1	−56.6	26.5	(63.2/−13.9/79.9)	246	Symons et al. (1989)
6	5		Dewey Lake Formation	−51	306.5	−53.8	310.3	−41.8	60.5	(63.2/−13.9/79.9)	250	2303, T
4	8	#	Bernal Formation	−49.9	298.1	−51.6	300	−45.1	52.6	(63.2/−13.9/79.9)	255	2489, T
4	15		Ochoan red beds	−54.8	299.3	−57.3	302.2	−47.6	60.4	(63.2/−13.9/79.9)	258	688, T
5	5		Guadalupian red beds	−51.5	306.7	−54.8	311.6	−41.9	62.2	(63.2/−13.9/79.9)	263	688, T
5	**3.8**		Intrusions Southern Illinois	−56.3	302.9			−46.6	59.5	(63.2/−13.9/79.9)	270	Domeier et al., 2011a
4	3.8		Downey Bluff sill	−53	308.7			−42	58.9	(63.2/−13.9/79.9)	272	Reynolds et al. (1997)
4	8.6		Hicks Dome breccia	−54.8	292.1			−50.8	52.3	(63.2/−13.9/79.9)	272	Reynolds et al. (1997)
3	10	#	Toroweap Formation	−51.9	303	−56.5	311	−43.2	63.6	(63.2/−13.9/79.9)	277	688, T
3	5		Leonardian subset	−51.7	302.1	−53.7	304	−44.5	57.1	(63.2/−13.9/79.9)	277	688, T
7	3.6		Artinskian Pictou red beds	−42.1	306.5	−41.4	306.4	−34.9	46.9	(63.2/−13.9/79.9)	280	2281, T
5	16.3		Churchland pluton	−33.5	306.3			−29	40.8	(63.2/−13.9/79.9)	282	1264, T
4	13.1	#	Fountain and Lykins Formations	−44.6	305.3	−47.8	308.8	−38.3	54	(63.2/−13.9/79.9)	283	504
5	2.1	#	Abo Formation	−46.8	304	−48.3	305.9	−40.1	52.7	(63.2/−13.9/79.9)	285	1311, T
3	10.2		Piedmont Mafic intrusions	−38.9	300.8			−35.9	41	(63.2/−13.9/79.9)	289	1527
5	1.5		Upper Casper Formation	−50.5	303	−56.2	310.3	−43.4	63	(63.2/−13.9/79.9)	291	1455, T
4	5	#	Elephant Canyon Formation	−37.5	296.6	−35.8	295.2	−36.7	34.4	(63.2/−13.9/79.9)	292	671, T
5	7.1	#	Cutler Formation, Lisbon Valley	−40.1	307.7	−42.1	310.1	−33.5	50	(63.2/−13.9/79.9)	292	1341, T
5	2	#	Ingelside Formation	−43.1	307.9	−46.5	311.7	−36	54.6	(63.2/−13.9/79.9)	292	1142, T
4	2	#	Cutler Formation	−41.6	300.4	−42.6	301.5	−38.3	44.7	(63.2/−13.9/79.9)	292	671, T
4	2.8	#	Minturn and Maroon Formations	−40.1	300.5	−40.3	300.8	−37	42.2	(63.2/−13.9/79.9)	298	1685, T
4	12.8	#	Upper Maroon Formation	−55.3	279.8	−60.6	285.1	−56.8	58	(63.2/−13.9/79.9)	299	504, T
5	3.9		Dunkard Formation	−44.1	301.5	−41.5	300.4	−38	43	(63.2/−13.9/79.9)	300	302, T
5	2.1		Laborcita Formation	−42.1	312.1	−43	313.4	−32.7	52.9	(63.2/−13.9/79.9)	301	1311, T
5	3.4	#	Wescogame Formation	−44.1	303.9	−46.3	306.8	−38.2	51.4	(63.2/−13.9/79.9)	301	1311, T
6	3.1	I	Glenshaw Formation	−28.6	299.9			−28.6	32.4	(63.2/−13.9/79.9)	303	Kodama (2009)
5	1.8		Lower Casper Formation	−45.7	308.6	−50.5	314.6	−37.6	59.8	(63.2/−13.9/79.9)	303	1455, T
5	6		Riversdale Group	−36	302	−30.2	301.5	−29	34.8	(63.2/−13.9/79.9)	310	1110, T
7	7.7	I	Shepody Formation, Nova Scotia	−27.2	298.3			−28.4	30.2	(63.2/−13.9/79.9)	317	Bilardello and Kodama (2010a)
6	8.3	I	Mauch Chunk	−22.6	294.4			−26.9	23.8	(63.2/−13.9/79.9)	320	Bilardello and Kodama (2010a)
7	15.3	I	Maringouin Formation, Nova Scotia	−27.9	297.2			−29.5	29.8	(63.2/−13.9/79.9)	322	Bilardello and Kodama (2010a)
4	6.5		New Brunswick volcanics I and redbeds	−19.5	315.8			−12.6	39.2	(63.2/−13.9/79.9)	330	Seguin et al. (1985)
6	8		Jeffreys Village Member	−27	311	−17.8	309.8				333	1534, T
7	9	I**	Deer Lake Formation	−18.6	304.2						335	Bilardello and Kodama (2010b)
3	16		Catskill Formation South	−27.4	303	−16.6	299.6				370	1693
4	9		Andreas red beds	−13	285	1.5	284.8				415	1388, T96
7	5.3		Wabash Reef	−17	305						420	1277, T96
6	5.8		Rose Hill Formation	−19.1	308.3						425	1218
4	7.3		Ringgold Gap sediments	−24	326.6	−16.9	321.7				438	1689
4	3.9		Tablehead Group limestone Mean	−13.4	329.3						470	2257, 1931, T96 (recalculated)
4	4.3		St. George Group limestone	−17.5	332.4						480	1928, T96
6	11.9		Oneota Dolomite	−10.3	346.5						490	1283, T96
5	8.5		Moore Hollow sediments	0.6	343	3.1	338.9				495	2383, T96

5	9.7		Morgan Creek	−10.6	338	−8.4	334.6					495	2376, T96
5	9		Point Peak	−5.2	345.8	−4.7	345					495	801, T96
5	7.1		Taum Sauk limestone	3.4	355.1							500	1284, T96
6	4.3		Royer Dolomite	−12.6	337.3							500	2289, T96
6	10		Florida Mountains	5.4	348.7							503	2375, T96
5	3.3		Tapeats Sandstone	−0.6	341.1	−1.7	342.6					508	1044, T96
5	6.2		Mont Rigaud and Chatham–Grenville	11.9	4.5							532	McCausland et al., 2007
			Greenland (102)										
6	7.4		Talerua Member lavas	−76.3	21.5			−75	44.1	(72.8/9.1/11.2)		39	Schmidt et al. (2005)
5	6.3		Nuussuaq lavas, Kanisut Member	−74.6	339.4			−77.6	11.6	(71.1/30.9/16)		54	Riisager et al. (2003b)
4	6		Kangerdlugsuaq dykes, Irminger	−63	0			−64.6	25.6	(71.4/30.2/16.4)		54.5	1604
4	15		Scoresby Sund lavas	−63	354			−65	19.8	(71.7/29.6/16.8)		55	450
3	4.2		Skaergaard Intrusion	−61	345			−63.8	9.9	(72/29/17.2)		55.5	1432
4	8.9		Kangerdlugssuaq Lavas	−63.4	5.1			−64.4	32	(72/29/17.2)		55.5	1844
6	3		Jacobsen Fjord dykes	−68	358			−69.6	28	(72/30.1/17.5)		59	1604
5	9		Jacobsen Fjord basalts	−56	3			−57.4	27.7	(71.9/30.3/17.5)		59.5	1604
6	3.2		Disko Island lavas combined	−67.5	15			−67.6	44.9	(71.8/30.8/17.5)		60.5	103
5	6		Svartenhuk lavas, Vaigat Formation	−76.2	37.9			−73.9	73.2	(71.8/30.8/17.5)		60.5	Riisager et al. (2003b)
5	6.9		Nuusuaq and Disko lavas, Vaigat Formation	−64.8	321.5			−69.4	−14.9	(71.8/30.8/17.5)		60.5	Riisager et al. (2003a)
6	5	I	Gipsdalen and Fleming Fjord Formations	−52.7	278.7			−67.9	36.6	(60.5/1.4/69.3)		209	Kent and Tauxe (2005)
3	11		Kap Stanton Formation	1	302							400	2301
			Stable “Europe” (301, 302, 401 from 250 Myr)										
4	3.6		West Eifel volcanics	−80.6	267.5			−80.6	−92.3	(18.3/−47/.1)		0.5	1513, T
4	4.4		East Eifel volcanics	−86.4	296.1			−86.4	−63.1	(18.3/−47/.1)		0.5	1505, T
3	12.9		Volcanics NW Germany	−84.3	357.7			−83.9	5.8	(18/−26.7/1)		8	56, T
5	1.8		Prado section, Teruel, Spain	−78.9	328.3			−78.9	−25.8	(17.9/−26.4/1.1)		9.5	Abels et al. (2009)
5	3.5		Cascante, Spain	−77.4	314.2			−77.7	−40.4	(18.5/−26.3/1.2)		10	Abdul Aziz et al. (2004)
5	6.9		Velay Oriental volcanics	−84.1	351.2			−83.6	3	(19.7/−25.7/1.4)		11.5	3324, T
5	1.5		Orera, Spain	−72.4	352			−71.9	−3.5	(19.6/−25.5/1.5)		12	Abdul Aziz et al. (2000)
4	4.4		Volcanics Germany	−77.8	310.8			−78.9	−36.2	(20/−19.7/2.9)		24	3282, T
3	3.4		Hocheifel volcanics	−80.8	2			−78	26.5	(26.8/−19.5/5.5)		34	1506, T
5	6.8		Lower Palaeogene mudstone	−63.7	358.6	−76.7	357.2	−72.2	30.6	(30.5/−15.7/10.3)		52	3534
5	1.5		Lundy island dikes, Wales	−83	335			−78.2	41.3	(34.5/−15.7/12.4)		59	755
5	3.5		Vaternish dyke swarm, Scotland	−76	340			−72.9	22.7	(34.5/−15.7/12.4)		59	85, T
5	1.2		Arran dikes, Scotland	−81.7	359.8			−74.9	46.3	(34.6/−15.7/12.5)		59.4	1041, T
5	2.8		Arran intrusives and extrusives	−80.2	339.6			−76	33.2	(34.6/−15.7/12.5)		59.5	6090
4	1.5		Sleat dikes, Scotland	−82.5	338			−77.6	40.6	(34.7/−15.7/12.5)		59.8	1174, T
5	5.7		Sky lavas, Scotland	−77.7	325.4			−76.2	18	(34.7/−15.7/12.5)		59.8	S. Rousse (Pers. Comm. 2011)
4	2.7		Ardnamurchan complex, Scotland	−77	355			−71.5	34.4	(34.8/−15.7/12.6)		60	1377, T
6	4.5		Faeroe flood volcanics	−71.4	334.7			−69.8	11.3	(34.8/−15.7/12.6)		60.1	3494, T
6	2.4		Rhum and Canna igneous, Scotland	−81	359			−74.3	44.8	(34.9/−15.7/12.7)		60.7	1169, T
6	4.7		Mull lavas, Scotland	−73.3	346.2			−69.5	23.1	(35/−15.7/12.8)		60.9	Ganerød et al. (2008)
5	4.7		Antrim Lava, Ireland	−78.9	347			−74	34.1	(35/−15.7/12.8)		61	Ganerød et al. (2010)
5	2.7		Muck and Eigg igneous	−74	351			−69.4	27.5	(35.1/−15.7/12.8)		61.2	1204, T
6	3.4		Aix-en-Provence, France	−79.1	344.5	−84.9	222.9	−82.4	95.9	(35.8/−16/14.6)		68	Cojan and Moreau (2006)
7	8		Aix-en-Provence sediments, France	−73	336			−69.8	21.1	(35.4/−15.7/15.2)		74	2394, T
5	3		Dagestan limstones, Caucasus	−74	341			−67.7	35.4	(37.5/−14/19.5)		86	3037, T
5	3		Dagestan limstones, Caucasus	−74	328			−70.4	28.7	(37.5/−14/19.5)		86	3037, T
4	5		Munsterland Turonian, Germany	−68	329			−65.1	22.3	(39.2/−13.6/21.8)		89.5	1507, T
5	4		Munster Basin limestone	−76	1			−62.9	54.7	(39.4/−13.7/24.2)		93	1495, T
6	**2.5**		Mongolia/Siberia Cretaceous Volcanics	−80.8	338.4			−63.2	70.6	(41.6/−10.1/34.1)		108	van Hinsbergen et al. (2008)
6	2.9		Berriasian limestones	−74	3			−48	82.4	(45.9/−3.4/48.4)		140	1397, T
5	6		Jura Blue limestone, Switzerland	−78	328			−56	87.9	(48.4/−1.1/52.8)		156.5	1337, T
3	3.9		Oxfordian sediments	−70	327			−54.5	74.3	(48.5/−1/53)		157	616, T
5	7		Terres Noires, France	−78	310			−59.5	88.7	(48.6/−.9/53.4)		158	3156, T
4	4		Subtatric Nappe sediments, Poland	−72	312			−59.3	77.2	(48.7/−.8/53.8)		159	1948, T
6	7.3		Limestones, Krakow–Czestochowa Upland	−72	330			−53.9	78.9	(48.7/−.8/53.8)		160	1948, T
7	6.3		Jurassic sediments	−63	300			−62.2	62.5	(49.8/.3/57)		168	1514, T
6	6.8		Scania basalts (179±6 Ma)	−69	283			−65.8	82.6	(49.4/.2/60.3)		179	2729, T
6	12		Thouars and Airvault Sections, France	−71	276			−65.6	90.9	(49.2/0/61.8)		184	1427, T
5	5.1		Paris Basin drillcore	−66	295.2			−60.6	75.2	(49.1/−.1/62.3)		186	3554

(continued on next page)

Table 1 (*continued*)

Q	α_{95}	Com	Formation	Lat	Lon	CLat	CLon	RLat	RLon	EULER	Age	GPDB RefNo/Reference
4	3		Liassic sediments	−77	315			−52.1	94.8	(48.7/0/63.6)	192	1467, T
5	7.5		Kerforne dykes, France	−61	259			−76	88.7	(48.1/.7/63.1)	198	2743, T
6	9		Hettangian–Sinemurian limestone	−55	280			−69.1	54	(47.8/1.1/62.5)	201	3141, T
7	3		Paris Basin sediments	−51	285			−65.8	44.1	(47.8/1.1/62.5)	201	3029, T
6	4.5		Andesites, Ukraine	−50	286.4			−65.3	41.7	(47.6/1.6/61.9)	204.2	Yuan et al. (2011)
6	8		Rhaetian sediments, Germany, France	−50	292	−58	272.9	−73.6	65.6	(47.3/2.2/61.1)	208	3141, T
5	5.1		Merci mudstone, Somerset	−50	308	−58.2	298.2	−61.7	60.7	(46.6/3.2/59.5)	215	3311, T
5	4.6		Sunnhordland dike	−50	305			−56.9	45.8	(46/3.9/58.2)	221	T, Walderhaug (1993)
6	6		Gipskeuper sediments	−49	311			−52.9	46.9	(46/3.9/58.2)	226	3141, T
5	2.9		Taimyr Sills, Siberia	−47.1	301.6			−57.8	39.2	(46/3.9/58.2)	228	Walderhaug et al. (2005)
6	3		Heming limestone, France	−54	321			−49.4	58.3	(46/3.9/58.2)	234	2411, T
6	12		Musschelkalk carbonates, Poland	−53	303			−59.1	50.4	(46/3.9/58.2)	234	3253, T
5	15		Bunter and Musschelkalk, Germany	−49	326	−56.5	318.6	−51.6	61.2	(46/3.9/58.2)	239	158, T
6	5		Upper Buntsandstein, France	−43	326	−47.8	322.2	−45.8	50.6	(46/3.9/58.2)	243	1028, T
6	3.8		Volpriehausen Formation, Germany	−49	348.2	−57	344.7	−39.2	71.2	(46/3.9/58.2)	246	Szurlies (2004)
6	7.8		Taimyr basalts, Siberia	−59.3	325.8			−49	67.4	(46/3.9/58.2)	248	Walderhaug et al. (2005)
7	3.3		German Trias, Lower Buntstein	−50.6	345.6	−58.8	341	−41.8	71.7	(46/3.9/58.2)	249	T, Szurlies et al. (2003)
3	10		Taimyr Siberian Traps, Siberia	−59	330			−46.9	68.2	(46/3.9/58.2)	250	2832
6	3.3		Siberian Traps, Siberia	−56.2	326			−47.7	63.2	(46/3.9/58.2)	251	Gurevitch et al. (2004)
3	13.9		Kotuy River Siberian Traps, Siberia	−52.7	328.4			−44.8	59.6	(46/3.9/58.2)	251	Pavlov et al. (2007)
5	2.1		Siberian Traps NSP1 pole	−56.4	321.7			−49.9	62	(46/3.9/58.2)	251	Pavlov et al. (2007)
6	5		Sudetes sediments, Poland	−50	343	−59.3	336.5	−44.1	70.7	(46/3.9/58.2)	251	3161, T
3	5.3		Stolbovaya River Siberian Traps, Siberia	−53.3	330.2			−44.2	61.1	(46/3.9/58.2)	251	Pavlov et al. (2007)
3	5		Big Nirundaiver intrusion and sediments, Siberia	−54.3	323			−48.4	59.5	(46/3.9/58.2)	251	Pavlov et al. (2007)
3	2.7		Moyero River Siberian Traps, Siberia	−58.5	314.5			−54.3	63.2	(46/3.9/58.2)	251	Gallet and Pavlov (1996); Pavlov et al. (2007)
6	9.7		Siberian Traps Mean recalculated, Siberia	−52.8	334.4			−41.8	62.3	(46/3.9/58.2)	251	Kravchinsky et al. (2002), recalculated
5	2.7		Dome de Barrot red beds, France	−46	327	−50	324.7	−45.5	54.7	(46/3.9/58.2)	255	652, T
6	4		Massif des Maures, France	−51	341	−55.4	338.1	−41.4	66.8	(46/3.9/58.2)	255	1408, T
5	3.5		Late Permian sediments, Urals	−45.6	350.2	−54.9	338.2	−41	66.2	(46/3.9/58.2)	260	Bazhenov et al. (2008)
5	5		Esterel sediments, France	−47	331	−50.6	327.7	−44.2	56.7	(46/3.9/58.2)	261	165, T
6	4		Brive Basin sediments, France	−49	343	−52.6	341.7	−38	65.3	(46/3.9/58.2)	261	3144, T
4	0		Permian red beds, Lodeve, France	−53	331	−58.6	326.4	−48.5	66.5	(46/3.9/58.2)	264	1207, T
5	1.5		Lodeve Basin, France	−49	334	−52.5	331.5	−43.1	60.7	(46/3.9/58.2)	264	1813, T
3	4.6		Upper Lodeve sandstone, France	−47	336	−49.3	334.7	−39.6	58.5	(46/3.9/58.2)	264	168, T
5	4		Saxonian red sandstone, France	−51	324	−56.4	318.8	−51.4	61	(46/3.9/58.2)	264	2361, T
5	6.1		Esterel extrusives, France	−51.5	322			−47.7	55.3	(46/3.9/58.2)	264	165, T
4	4.1		Cracow volcanics B	−50	344			−35.3	63.8	(46/3.9/58.2)	269	Nawrocki et al. (2008)
5	**2.5**		Lunner dikes, Norway	−51	343			−36.4	64.3	(46/3.9/58.2)	271	Dominguez et al. (2011)
5	5.9		Lunner dikes, Norway	−53	344			−37.1	66.7	(46/3.9/58.2)	271	3188, T (redated)
4	8.6		Bohuslan dikes combined, Sweden	−51	345			−35.4	65.3	(46/3.9/58.2)	275	1155, T
4	11		Scania melaphyre dikes, Sweden	−54	352			−34.1	71.4	(46/3.9/58.2)	279	2222, T
4	7		Bohemian quartz porphyry, Germany	−37	341			−28.3	50.6	(46/3.9/58.2)	280	3145, T
3	14		Mauchline lavas, Scotland	−47	337			−37.1	57.3	(46/3.9/58.2)	280	3093, T
5	10		Bohemian Massif igneous, Germany	−42	346			−29	57.8	(46/3.9/58.2)	280	2356, T
5	1		Oslo volcanics, Norway	−47	337			−37.1	57.3	(46/3.9/58.2)	281	915, T
4	13.4		Ringerike lavas, Norway	−44.6	337.4			−35.4	55.2	(46/3.9/58.2)	281	1830
4	6.9		Sarna alkaline intrusion, Sweden	−38	346			−26.2	54.6	(46/3.9/58.2)	281	1735, T
5	6.5		Trachytes, Ukraine	−49.4	359.7			−27.4	71.4	(46/3.9/58.2)	282.6	Yuan et al. (2011)
4	6.7		Moissey volcanics, France	−41	352			−25.1	60.6	(46/3.9/58.2)	285	1205, T
5	3.2		Intrasudetic Basin volcanics, Poland	−43	352			−26.5	62.1	(46/3.9/58.2)	285	3161, T
5	5.1		North Sudetic Basin sediments, Poland	−44	4	−48.6	4.1	−24.9	73.2	(46/3.9/58.2)	285	3161, T
5	2		Krkonose Basin oil shales, Czech Republic	−40	346	−42.4	345.2	−29.6	57.7	(46/3.9/58.2)	285	2444, T
3	7.7		Lower Lodeve sandstone	−44	350	−39.8	−9.4	−25	58.8	(46/3.9/58.2)	285	168, T
5	6.3		Mount Hunneberg Sill, Sweden	−38	346			−26.2	54.6	(46/3.9/58.2)	285	2211, T
4	8.1		North Sudetic Basin volcanics, Poland	−42	354			−24.8	62.5	(46/3.9/58.2)	285	3161, T
5	2		Lodeve Basin, France	−42	349	−40.5	−9.8	−25.7	59	(46/3.9/58.2)	285	1813, T
4	17		Lodeve B Component, France	−49	342	−52.5	340.1	−38.7	64.5	(46/3.9/58.2)	285	2454, T
4	6.8		Intrasudetic basin sediments, Poland	−37	340	−38.5	339.4	−30.2	50.9	(46/3.9/58.2)	285	3161, T
4	7.9		Krakow volcanics, Poland	−43	345			−30.2	58.1	(46/3.9/58.2)	285	275, T
5	4		Bohemian red beds, Czech Republic	−41	345	−44	343.5	−31.6	58.1	(46/3.9/58.2)	285	167, T
3	13.2		Lower Silesia volcanics, Poland	−40	352			−24.3	59.8	(46/3.9/58.2)	285	465, T (recalculated)

5	4	Exeter Lavas, UK	−50	330			−42.6	57.1	(46/3.9/58.2)	286	165, T
4	5.9	Black Forest volcanics, Germany	−49	356			−28.8	69.1	(46/3.9/58.2)	286	170, T (recalculated)
4	10	Exeter Lavas, UK	−48	343			−34.5	61.4	(46/3.9/58.2)	286	411, T (recalculated)
3	1	Black Forest rhyolites, Germany	−42	353			−25.3	61.9	(46/3.9/58.2)	286	2941, T
4	5.8	Thuringer Forest sediments, Germany	−41.5	340	−45.3	338.1	−35.5	56.3	(46/3.9/58.2)	287	1792, T
4	2.4	Stabben Sill, Norway	−32	354			−17.3	55.4	(46/3.9/58.2)	291	1540, T
3	15.9	Saar–Nahe volcanics, Germany	−41	349			−26.7	58.8	(46/3.9/58.2)	291	712, T
3	13	Nahe volcanics, Germany	−46	347			−31.2	61.8	(46/3.9/58.2)	291	940, T
6	13	Sudetic Mountain granitoids, Poland	−42	346			−29	57.8	(46/3.9/58.2)	293	2446, T
4	4.8	Great Whin Sill, UK	−44	339			−34.1	55.5	(46/3.9/58.2)	294	585, T
5	3.5	Hadrian's Wall–Pennines Sill and Hett Dike (Whin Sill), UK	−32.9	347.1			−21.9	51.4	(46/3.9/58.2)	294	T, Liss et al. (2004)
5	6.3	Holy Island Sill and Dyke (Whin Sill), UK	−35.4	346.8			−23.9	53.1	(46/3.9/58.2)	294	T, Liss et al. (2004)
4	4	Nideck–Donon volcanics, France	−47	348			−31.3	63.2	(46/3.9/58.2)	294	1010, T
3	19	Lower Nideck volcanics, France	−42	348			−27.9	59	(46/3.9/58.2)	294	174, T
4	4.8	Cracow volcanics A, Poland	−44	355			−25.7	64.6	(46/3.9/58.2)	294	Nawrocki et al. (2008)
5	8.1	Alnwick Sill, High Green and St. Oswalds Chapel Dyke (Whin Sill), UK	−47.1	337.1			−37.1	57.5	(46/3.9/58.2)	294	T, Liss et al. (2004)
5	6.5	Scania dolerites, Sweden	−38	348			−25.1	55.8	(46/3.9/58.2)	294	2222, T
5	11	Scania dolerite dikes, Sweden	−37	354			−21.1	58.9	(46/3.9/58.2)	294	2211, T
4	7.1	Thuringer Forest volcanics, Germany	−37.1	350			−23.3	56.4	(46/3.9/58.2)	295	1792, T
4	13.6	Silesia volcanics, Poland	−43	354			−25.5	63.3	(46/3.9/58.2)	296	465, T
3	7.1	Arendal diabase dykes, Norway	−42.5	339.6			−32.8	54.5	(46/3.9/58.2)	297	175, T
4	2.9	Ny–Hellesund sills, Norway	−39	341			−29.7	52.3	(46/3.9/58.2)	297	626, T
5	1.3	Peterhead dyke, Scotland	−41	342			−30.5	54.6	(46/3.9/58.2)	297	1535, T
6	3	Donets basin, Ukraine	−43	345	−49.9	337.3	−38.6	60.4	(46/3.9/58.2)	297	Iosifidi et al. (2010)
5	2.4	Svedlodarsk, Karamysh Formation, Donbas	−48.4	349.8	−56.1	341.2	−40.3	68.8	(46/3.9/58.2)	299	Meijers et al. (2010)
5	4	Mount Billinger sill, Sweden	−31	354			−16.6	54.7	(46/3.9/58.2)	299	2211, T
5	2.2	Svetlodarsk, Kartamysh Formation, Donbas	−48.2	348.3	−55.9	339.4	−41	67.9	(46/3.9/58.2)	299	Meijers et al. (2010)
6	4	Donets basin, Ukraine	−42	359	−45.7	356.5	−26.3	66.8	(46/3.9/58.2)	301	Iosifidi et al. (2010)
5	2	Debaltsevo Donbas, Ukraine	−48.2	342.3			−35	61.3	(46/3.9/58.2)	303	Meijers et al. (2010)
3	3	Wackerfield dyke, England	−49	349			−32.2	65.4	(46/3.9/58.2)	303	180, T
5	5.2	Queensferry sill, Scotland	−38.3	354			−22	59.8	(46/3.9/58.2)	305	2447, T
5	9	Westphalian–Stephanian red beds, Czech Republic	−38	343	−40.3	341.5	−30.3	53.7	(46/3.9/58.2)	305	167, T
5	2.9	Tashkovska Donbas, Ukraine	−38.4	339.5			−30.1	50.9	(46/3.9/58.2)	312	Meijers et al. (2010)
6	7	Burntisland–Kinghorn lavas, Scotland	−14	332						332	2447, T96 (redated)
6	8.2	Derbyshire Lavas, England	−14.3	335.9						335	2440, T
6	11	Cheviot Hills igneous, England	4	323						396	190, T96
6	7	Old Red Sandstone lavas and sediments, Scotland	−5	320						410	194, T96
7	3	Strathmore lavas, Scotland	2	318						410	1536, T96
6	7.3	Devonian sediments, Podolia, Ukraine	3.7	325.5						411	2664
5	6	Lorne Plateau lavas, Scotland	2	321						412	193, T96
4	2.5	Glenbervie ignimbrite, Scotland	−8	335						415	2565, T96
4	4.3	Lintrathen ignimbrite, Scotland	−1	325						415	2565, T96
4	4.9	Middle Silurian limestone, Dniester basin, Ukraine	−17	350						419	Jelenska et al. (2005)
7	9.1	Ringerike sandstone, Oslo, Norway	−19	344	−13.6	−16				421	1830, T96
3	5.7	Foyers granite, Scotland	−27	346						421	1530, T96
3	8	Gotland Medby limestone	−23	351						422	1734, T96
4	4.6	Yaruga limestone and dolomite, Dniester basin, Ukraine	−15	350						424	Jelenska et al. (2005)
5	7.9	Ratagen Complex, Scotland	−15	347						425	1200, T96
3	6	Gotland Follingbo limestone, Sweden	−21	344						425	1734, T96
4	2	Gotland Dacker limestone, Sweden	−19	349						426	1734, T96
5	5.1	Gotland Visby limestone, Sweden	−19	352						427	2363, T96
3	5	Strontian granite, Scotland	−21	344						430	1530, T96
4	5.2	Peterhead granite, Scotland	−21	358						432	1535, T96
5	13.4	Swedish Limestone I(N)	3	35						458	2362, T96
6	4.8	Vestergotland (N3), Sweden	5	34						459	2362, T96
5	4.9	Llandeilian limestone, St. Petersburg, Russia	12	41.9						463	Pavlov et al., 2008 EPSL
6	4.4	Vestergotland (N1–N2 and R13), Sweden	14	49						466	2362, T96
4	6.7	Dapingian–Darriwilian limestone, Estonia	11.3	39.1						467	Plado et al., 2010 GJI 180
6	9.2	Komstad Limestone, Sweden	19	51						471	Torsvik and Rehnström (2003)
6	6.8	Gullhøgen (R1 + R2), Sweden	18.7	54						472	2959, T96
4	7.1	Florian limestone, Estonia	25	50.9						472	Plado et al., 2010 GJI 180
5	9	Swedish Limestones	30	55						475	2541, T96
6	5.1	Swedish Limestones I(R)	18	46						475	2438, T96

(continued on next page)

Table 1 (*continued*)

Q	α_{95}	Com	Formation	Lat	Lon	CLat	CLon	RLat	RLon	EULER	Age	GPDB RefNo/Reference
6	4		Narva Ordovician limestone, Russia	18	55						477	Khramov and Iosifidi (2009)
5	3.6		St Petersburg Limestone, Russia	34.7	59.1						478	3179
5	5		Narva Cambrian sandstone, Russia	22	87	34.2	79.8				500	Khramov and Iosifidi (2009)
3	6.8		Andrarum limestone, Sweden	52	111						500.1	3425
4	6.9		Tornetrask Formation/Dividal Group, Sweden	58.4	122.5	68.7	102.2				535	Rehnström and Torsvik (2003)
			West Gondwana									
			Amazonia (S America, 201)									
3	10		El Loa Formation and associated ignimbrites, Chile	−85.4	303.8			−85.5	−37.4	(62.1/−40.5/2.8)	8.5	3323, T
3	10		Lipiyoc Formation, Puna, Argentina	−85.7	80.5			−84.6	75.6	(62.1/−40.5/2.8)	8.5	3027, T
5	11.4		Remedios, Sao Jose formations, Fernando de Noronha, Brazil	−84.5	316			−84.4	−26.3	(62/−40.6/3.1)	9.5	1404, T
5	5.9		Itatiaia and Passa Quatro Complexes, Brazil	−79.5	0			−69.6	46.8	(63.5/−33.4/26.2)	70.5	3261, T
6	2.6		Pocos de Caldas Alkaline Complex, Brazil	−83.2	320.1			−71.8	48.8	(61.6/−34.3/33.8)	84	3261, T
5	4.2		Sao Sabastiao Island Intrusions, Brazil	−79.4	331.9			−67.5	44.3	(61.2/−34.3/34.4)	85	3261, T
3	4.8		Intrusives, Cabo de Santo Agostinho, Brazil	−87.6	315.1			−69.5	65.2	(58.2/−34.6/38.7)	92	1448, T
4	3		Cabo Magmatic Province, Brazil	−87.9	335.9			−63.5	69.8	(54.9/−34.8/44.9)	102	Font et al. (2009)
4	2.8		East Maranhao intrusives, Brazil	−83.6	81			−53.7	84.1	(51.8/−35/52.4)	118	1431, T
6	2.6		Florianopolis dyke swarm, Santa Catarina Island, Brazil	−89.1	3.3			−56.3	76.3	(51/−34.3/53.6)	123.5	3190, T
6	2		Ponta Grossa dykes, Brazil	−82.4	30.3			−48.1	77.9	(50.1/−32.8/54.8)	130	2958, T
6	2.4		Northeast Parana Magmatic Province Combined, Brazil	−83	71.4			−49.6	85.6	(50/−32.5/55.1)	132	3422
4	14.1		Dykes, Rio Grande do Norte, Brazil	−80.6	275			−59.3	63.3	(50/−32.5/55.1)	146	1509, T
3	9.3		West Maranhao Basalts, Brazil	−85.3	262.5			−58.5	72.7	(50/−32.5/55.1)	175	1431, T
5	3.8		Anari and Tapirapua Formations, Brazil	−65.5	250.3			−70.6	34.3	(50/−32.5/55.1)	196.6	3316, T
5	**4**		French Guyana dikes, Brazil	−81.2	235.1			−63.6	72.7	(50/−32.5/55.1)	198	3378
4	$\overline{4}$.9		Bolivar dykes, Venezuela	−66.9	245.6			−71.9	40.3	(50/−32.5/55.1)	202.5	150, T
4	10		Dolerite dykes, Suriname	−82	320			−52.7	66.4	(50/−32.5/55.1)	232	701, T
6	6		Mitu Group red beds, Peru	−71.4	303.6	−60	294.1	−50.4	29.1	(50/−32.5/55.1)	248.5	3524, T
6	6.6		Independencia Group	−80.7	7	−70.7	325.5	−45.5	52.9	(50/−32.5/55.1)	260	Rapalini et al. (2006)
4	4.5		Copacabana Group sediments, Peru	−68.2	321.3	−56.1	305.2	−43.4	29.2	(50/−32.5/55.1)	280	Rakotosolofo et al. (2006)
4	4.1		Santa Fe Group, Brazil	−65.7	330.9	−53.2	324	−33.7	36	(50/−32.5/55.1)	300	Brandt et al. (2009)
3	11.2		Itarare Subgroup, Tubarao Group, Brazil	−57	357	−48.3	338.2	−24.3	41.3	(50/−32.5/55.1)	310	798, T
			Parana (S America, 202)									
3	6		Rio de Los Molinos dykes 1, Cordoba, Argentina	−77	18			−66.8	52.3	(63.9/−33.6/24.7)	65.5	102, T
4	3.7		Serra Geral basalts, Brazil	−84.6	115.4			−57	86.1	(51.7/−35/52.6)	119	765, T
3	10.4		Vulcanitas Cerro Colorado Formation, Cordoba, Argentina	−81	14			−49.2	71.8	(51.5/−34.9/53)	121	123, T
5	5.9		El Salto–Almafuerte lavas, Cordoba, Argentina	−72	25			−39.1	73.6	(50.9/−34.2/53.7)	124	1087, T
3	11		Rio de Los Molinos dykes 2, Cordoba, Argentina	−79	8			−43	71.3	(47.5/−33.3/56.1)	139.5	102, T
3	18.1		Sierra de las Animas volcanic Complex, Uruguay	5.9	338.1			24.1	12.1	(47.6/−33.3/56.2)	510	3513
			Colorado (S America, 290)									
4	8		Pirgua basalts and red beds, Argentina	−85	222			−73	71.4	(56.9/−34.7/40.9)	95.5	1131, T
5	8.7		Marifil Formation, North Patagonia, Argentina	−83	138			−53.3	90.1	(47.5/−33.3/57.3)	183	3535, T
6	4.5		Mendoza–Neuquen sediments and volcanics	−74	67			−38.1	89.4	(47.5/−33.3/57.3)	183	Iglesia-Llanos et al. (2006)
5	**6.8**		Lepa-Osta Arena Formation	−75.5	129.4			−51	102	(47.5/−33.3/57.3)	187	3314
6	$\overline{4.5}$		Mendoza sediments and volcanics	−51	223			−84.7	−21.3	(47.5/−33.3/57.3)	195	Iglesia-Llanos et al. (2006)
4	7.6		Los Colorados Mendoza	−81.8	298.3			−52.4	65.2	(47.5/−33.3/57.3)	216	Vizán et al. (2004)
4	7		Amana Formation, Paganzo Group, Argentina	−83	317	−69.1	298.5	−49.7	45.5	(47.5/−33.3/57.3)	240	1132, T
6	**6.4**		Puesto Viejo Formation Volcanics, Mendoza	−76	313.4			−48.1	57.7	(47.5/−33.3/57.3)	240	Domeier et al. (2011c)
6	**4.9**		Puesto Viejo Formation Sediments, Mendoza	−89.2	346.1	−75.1	293.5	−52.6	54.2	(47.5/−33.3/57.3)	240	Domeier et al. (2011c)
6	$\overline{3.3}$		Sierra Chica, La Pampa	−80.1	348.6			−44.9	68.6	(47.5/−33.3/57.3)	263	Domeier et al. (2011b)
6	**4.1**		Upper Choiyoi Group, Mendoza	−75.7	326			−45.3	59.5	(47.5/−33.3/57.3)	264	Domeier et al. (2011c)
4	$\overline{5.2}$		Tambillos, Uspallate Basin, Argentina	−80.6	308.3			−50.7	63.7	(47.5/−33.3/57.3)	267	2475
4	2.8		La Colina Formation, Paganzo	−80.6	268.8	−66.7	285.5	−53.7	39.6	(47.5/−33.3/57.3)	283	Geuna and Escosteguy (2004)
3	2.5		Middle Paganzo II, Los Colorados Lower Beds, Argentina	−59.5	357.5	−55.2	332.3	−29.2	43.2	(47.5/−33.3/57.3)	283	620, T
3	3.1		La Colina Formation, Los Colorados 1, Argentina	−74	313	−60.9	301.3	−45.1	35.2	(47.5/−33.3/57.3)	283	166, T
4	4.9		Rio del Penon Formation sediments, Argentina	−76.8	293.7	−62.4	292.2	−49.6	34.4	(47.5/−33.3/57.3)	290	Geuna and Escosteguy (2004)
4	7		Punta del Agua Formation volcanics, Argentina	−73.1	272.4			−58.4	50.8	(47.5/−33.3/57.3)	290	Geuna and Escosteguy (2004)
3	5		La Colina basalt, Argentina	−66	348			−33.4	57.8	(47.5/−33.3/57.3)	300	178, T
4	5.7		La Tabla Formation, Chile	−51	347			−20.8	48.8	(47.5/−33.3/57.3)	310	1420, T
6	5		La Colina Formation, Argentina	−49	343	−45.4	323.6	−25.1	31.5	(47.5/−33.3/57.3)	310	1144, T

6	9.6	Pular and Cas formations, Chile	−57	350			−25.2	53.6	(47.5/−33.3/57.3)	310	1420, T
		Patagonia (S America, 291)									
5	**5.7**	Eocene volcanics Patagonia	−81	337.4			−74.4	33.2	(57.2/−31.2/19.4)	47	Somoza (2007)
6	4.3	Patagonian Plateau basalts, Chile, Argentina	−78.7	358.4			−68.8	45.5	(63.4/−33.4/26.5)	71.5	2374, T
5	2	San Bernardo, Patagonia	−86.8	35.2			−66.7	71.5	(58.2/−34.6/38.7)	92	Somoza and Zaffarana (2008)
4	**3.8**	Cerro Barcino sediments, Argentina	−87	159	−77.5	283.2	−60.9	51.4	(52/−35/52.1)	116	Geuna et al. (2000)
5	5.5	Posades and Sierra Colorado ignimbrites, Argentina	−81	172			−57.9	90.4	(47.5/−33.3/58)	156.5	3535
4	4.9	Chon Aike Formation, combined result, Argentina	−85	197			−55.8	82	(47.5/−33.3/59.2)	167	133, T
		Southern Africa (701)									
5	**5.2**	Cretaceous Kimberlites 1, South Africa, Lesotho	−64.1	46.1						90.5	2293, T
6	**9.7**	Cretaceous Kimberlites 2, South Africa	−47.6	89.9						129	2293, T
5	3.1	Kaoko lavas, Namibia	−48.3	86.6						132	126, T
4	13.3	Batoka basalts, northern Zimbabwe	−64	80.6						180	T, Jones et al. (2001)
3	15.8	Hoachanas lavas, Namibia	−61.9	71.9						183	126, T
5	3.2	Stormberg lavas (Lesotho basalts), South Africa	−71.6	93.5						183	3090, T
4	11	Stormberg lavas, Sani Pass and Maseru, Lesotho	−70.5	88.7						183	984, T
3	7	Karroo lavas, Central Africa, Zimbabwe, Mozambique	−57	84						183	635, T
5	9.5	Karroo dolerites combined, South Africa, Zimbabwe	−65.4	75.1						183	317, T
5	8.7	Marangudzi Ring Complex, Zimbabwe	−70.7	106.7						186	470, T
3	4.6	Red sandstone Formation, Zambia	−68	50.5	−54.7	39.5				221.5	323, T
3	6	Cassanje Series, Angola	−54	80	−49	62.6				248.5	1960, T
5	7.6	Karroo Basin	−50.9	86.3	−48	63.8				251	De Kock and Kirschvink (2004)
6	5.6	K1 Dwyka Varves, Zimbabwe, Zambia, Tanzania	−26.5	26.5	−21.6	27.7				281.5	435, T
6	12	Dwyka Group combined	−25	67	−25.2	53.6				315	3489, T
4	7	Bokkeveld Group, Cape Province, South Africa	10	15	−3.3	16				398.5	1416, TV
5	18	Pakhuis, Cedarberg Formations, Cape Province, South Africa	25	343	17	−11				446.5	1416, TV
6	9	Graafwater Formation, Cape Province, South Africa	28	14	13.9	13.8				482.5	1416, TV
		Meseta (707)									
4	14	Intrusives, Beni Mellal, Morocco	−46	78						120	1859, T
6	9	Beni Mellal volcanics, Morocco	−44	71			−42.6	73.6	(33.6/26/2.3)	173.5	148, TV
4	11	Beni Mellal basalts, Morocco	−45	68			−43.7	70.7	(33.6/26/2.3)	173.5	1859, T
5	6	Argana Flows. Morocco	−69.2	55.5			−68.2	61	(33.6/26/2.3)	201	Ruiz-Martinez et al. (2012)
3	7	Morrocan Intrusives, Morocco	−71	36			−70.5	42.7	(33.6/26/2.3)	201	148, T
5	**19**	Central Atlantic Magmatic Province, Morocco	−73	61.3			−71.8	67.4	(33.6/26/2.3)	201	T, Knight et al. (2004)
3	4.6	Taztot Trachyandesite, Morocco	−38.7	56.8			−37.7	59.4	(33.6/26/2.3)	273	723, T
5	4.7	Chougrane red beds, Morocco	−32.2	64.1	−33.4	66	−32.1	68.3	(33.6/26/2.3)	273	723, T
3	7.8	Djebel Tarhat red beds, Morocco	−24	63.8	−23.3	62.3	−22.1	64.3	(33.6/26/2.3)	273	1080, T
3	20.9	Volcanics, Mechra ben Abou and Chougrane, Morocco	−36	58			−34.9	60.5	(33.6/26/2.3)	280.5	1859, T
		Somalia (709)									
3	4.1	Afar Stratoid Series, Ethiopia	−87.5	359.3			−87.5	−2.3	(52.4/6.3/−.1)	1	3336, T
3	5.7	Stratoid Basalts, Ethiopian Afar, Ethiopia	−87.2	37.1			−87.3	34.3	(50.2/6.5/−.2)	2	3559, T
3	4.1	Gamarri section lavas, Afar Depression, Ethiopia	−79.7	350.2			−79.6	−11	(50.3/6.4/−.3)	2.5	3234, T
5	3.8	Ngorora Formation, Kenya	−85.7	75.8	−84.4	65.5	−85.1	59.6	(50.4/6.4/−1.3)	11.5	3111, T
4	8.8	East African volcanics, Kenya and Tanzania	−86.5	6.6			−86.4	−7.5	(50.4/6.4/−1.3)	12	774, T
3	10	Volcanics, Kenya	−80.1	214.2			−79.7	−142.7	(50.3/6.4/−1.3)	13.5	1517, T
5	3.1	Turkana Lavas, Kenya	−84.6	343.3			−84.2	−25.5	(50.4/6.4/−1.3)	17	774, T
4	8.4	Southern Plateau volcanics, Ethiopia	−75.1	350.3			−74.8	−14.2	(50.3/6.4/−1.5)	34	2764, T
4	3	Lupata series volcanics, Mozambique	−61.8	79.5			−62.7	77.8	(50.3/6.4/−1.5)	111	992, T
3	9.3	Mlanje Massif syenite, Malawi	−60	82			−60.9	80.4	(50.3/6.4/−1.5)	124.5	401, T
3	5	K3 beds, Galula coalfield, Tanzania	−46	40	−33.3	36.9	−33.7	35.2	(50.3/6.4/−1.5)	257	324, T
5	1.9	Ntonya Ring Structure, Malawi	27.5	344.8			27.8	−15.9	(50.3/6.4/−1.5)	522	404, TV
4	5	Sinyai dolerite, Kenya	−28.4	319.1			−27.7	−42.4	(50.3/6.4/−1.5)	547	3106, TV
		Northwest Africa (714)									
4	6.7	Famara Volcanics, Canary Islands	−87.5	358.2						7.5	2938, T
3	5.2	Basalt Series II, Canary Islands	−77.8	326.2						8	1493, T
4	4.1	Miocene volcanics, Canary Islands	−81.9	294.4						13	25, T
3	2.3	Massif de Cavallo, Algeria	−86.8	202.9						13	555, T
5	8	Basalt Series I, Canary Islands	−72	71.2						81	1493, T

(continued on next page)

Table 1 (*continued*)

Q	α_{95}	Com	Formation	Lat	Lon	CLat	CLon	RLat	RLon	EULER	Age	GPDB RefNo/Reference
6	6.3		Upper Jurassic sediments, Tunisia	−65.2	20.3			−65.3	25.8	(33.6/26/2.3)	152.5	1167, T
3	19.2		Intrusive rocks, Nigeria	−62.5	61.6			−61.3	65.8	(33.6/26/2.3)	160	1081, T
5	7.4		Diabase dykes and sills, Liberia	−68.5	62.4			−67.3	67.4	(33.6/26/2.3)	185.5	140, T
4	4.1		Hank volcanics, North Mauritania	−69.4	52			−68.5	57.7	(33.6/26/2.3)	187	3259, T
4	6.1		Hodh volcanics, South Mauritania	−71.4	60.2			−70.2	66	(33.6/26/2.3)	187	3260, T
4	6.2		Freetown Complex, Sierra Leone	−82.9	32.7			−82.4	48.7	(33.6/26/2.3)	193	3287, T
5	**4.1**		Ighrem and Foum Zguid dykes, Morocco	−73	64.7			−71.7	70.6	(33.6/26/2.3)	200	Palencia-Ortas et al. (2011)
6	2.6		Zarzaitine Formation, Algeria	−70.9	55.1	−76.2	78.9	−74.6	84.4	(33.6/26/2.3)	206.5	2932, T
5	6		Serie d'Abadla, Upper Unit, Morocco	−29	60	−26.8	56.5	−25.7	58.6	(33.6/26/2.3)	273	1459, T
5	3.6		Abadla Formation, Lower Unit, Algeria	−29.1	57.8	−26.3	54.2	−25.4	56.3	(33.6/26/2.3)	275	3275, T
5	2.8		Upper El Adeb Larache Formation, Algeria	−38.5	57.5	−33.7	52.4	−32.8	54.8	(33.6/26/2.3)	286.5	2540, T
4	4.1		Lower Tiguentourine Formation, Algeria	−33.8	61.4	−29	55.5	−28	57.7	(33.6/26/2.3)	290	2728, T
5	3.5		Lower El Adeb Larache Formation, Algeria	−28.7	55.8	−20.9	48.3	−20.1	50.3	(33.6/26/2.3)	307	2540, T
6	4.6		Illizi Basin sediments, Algeria	−28.3	58.9	−21.1	51.5	−20.2	53.4	(33.6/26/2.3)	309	3484, T
5	2.6		Reggane Basin, Harsi Bachir Formation, Algeria	−32.8	55.7	−27.8	49.9	−27	52.1	(33.6/26/2.3)	310	Derder et al. (2009)
4	4.5		Oubarakat and El-Adeb Larache Formations, Algeria	−28.2	55.5	−20.3	47.8	−19.6	49.8	(33.6/26/2.3)	317	3481, T
7	5.3		Reggane Basin, Algeria	−26.6	44.7	−17.5	36.2	−17.1	38.1	(33.6/26/2.3)	320	3402, T
5	5.9		Tin Serrinine Basin intrusions	−18.8	31.2			−18.6	33.2	(33.6/26/2.3)	348	Derder et al. (2006).
5	3.7		Griotte limestones, Algeria	−21	19.9			−21.2	21.9	(33.6/26/2.3)	365	2725, TV
6	3.7		Ben-Zireg limestones, Algeria	−19.2	19.8			−19.4	21.8	(33.6/26/2.3)	365	2521, TV
5	6.6		Air intrusives, Niger	−43.4	8.6			−43.9	11.7	(33.6/26/2.3)	409	1364, TV
			Northeast Africa (715)									
5	2.5		Main Ethiopian Rift basalts	−87.6	346.9						1.5	Kidane et al. (2006)
5	3.1		Hadar Basin, Ethiopia	−84.9	127.9						3	Dupont-Nivet et al. (2008a)
5	7.4		South Holhol–Djibouti	−86.1	336.5						4	Audin et al. (2004)
5	11.2		Volcanics, Jebel Soda, Libya	−69	4						11.5	60, T
5	8.3		Volcanics, Jebel Soda, Libya	−78.4	16.1						11.5	50, T
5	2.6		Blue Clay Formation, Malta	−73	0.5	−83.2	341.7				13.5	Abels et al. (2005)
4	12.7		Ethiopian Flood basalts, Abbay and Kessen gorges, Ethiopia	−83	13.3						26.5	3496, T
6	6		Qatrani Formation, Egypt	−79.6	332.2	−79.5	258.6				29	3280, T
5	5.4		Ethiopian Traps, Ethiopia	−77.9	32.8						30	3209, T
5	6.4		Iron ores combined, Baharia Oasis, Egypt	−83.5	318.6						37	1500, T
6	4		Fayum Province, Egypt	−71	340	−76.5	308.4				37.5	Lotfy and van der Voo (2007)
6	4.2		Mokattam limestone, Egypt	−78.1	342.8						42.5	3280, T
6	6		Fayum Province, Egypt	−68	338	−73	314.8				44.5	Lotfy and van der Voo (2007)
3	5.8		Basalts, Wadi Abu Tereifiya, Egypt	−69.4	9.4						44.5	1141, T
5	8.5		Wadi Natash volcanics, Egypt	−69.3	78.1			−69.4	78.3	(39.9/−61.4/−.2)	93	1500, T
3	18.1		Wadi Natash volcanics, Egypt	−75.7	48.3			−75.9	48.4	(40.1/−61.4/−.2)	94.5	3260, T
3	11.5		Upper Triassic Sediments, Southern Tunisia	−54.9	43.3	−59.7	27	−60.2	26.5	(40.5/−61.4/−.7)	221.5	3020, T
4	5.5		Al Azizia Formation, Kaf Bates, Libya	−54.5	45.8			−55	45.6	(40.5/−61.4/−.7)	231	3408, T
5	3.8		Al Azizia Formation, Al Azizia, Libya	−59.3	34.1			−59.8	33.7	(40.5/−61.4/−.7)	231	3408, T
4	6		Jebel Nehoud Ring Complex, Kordofan, Sudan	−40.8	71.3			−41.2	71.2	(40.4/−61.4/−.7)	280	3504, T
3	10.8		Gilif Hills volcanics, Bayuda Desert, Sudan	25.9	11.6			25.4	11.2	(40.4/−61.4/−.7)	377	2189, TV
6	9.2		Salala Ring Complex, Sudan	39.6	329.5			39.3	−30.6	(40.4/−61.4/−.7)	463	2715, TV
			East Gondwana									
			India–Pakistan (501)									
4	5.4		Mount Pavagarh Traps, Gujrat, India	−39.2	105.6			−73.4	66.6	(18.8/22.6/−39.2)	64	94, T
6	**5.7**		Mahabeleshwar Plateau lavas	−39	100.8			−72	54.5	(19/21.9/−40.2)	65	Jay et al. (2009)
4	6.7		Deccan Traps, Mahabaleshwar, India	−40	96			−70.6	42.6	(19.2/21.5/−40.7)	65.5	107, T
6	5.9		Deccan Traps, Nagpur to Bombay traverse, India	−38.4	102.4			−72.7	57.9	(19.2/21.5/−40.7)	65.5	393, T
3	3.8		Deccan Traps, Western Ghats, India	−34.5	103.6			−69.8	66.8	(19.2/21.5/−40.7)	65.5	705, T
5	9.4		Deccan dyke swarms, western India	−37.2	100.5			−70.8	56.2	(19.2/21.5/−40.7)	65.5	3094, T
3	3.8		Deccan Traps, Jalna, India	−39	99			−71.5	49.9	(19.2/21.5/−40.7)	65.5	686, T
4	10.1		Central Kerala dykes, India	−34.6	94			−67.6	42.9	(20.2/19.3/−43.8)	69	2754, T
4	12		Central Kerala gabbro dyke, India	−21.6	119.4			−74.9	73.7	(19.8/27.2/−59.2)	88	2754, T
5	7.5		St. Mary Islands, western India	−14.2	117.8			−66.7	79.4	(20.2/27.6/−58.5)	91.2	T, Torsvik et al. (2000)
3	4		Rajmahal Traps, West Bengal and Bihar, India	−3	118			−49.8	86.8	(23.4/31.3/−53.8)	116	633, T
6	3.5		Rajmahal Traps, Bihar, India	−7	117			−53.3	83.2	(23.4/31.3/−53.8)	116	678, T
6	8.3		Rajmahal Traps, West Bengal, India	−9.3	124.8			−57.6	95.2	(23.4/31.3/−53.8)	116	2977, T

4	5.5	Rajamahal Traps, North Rajmahal Hills, India	−6.5	120.2			−53.8	88.5	(23.4/31.3/−53.8)	116	T, Tarduno et al. (2001)
3	7	Sylhet Traps, Khasi Hills, India	−16	121			−63	84.4	(23.5/31.4/−53.7)	116.5	985, T
5	2.4	Rajmahal Traps, Bihar, India	−9.4	116.6			−55.1	81.1	(23.5/31.5/−53.6)	117	3095, T
5	4.6	Pachmarhi beds, Central India	−10.1	130.1	−2.4	118.5	−45.1	71.3	(29.8/42.1/−60.5)	206.5	593, T
4	4.6	Mangli Beds, Central India	7.3	124.3	12.2	110.9	−28.7	73.5	(29.8/42.1/−60.5)	243	593, T
5	6	Panchet clays, Karanpura Coalfields, India	7.5	120.5	13.4	109.1	−26.7	72.5	(29.8/42.1/−60.5)	248.5	162, T
6	4.3	Wargal and Chidru Formations, Salt Range, Pakistan	2.2	125.8			−44.6	83.5	(29.8/42.1/−60.5)	250.5	2467, T
3	1.8	Kamthi beds, Tadoba, India	4.1	102.8	10.2	94.5	−20.3	58.1	(29.8/42.1/−60.5)	250.5	593, T
6	6.5	Kamthi red beds, Wardha Valley, Central India	4	129	9.5	115.1	−33.2	75.8	(29.8/42.1/−60.5)	250.5	163, T
3	12.1	Alozai Formation, Baluchistan, Pakistan	18.1	111			−23.8	77	(29.8/42.1/−60.5)	289.5	1236, T
		Arabia (503)									
5	4.1	Volcanics, Syria	−82.4	62.2			−82.9	57.8	(36.5/18/−.8)	2.5	Abou Deeb et al. (1999); Abou Deeb and Tarling (2005)
5	3.4	Volcanics, Syria	−76	13.5			−75.2	−3.1	(36.5/18/−4.5)	19	Abou Deeb et al. (1999); Abou Deeb and Tarling (2005)
5	**3.6**	Afro-Arabian flood volcanic province, Yemen	−74.2	69.1			−77.7	46.7	(35.7/20.4/−7.1)	29	Riisager et al. (2005)
3	7.2	Abu Durba sediments, SW Sinai, Egypt	−25.6	64	−13.4	58.4	−17.7	51.5	(37.1/17.1/−8.9)	306.5	2784, T
		Madagascar (702)									
5	4.4	Antanimena and Mailaka volcanics	−74	43.7						86.5	3481, T
4	7.6	Volcanics, Massif d'Androy Andria	−64	63						87	547, T
4	4.9	Volcanics, Antanimena Andria	−66.1	49.7						87	708, T
4	4.4	Volcanics, Southeast Coast Andria	−65.8	35.6						87	708, T
4	8.9	Volcanics, Mangoky–Anilahy Andria	−73.7	73.1						87	708, T
5	4.3	Dolerites, east Madagascar	−65.5	38						87	3211, T
4	6.9	Volcanics, Mailaka Andria	−70.3	63.1						87	708, T
5	2.4	Volcanics, Southwest Madagascar	−76.8	68.2						87	3210, T
5	10.7	d'Analava complex	−66.7	43.5						91	T, Meert and Tamrat (2006)
3	5.9	Isalo Group	−74	97.1	−65.2	70.8	−50.9	59.5	(14.8/137.5/−15.4)	206.5	147, T
3	7.6	Combined Sakamena Rakotosolofo et al. 1999	−76.7	110.8	−68.4	73.5	−54.3	60.4	(14.8/137.5/−15.4)	250.5	T, 3329
3	9.5	Combined Sakoa Rakotosolofo et al. 1999	−51.3	72.6	−42.5	60.2	−27.8	54.4	(14.8/137.5/−15.4)	305	3329, T
5	11	Carion Granite	−6.8	1			3.1	−2.6	(14.8/137.5/−15.4)	509	3405, TV
4	14	Stratoid Granites	−6.8	352.7			1.6	−10.7	(14.8/137.5/−15.4)	521	Meert et al. (2003)
		Australia (801)									
5	1.8	Tarakohe Quarry, New Zealand (Australian Plate)	−78.4	103.1	−70.3	148.6	−80.2	155.3	(12/48.8/−10.4)	17.5	Turner et al. (2007)
5	3.6	Barrington Volcano,New South Wales	−70.5	125.6			−80.2	19	(14.1/57/−24.4)	53	592
5	1.8	Otway Group sediments	−48.9	148.7	−45.1	146.8	−56.4	93.9	(17.2/103.2/−36)	112	1201
5	3.7	Prospect dolerite, Sydney Basin	−53	179.6			−59.2	64.5	(19.5/117.8/−56.2)	168	1177
4	6	Garrawilla volcanics and Nombi extrusives, New South Wales	−46.1	175.2			−57.3	78.3	(19.5/117.8/−56.2)	180	780
5	2.9	Tasmanian dolerite	−50.7	174.5			−56.6	69.9	(19.5/117.8/−56.2)	183	1113
6	5.1	Newcastle range volcanics	−63.8	124.5			−31.5	48.8	(19.5/117.8/−56.2)	321	3561
6	6	Brewer Conglomerate, Northern Territory	−47.1	41	−49.3	54.7	2.2	28.5	(19.5/117.8/−56.2)	367	2726, TV
6	7.8	Reef Complex, Canning Basin	−49.1	38			3.6	17.7	(19.5/117.8/−56.2)	370	1345, TV
6	15.2	Canning Basin Reef Complexes, Western Australia	−62	23.2			−10	10.7	(19.5/117.8/−56.2)	370	2942, TV
5	5	Canning basin, Upper Frasnian	−63	38.6			−10.3	18	(19.5/117.8/−56.2)	376	E. Tohver, pers.comm. (2012)
5	3	Tumblagooda Sandstone, Carnarvon Basin	−26.7	33.7	−30.4	46	21.9	25.2	(19.5/117.8/−56.2)	465	206, TV
4	13	Jinduckin Formation, Northern Territory	−13	25			38.3	1.5	(19.5/117.8/−56.2)	493	202, TV
6	7.4	Chatswood limestone and Ninmaroo Formation, Western Queensland	3.1	54.1			52.7	45	(19.5/117.8/−56.2)	495	3082, TV
3	3.8	Black Hill Norite, South Australia	−37.5	34.4			15.2	14.8	(19.5/117.8/−56.2)	500	2971, TV
6	10	Hugh River shale, Jay Creek limestone	−19.3	39.1			33.4	19	(19.5/117.8/−56.2)	510	Mitchell et al. (2010)
3	10.1	Lake Frome Group Combined, Flinders Ranges, South Australia	−31.4	26.9	−31.3	26.7	20.6	7.4	(19.5/117.8/−56.2)	510	1769, TV
3	10.4	Giles Creek dolomite, Ross River, Amadeus Basin	−38.3	24.5			13.4	6.9	(19.5/117.8/−56.2)	510	1769, TV
3	12.3	Cambrian sediments, Kangaroo Island, South Australia	−33.8	15.1	−32.8	13.9	16.4	−3.2	(19.5/117.8/−56.2)	515	1769, TV
7	6.7	Todd River dolomite, Northern Territory	−43.2	339.9			−6.2	−20.8	(19.5/117.8/−56.2)	522	1070, TV
6	14.4	Billy Creek Formation, Aroona Creek and Wirrealpa limestone, Flinders Ranges	−37.4	20.1			13.5	3.2	(19.5/117.8/−56.2)	523	1769, TV
6	7.3	Pertaoorta Group, Areyonga Gorge, Amadeus Basin	−32.7	11.5	−28.7	5.7	17.4	−11.7	(19.5/117.8/−56.2)	525	1769, TV
6	4.1	Upper Arumbera sandstone, Northern Territory	−46.6	337.3	−37.4	331.7	−6.5	−29.4	(19.5/117.8/−56.2)	534	1070, TV
5	11.4	Hawker Group, Flinders Ranges, South Australia	−21.3	14.9			27.5	−6.6	(19.5/117.8/−56.2)	535	1769, TV
6	16	Brachina Formation, Adelaide Geosyncline, South Australia	−33	328	−20.2	326.5	1.6	−45.3	(19.5/117.8/−56.2)	550	1648, TV
		East Antarctica (802)									
5	4	McMurdo Sound volcanics	−85.5	143.6			−85.5	141.7	(8.3/−49.4/.2)	1	Tauxe et al. (2004)
5	**6.3**	McMurdo volcanics combined	−87.3	137.3			−87.3	130.8	(8.2/−49.4/.3)	2	1319, T

(continued on next page)

Table 1 (*continued*)

Q	α_{95}	Com	Formation	Lat	Lon	CLat	CLon	RLat	RLon	EULER	Age	GPDB RefNo/Reference
5	7		James Ross Island volcanics	−86.4	28.5			−85.7	30.7	(8.2/−49.4/.8)	5	Kristjánsson et al. (2005)
5	**2.3**		Kerguelen islands (Antarctic Plate)	−85.5	9.3			−81.7	25.3	(11.6/−48.2/4.2)	27	Camps et al. (2007)
5	4.4		Lavas and dykes, Vestfjella	−51.4	203.4			−55	98.6	(10.5/148.8/−58.2)	164	1548, T
4	3.4		Ferrar dolerites, Northern Prince Albert Mountains	−47.8	225.5			−69.3	91.3	(10.5/148.8/−58.2)	183	2721, T
3	3.3		Ferrar dolerite sill, Mount Cerberus	−57.8	224.3			−61.5	75.7	(10.5/148.8/−58.2)	183	1838, T
5	2.4		Ferrar dolerites, Wright Valley	−45.3	208			−59.4	108.3	(10.5/148.8/−58.2)	183	1599, T
5	10.2		Ferrar dolerite, McMurdo Sound	−50.5	211.4			−60	97.1	(10.5/148.8/−58.2)	183	1657, T
4	6.9		Storm Peak Lavas, Queen Alexandra Range	−44.1	231.5			−74.9	91.3	(10.5/148.8/−58.2)	193	808, T
5	3.8		Vestfjella lavas and dykes	−41.8	226.5			−73.2	105.8	(10.5/148.8/−58.2)	195	1154, T
5	5.2		Vanda lamprophyre and porphyry, Wright Valley	−2.5	23.8			37.8	−2.5	(10.5/148.8/−58.2)	471.5	1599, TV
5	7.6		South Victoria Land intrusives	−3.5	22.7			36.3	−2.7	(10.5/148.8/−58.2)	475	2966, TV
5	7.2		Teall Nunatak, Victoria Land	−11	21			29.6	2	(10.5/148.8/−58.2)	479	3187, TV
4	10.9		Lamprophyre dykes, Taylor Valley	−9.3	26.7			34.5	5.7	(10.5/148.8/−58.2)	484	1079, TV
4	12		Killer Ridge/Mount Lok	−7	21.4			32.8	−0.9	(10.5/148.8/−58.2)	499	3298, TV
4	8.1		Granitic rocks, Wright Valley	−5.4	18.5			32	−4.6	(10.5/148.8/−58.2)	500	1599, TV
3	4.5		Sør Rondane intrusives, Queen Maud Land	−28.5	9.5			9.5	6.1	(10.5/148.8/−58.2)	515	546, TV

Table 2
Relative fits of Greenland/Europe vs. North America and Europe vs. Greenland.

	Greenland vs. North America			Europe vs. Greenland			Europe vs. North America		
Age	Lat	Long	Angle	Lat	Long	Angle	Lat	Long	Angle
220				65.1	126.1	−18.9	78.6	161.9	−31.0
215				62.2	126.8	−17.8	77.4	160.3	−29.7
210				58.9	127.3	−16.8	76.0	159.0	−28.5
205				55.1	127.9	−15.8	74.5	157.7	−27.2
200				50.9	128.4	−14.9	72.8	156.6	−26.0
195				46.2	128.8	−14.1	71.0	155.6	−24.8
190				40.9	129.2	−13.3	69.0	154.8	−23.6
185				40.9	129.2	−13.3	69.0	154.8	−23.6
180				40.9	129.2	−13.3	69.0	154.8	−23.6
175				40.9	129.2	−13.3	69.0	154.8	−23.6
170				40.7	129.1	−13.3	69.0	154.8	−23.5
165				40.5	129.0	−13.2	69.0	154.8	−23.4
160				40.3	128.9	−13.1	69.0	154.8	−23.3
155				40.1	128.8	−13.0	69.0	154.8	−23.2
150				39.9	128.6	−12.9	69.0	154.8	−23.1
145				39.7	128.5	−12.8	69.0	154.8	−23.1
140				39.7	128.5	−12.8	69.0	154.8	−23.1
135				39.7	128.5	−12.8	69.0	154.8	−23.0
130				39.7	128.5	−12.8	69.0	154.8	−23.0
125	67.5	−118.5	−14.0	39.7	128.5	−12.8	69.0	154.8	−23.0
120	67.5	−118.5	−13.8	40.3	128.8	−12.9	69.0	154.7	−23.1
115	67.4	−118.6	−13.6	39.6	128.7	−12.8	68.5	154.2	−22.7
110	67.2	−118.8	−13.3	38.2	128.4	−12.6	67.7	153.3	−22.1
105	67.1	−119.0	−13.0	36.6	128.1	−12.5	66.8	152.3	−21.5
100	66.9	−119.2	−12.7	36.6	127.3	−12.3	66.8	151.6	−21.1
95	66.7	−119.4	−12.4	36.6	126.4	−12.1	66.7	150.8	−20.6
90	66.3	−120.2	−11.9	37.4	125.5	−12.0	66.6	149.9	−20.2
85	65.6	−121.9	−11.2	39.4	124.5	−12.1	66.6	149.2	−19.8
80	63.5	−125.3	−9.8	39.7	124.3	−12.1	64.1	148.0	−18.7
75	60.1	−129.8	−8.2	39.4	125.0	−12.1	60.2	147.5	−17.4
70	54.7	−135.0	−6.7	39.2	125.8	−12.1	55.7	147.1	−16.2
65	47.7	−136.8	−5.2	43.1	125.4	−12.1	54.9	146.6	−15.1
60	36.4	−137.5	−3.9	48.3	124.5	−12.2	55.6	145.8	−14.1
55	28.7	−130.8	−3.1	52.4	123.5	−12.0	58.6	144.8	−13.1
50	53.3	−109.3	−3.0	53.2	126.1	−10.0	64.4	141.0	−11.7
45	62.8	−99.1	−2.3	56.3	128.9	−8.9	65.8	137.5	−10.3
40	62.8	−99.1	−1.3	60.9	129.5	−8.3	66.7	135.6	−9.2
35	63.1	−99.1	−0.4	66.1	130.8	−7.8	67.7	132.9	−8.1
30				68.3	131.7	−7.0	68.3	131.7	−7.0
25				68.6	132.0	−6.1	68.6	132.0	−6.1
20				68.9	132.5	−5.1	68.9	132.5	−5.1
15				67.9	132.7	−3.7	67.9	132.7	−3.7
10				66.4	133.0	−2.3	66.4	133.0	−2.3
5				66.4	133.0	−1.2	66.4	133.0	−1.2

Table 3
APWP for Laurentia (North America and Greenland corrected for pre-drift position and seafloor spreading). APWP's are listed without correction for inclination shallowing in clastic sedimentary rocks (RM), or corrected for inclination shallowing using a flattening factor of 0.6 (RM f = 0.6). The latter APWP is also calculated using the spherical spline method using a moderate smoothing factor (300) and input poles were weigthed by their Q-factor (Spline 300 Q f = 0.6). N = number of input poles (*Note*: If N = 1 then we report α_{95} for that single study; If N = 0 then we have linearly interpolated the pole); A_{95} = 95% confidence circle; Plat/Plon = Pole latitude/longitude; GCD = Great Circle Distance between the RM f = 0.6 model and the spherical spline path. RM = Running Mean path with 20 Myr sliding window. Age is in million years. The recommended APWP is shown with **bold** numbers.

		RM			RM f = 0.6			Spline 300 Q f = 0.6		
Age	N	A_{95}	Plat	Plon	A_{95}	Plat	Plon	Plat	Plon	GCD
0	15	2.2	−87.5	295.4	2.3	−88.0	322.8	**−88.5**	**305.0**	**0.8**
10	16	2.2	−87.4	283.7	2.4	−88.4	334.3	**−86.7**	**314.2**	**1.9**
20	11	3.7	−84.0	325.4	3.6	−84.1	338.1	**−84.7**	**332.6**	**0.8**
30	14	3.1	−82.8	341.9	3.1	−82.8	341.9	**−82.4**	**346.5**	**0.8**
40	15	2.8	−81.7	338.1	3.2	−81.8	344.8	**−81.3**	**350.3**	**0.9**
50	20	4.0	−76.0	349.6	4.2	−75.7	358.4	**−77.4**	**2.7**	**2.0**
60	21	3.8	−74.2	355.6	3.9	−73.8	5.0	**−73.2**	**9.1**	**1.3**
70	14	4.6	−75.3	7.5	4.9	−75.0	18.0	**−75.7**	**15.0**	**1.1**
80	7	7.0	−74.4	14.6	7.9	−74.5	21.3	**−75.9**	**22.8**	**1.4**
90	4	6.3	−74.7	18.6	6.3	−74.7	18.6	**−75.7**	**17.2**	**1.0**
100	3	13.1	−75.6	0.7	13.1	−75.6	0.7	**−75.0**	**5.2**	**1.3**
110	7	4.7	−75.4	10.0	4.7	−75.4	10.0	**−74.2**	**5.4**	**1.8**
120	10	3.2	−72.5	16.6	3.2	−72.5	16.6	**−72.7**	**15.1**	**0.5**
130	7	4.0	−71.3	18.2	4.0	−71.3	18.2	**−71.3**	**19.2**	**0.3**
140	3	18.3	−63.3	357.1	7.1	−62.6	18.2	**−67.8**	**15.8**	**5.3**
150	5	12.5	−62.4	341.4	12.9	−64.1	359.8	**−66.2**	**357.6**	**2.2**
160	7	9.2	−62.7	319.3	10.6	−66.8	337.9	**−62.7**	**342.6**	**4.6**
170	6	10.6	−63.3	305.4	12.4	−67.0	316.1	**−65.9**	**317.0**	**1.1**
180	8	6.8	−65.9	275.3	6.0	−67.8	277.2	**−67.0**	**283.4**	**2.5**
190	16	3.5	−65.2	264.6	3.2	−66.5	264.9	**−66.6**	**264.5**	**0.2**
200	19	2.8	−63.5	262.8	2.6	−64.2	262.8	**−64.7**	**260.9**	**1.0**
210	27	2.3	−59.8	269.7	2.1	−61.3	270.0	**−61.1**	**267.0**	**1.4**
220	28	2.5	−56.0	278.2	2.5	−58.0	279.2	**−57.3**	**279.6**	**0.8**
230	19	3.3	−52.1	288.0	3.5	−54.5	290.1	**−53.9**	**291.6**	**1.1**
240	13	4.4	−50.2	292.4	4.7	−53.2	295.3	**−52.3**	**292.8**	**1.8**
250	4	12.5	−50.8	293.2	13.6	−53.1	294.8	**−53.0**	**295.8**	**0.6**
260	5	3.5	−52.8	302.7	3.5	−54.9	305.4	**−55.1**	**303.9**	**0.9**
270	7	4.2	−51.7	303.3	4.9	−53.1	305.3	**−53.0**	**305.1**	**0.1**
280	10	4.8	−47.4	303.4	5.2	−48.5	304.8	**−45.9**	**306.1**	**2.8**
290	13	3.9	−43.1	302.0	4.6	−44.4	303.6	**−45.1**	**305.9**	**1.8**
300	13	4.4	−42.4	302.2	5.5	−43.6	304.0	**−42.9**	**304.1**	**0.7**
310	8	7.0	−36.4	302.1	8.0	−36.4	302.9	**−33.4**	**300.3**	**3.7**
320	5	9.4	−26.9	301.6	8.2	−25.7	301.5	**−25.8**	**298.7**	**2.6**
330	5	8.8	−23.3	304.6	8.7	−21.5	304.4	**−20.1**	**305.1**	**1.4**
340	3	11.0	−21.8	310.3	8.5	−18.7	309.9	**−17.7**	**305.7**	**4.2**
350			−23.2	308.5		−18.1	306.5	**−16.3**	**303.3**	**3.5**
360			−24.6	306.8		−17.4	303.0	**−14.9**	**301.0**	**3.1**
370	1	16.0	−27.4	303.0	16.0	−16.6	299.6	**−13.1**	**298.6**	**3.6**
380			−19.5	297.9		−12.2	296.0	**−9.7**	**293.7**	**3.3**
390			−11.4	293.3		−7.8	292.4	**−5.8**	**289.5**	**3.5**
400	1	11.0	−3.3	289.0	11.0	−3.3	289.0	**−4.2**	**288.3**	**1.1**
410	3	19.2	−11.2	292.9	21.9	−6.3	292.7	**−9.2**	**295.0**	**3.7**
420	3	19.3	−16.6	299.4	26.2	−11.7	299.2	**−14.2**	**301.9**	**3.6**
430	3	17.5	−20.3	313.1	13.0	−17.8	311.7	**−18.8**	**313.2**	**1.8**
440	1	7.3	−24.0	326.6	7.3	−16.9	321.7	**−18.8**	**321.2**	**1.9**
450			−21.1	328.1		−16.5	324.8	**−17.8**	**325.2**	**1.4**
460			−18.3	329.5		−16.0	327.8	**−16.8**	**328.3**	**0.9**
470	2	11.1	−15.4	330.8	11.1	−15.4	330.8	**−15.7**	**330.7**	**0.3**
480	3	14.7	−13.8	336.1	14.7	−13.8	336.1	**−13.9**	**335.8**	**0.3**
490	7	7.9	−7.5	342.7	8.3	−6.8	341.5	**−8.5**	**340.9**	**1.8**
500	8	6.2	−3.8	344.5	6.6	−3.3	343.6	**−2.4**	**344.2**	**1.1**
510	4	12.9	−1.1	345.6	12.7	−1.4	346.0	**3.8**	**349.4**	**6.2**
520			5.5	354.9		5.3	355.1	**9.1**	**356.7**	**4.1**
530	1	6.2	11.9	4.5	6.2	11.9	4.5	**9.4**	**0.3**	**4.9**

150 Ma). Similarly, latitudinal velocities for Africa are reduced to ~6 cm/yr or less since the Late Carboniferous (Fig. 20b).

The magnitude of TPW not only affects APWPs, but also the magnitude of net lithospheric rotation (NR) derived from a palaeomagnetic reference frame. If mantle convection is the principal driving-force for plate motions, NR should approximate zero, and small deviations, typically less than 0.2°/M.y. for the past 50 Ma (thick light brown line in Fig. 25c), are commonly explained by lateral viscosity variations (O'Connell et al., 1991; Ricard et al., 1991). In an ideal world, NR calculations require absolute plate motion models (mantle models) and plate polygons for both continental and oceanic lithosphere (Torsvik et al., 2010b). Unfortunately, global absolute plate models are increasingly unreliable prior to the Late Cretaceous (~83 Ma) due to (1) models of hotspot motion becoming poorer, (2) lack of hotspot tracks, and (3) lack of relative plate circuits between the Pacific and Indo-Atlantic realm (Doubrovine and Tarduno, 2008a,b).

We have previously estimated NR back to the Late Jurassic (Fig. 25c) based on mantle models (0–100 Ma) and a TPW-corrected global palaeomagnetic model back to 150 Ma (Torsvik et al., 2010b). We observed that NR fluctuated and gradually increased back in time, but by removing a linear time-trend we estimated an average of 0.12°/Myr for the past 150 Myr. A pronounced peak between 60 and 50 Ma (0.33°/M.y.) was attributed to the unprecedented acceleration and deceleration of the Indian plate. As a comparison and as a TPW sensitivity test we here calculate NR

Table 4
APWP for Stable Europe/Baltica (Siberia after 251 Ma). The recommended APWP is shown with **bold** numbers. See Table 3 for more information.

		RM			RM f = 0.6			Spline 300 Q f = 0.6		
Age	N	A95	Plat	Plon	A95	Plat	Plon	Plat	Plon	GCD
0	5	5.5	−82.5	312.2	5.5	−82.5	312.2	**−83.7**	**290.3**	**2.9**
10	7	5.2	−81.8	327.2	5.2	−81.8	327.2	**−80.2**	**331.1**	**1.7**
20	4	7.6	−78.6	331.6	7.6	−78.6	331.6	**−78.0**	**336.9**	**1.2**
30	2	21.1	−80.3	332.6	21.1	−80.3	332.6	**−78.9**	**340.6**	**2.0**
40	1	3.4	−80.8	2.0	3.4	−80.8	2.0	**−79.2**	**346.6**	**3.1**
50	8	4.7	−78.0	346.2	2.5	−79.6	344.2	**−78.9**	**349.8**	**1.2**
60	13	3.0	−77.2	346.1	2.2	−78.1	345.0	**−77.7**	**344.1**	**0.5**
70	7	3.1	−75.7	345.5	3.1	−75.7	345.5	**−74.7**	**338.3**	**2.1**
80	4	3.9	−72.3	333.2	3.9	−72.3	333.2	**−73.5**	**336.7**	**1.6**
90	4	6.2	−73.4	338.1	6.2	−73.4	338.1	**−74.2**	**339.0**	**0.9**
100	2	14.3	−78.6	352.0	14.3	−78.6	352.0	**−77.6**	**343.2**	**2.1**
110	1	2.5	−80.8	338.4	2.5	−80.8	338.4	**−79.7**	**348.2**	**2.0**
120			−78.8	349.8	0.0	−78.8	349.8	**−78.7**	**359.0**	**1.8**
130			−76.5	357.5	0.0	−76.5	357.5	**−77.1**	**2.4**	**1.3**
140	1	2.9	−74.0	3.0	2.9	−74.0	3.0	**−75.3**	**1.7**	**1.3**
150	6	5.0	−74.7	328.5	5.0	−74.7	328.5	**−75.7**	**342.3**	**3.7**
160	6	5.7	−72.5	316.5	5.7	−72.5	316.5	**−72.9**	**318.0**	**0.6**
170	3	14.4	−69.0	302.7	14.4	−69.0	302.7	**−67.7**	**297.8**	**2.2**
180	3	6.6	−68.9	285.5	6.6	−68.9	285.5	**−68.5**	**287.2**	**0.7**
190	4	12.2	−69.9	281.7	12.2	−69.9	281.7	**−66.6**	**281.8**	**3.3**
200	6	10.9	−58.0	284.0	10.4	−59.3	280.3	**−57.7**	**279.7**	**1.7**
210	5	6.7	−51.6	290.5	6.1	−54.7	284.5	**−53.9**	**287.4**	**1.9**
220	4	3.4	−49.1	306.4	6.8	−51.2	304.2	**−51.8**	**300.2**	**2.6**
230	6	5.8	−50.7	311.2	5.1	−51.8	309.7	**−51.3**	**309.7**	**0.5**
240	8	7.1	−52.9	328.5	5.8	−56.3	325.2	**−54.5**	**321.8**	**2.6**
250	16	3.7	−52.8	332.8	2.6	−55.6	329.8	**−56.3**	**331.4**	**1.1**
260	20	2.8	−52.0	332.2	2.2	−54.5	329.8	**−54.1**	**332.2**	**1.4**
270	16	3.3	−48.9	339.1	3.6	−51.1	337.4	**−51.5**	**338.5**	**0.8**
280	29	2.4	−44.7	346.5	2.4	−45.1	346.3	**−46.0**	**345.4**	**1.1**
290	47	1.7	−42.3	347.0	1.9	−43.1	346.5	**−42.3**	**347.3**	**1.0**
300	27	2.3	−41.5	347.9	2.7	−42.6	347.0	**−44.2**	**346.6**	**1.6**
310	6	6.3	−42.5	347.8	5.9	−43.5	347.0	**−39.7**	**343.1**	**4.8**
320			−28.5	339.9	0.0	−29.0	339.6	**−29.6**	**337.9**	**1.6**
330	2	8.3	−14.2	334.0	8.3	−14.2	334.0	**−18.2**	**334.6**	**4.1**
340	2	8.3	−14.2	334.0	8.3	−14.2	334.0	**−9.3**	**333.1**	**4.9**
350			−10.6	331.7	0.0	−10.6	331.7	**−2.5**	**331.5**	**8.1**
360			−6.9	329.5	0.0	−6.9	329.5	**2.0**	**329.7**	**8.9**
370			−3.3	327.3	0.0	−3.3	327.3	**4.6**	**327.3**	**7.9**
380			0.4	325.2	0.0	0.4	325.2	**5.9**	**324.6**	**5.5**
390	1	11.0	4.0	323.0	11.0	4.0	323.0	**5.9**	**321.7**	**2.3**
400	3	8.2	0.3	320.3	8.2	0.3	320.3	**4.7**	**319.2**	**4.5**
410	7	10.0	−3.4	327.6	10.0	−3.4	327.6	**−0.2**	**322.5**	**6.0**
420	16	7.3	−13.0	338.6	7.3	−12.6	338.6	**−12.9**	**340.1**	**1.5**
430	10	3.3	−20.1	348.5	3.5	−19.5	348.5	**−19.8**	**355.5**	**6.6**
440			−8.7	12.2	0.0	−8.4	12.2	**−17.0**	**9.7**	**8.9**
450	2	4.9	4.0	34.5	4.9	4.0	34.5	**−6.5**	**24.5**	**14.5**
460	5	7.2	9.1	39.7	7.2	9.1	39.7	**7.0**	**38.1**	**2.7**
470	10	5.8	20.2	49.9	5.8	20.2	49.9	**17.8**	**48.7**	**2.6**
480	7	5.8	23.4	52.9	5.8	23.4	52.9	**27.3**	**58.8**	**6.6**
490	2	86.3	37.6	96.5	66.7	44.2	93.1	**34.7**	**72.0**	**18.7**
500	2	86.3	37.6	96.5	66.7	44.2	93.1	**40.3**	**85.1**	**7.0**
510	2	86.3	37.6	96.5	66.7	44.2	93.1	**46.7**	**93.3**	**2.6**
520			48.7	106.8	0.0	56.5	96.1	**54.5**	**98.6**	**2.4**
530	1	6.9	58.4	122.5	6.9	68.7	102.2	**63.5**	**102.0**	**5.1**

Table 5
APWP for Laurussia/Laurasia (<251 Ma). The recommended APWP is shown with **bold** numbers. See Table 3 for more information.

		RM			RM f = 0.6			Spline 300 Q f = 0.6		
Age	N	A95	Plat	Plon	A95	Plat	Plon	Plat	Plon	GCD
0	20	2.1	−86.3	300.7	2.3	−86.6	313.4	**−87.9**	**289.1**	**1.7**
10	23	2.4	−85.9	305.8	2.4	−86.4	325.5	**−83.8**	**326.2**	**2.6**
20	15	3.3	−82.8	319.7	3.3	−83.1	327.3	**−83.0**	**327.2**	**0.2**
30	16	2.9	−83.4	328.5	2.9	−83.4	328.5	**−83.0**	**333.1**	**0.7**
40	16	2.8	−82.5	322.8	3.1	−83.0	329.0	**−82.9**	**339.0**	**1.2**
50	28	2.9	−78.1	339.9	2.9	−79.0	346.8	**−80.7**	**343.1**	**1.9**
60	34	2.5	−77.1	343.0	2.4	−78.0	349.7	**−77.9**	**350.3**	**0.1**
70	21	3.2	−78.5	346.9	3.5	−79.3	355.1	**−79.9**	**347.0**	**1.6**
80	11	5.1	−77.6	347.0	5.9	−78.5	350.6	**−80.3**	**355.0**	**2.0**
90	8	5.0	−77.4	349.6	5.0	−77.4	349.6	**−76.7**	**345.9**	**1.1**
100	5	6.2	−78.7	348.2	6.2	−78.7	348.2	**−78.0**	**345.6**	**0.9**
110	8	4.1	−80.0	355.0	4.1	−80.0	355.0	**−78.5**	**359.0**	**1.8**
120	10	3.2	−78.0	14.0	3.2	−78.0	14.0	**−78.3**	**12.7**	**0.4**
130	8	3.6	−76.8	16.3	3.6	−76.8	16.3	**−74.3**	**26.5**	**3.5**
140	4	11.8	−68.7	2.6	6.8	−70.3	22.7	**−70.7**	**22.7**	**0.4**
150	11	6.5	−70.0	339.1	6.7	−72.5	348.1	**−70.2**	**359.3**	**4.3**
160	13	6.0	−66.4	322.6	6.2	−70.2	330.4	**−69.7**	**335.7**	**1.9**
170	9	7.8	−62.9	310.5	8.5	−66.3	315.0	**−65.2**	**313.1**	**1.3**
180	11	5.5	−61.8	287.2	4.8	−63.3	287.7	**−64.6**	**290.6**	**1.8**
190	20	3.7	−60.4	281.1	3.4	−61.4	281.0	**−62.6**	**280.6**	**1.2**
200	25	3.0	−57.0	282.6	2.8	−57.8	281.6	**−56.5**	**279.3**	**1.8**
210	32	2.2	−53.7	291.9	2.1	−55.5	290.9	**−55.2**	**288.8**	**1.2**
220	32	2.3	−50.9	302.9	2.4	−53.0	303.0	**−52.4**	**303.8**	**0.8**
230	25	2.8	−48.7	312.5	2.8	−51.0	313.3	**−50.2**	**314.6**	**1.1**
240	21	4.0	−49.1	321.3	3.7	−52.3	321.5	**−52.4**	**321.1**	**0.2**
250	20	3.9	−51.9	329.5	3.2	−54.5	327.5	**−55.1**	**328.7**	**0.9**
260	25	2.3	−51.6	331.0	1.9	−54.0	329.5	**−54.0**	**331.6**	**1.2**
270	23	2.8	−49.1	335.5	2.9	−51.0	334.8	**−51.6**	**334.0**	**0.8**
280	39	2.6	−45.0	341.8	2.6	−45.6	342.0	**−45.0**	**340.9**	**1.0**
290	60	2.1	−42.2	342.7	2.2	−43.1	342.6	**−42.7**	**343.5**	**0.7**
300	40	2.9	−41.3	341.3	3.0	−42.4	341.2	**−43.2**	**340.2**	**1.1**
310	14	6.2	−37.9	336.4	6.4	−38.3	336.5	**−33.7**	**332.8**	**5.5**
320	6	9.3	−26.6	331.0	8.9	−25.6	331.0	**−23.5**	**327.4**	**3.9**
330	7	6.3	−19.0	333.1	6.0	−17.7	333.1	**−16.7**	**333.0**	**0.9**
340	5	6.2	−17.6	336.7	4.8	−15.8	336.7	**−14.4**	**335.1**	**2.0**
350			−20.6	334.8		−15.6	333.9	**−13.0**	**335.4**	**2.5**
360			−22.5	332.8		−14.5	331.2	**−11.4**	**332.9**	**3.5**
370	1	16.0	−24.8	330.8	16.0	−13.8	328.6	**−8.4**	**329.9**	**5.6**
380			−11.4	325.8		−5.8	324.9	**−3.8**	**326.1**	**2.3**
390	2	10.9	2.2	321.3	10.9	2.2	321.3	**1.4**	**322.5**	**1.4**
400	4	5.0	0.4	320.1	5.0	0.4	320.1	**3.9**	**319.2**	**3.7**
410	10	7.7	−4.7	326.2	7.8	−3.2	326.3	**0.3**	**321.8**	**5.8**
420	19	6.5	−13.1	337.1	6.7	−12.0	337.1	**−12.4**	**337.6**	**0.6**
430	13	4.9	−19.6	348.3	4.6	−18.7	348.0	**−22.2**	**354.7**	**7.2**

purely based on reconstructions of the continental lithosphere (28–39% of the Earth's surface) through time, but extended back to the Late Carboniferous. Mean NR is higher, as expected, averaging to 0.45 ± 0.25°/M.y. for the past 300 Myr with conspicuous peaks at 110–105 Ma and 150–145 Ma, which reaches almost 1°/M.y. Because TPW is associated with toroidal components of plate motion, these and many other highs are reduced after TPW correction resulting in the lowering of the NR mean to 0.35 ± 0.21° for the past 300 Ma and 0.28 ± 0.14° for the past 150 M.y. NR calculated from only continental lithosphere should generally be considered as maximum values, but except for a notable spike between 40 and 50 Ma, such simplified NR estimates for the past 150 M.y. (corrected for TPW) show gross similarities with 'properly' determined NR. Interestingly, NR estimates purely based on continental lithosphere are considerable lower than the HS3 model of Gripp and Gordon (2002). The latter model (NR = 0.43°/M.y.) is widely used in the geodynamic community but not recommended (Torsvik et al., 2010b).

8. Conclusions and future outlook

In this extensive review of Phanerozoic palaeomagnetic poles, mostly derived from the cratonic elements of Gondwana, Laurentia, Baltica/Europe and Siberia, we have constructed new APWPs for Laurentia and Baltica, their Caledonian (Silurian) merger into Laurussia, and subsequent Late Permian merger of Laurussia and Siberia into Laurasia. After the main Pangaea assembly phase (~320 Ma), palaeomagnetic poles from Gondwana and Laurussia/Laurasia were combined to a Global APWP (GAPWaP). We have generated APWPs without/with correction for potential inclination error and conclude that all detrital sedimentary poles should be corrected for inclination shallowing, unless previously corrected using either the inclination–elongation method or anisotropy of magnetic susceptibility information (Tauxe and Kent, 2004;

Table 6
a. Relative fits for Gondwana (South Africa is fixed). Fits at 160 Ma are used back to 550 Ma.

	NW Africa			NE Africa			Somalia			Madagascar			India			Arabia		
AGE	Lat	Long	Angle	Lat	Long	Angle	Lat	Long	Angle	Lat	Long	Angle	Lat	Long	Angle	Lat	Long	Angle
160	33.6	26.0	2.3	40.5	−61.4	−0.7	9.9	143.0	−0.2	14.7	137.6	−15.6	29.9	42.3	−60.5	37.1	17.2	−8.9
155	33.6	26.0	2.3	40.5	−61.4	−0.7	9.9	143.0	−0.2	10.7	130.3	−13.2	27.1	41.4	−61.6	37.1	17.2	−8.9
150	33.6	26.0	2.3	40.5	−61.4	−0.7	9.9	143.0	−0.2	4.6	120.2	−11.1	24.3	40.6	−62.8	37.1	17.2	−8.9
145	33.6	26.0	2.3	40.5	−61.4	−0.7	9.9	143.0	−0.2	0.8	118.8	−9.1	22.8	39.2	−62.5	37.1	17.2	−8.9
140	33.6	26.0	2.3	40.5	−61.4	−0.7	9.9	143.0	−0.2	0.6	−55.4	7.4	22.1	37.7	−61.4	37.1	17.2	−8.9
135	33.6	26.0	2.3	40.5	−61.4	−0.7	9.9	143.0	−0.2	1.1	−56.9	5.9	21.3	36.4	−61.5	37.1	17.2	−8.9
130	33.7	26.0	2.0	40.5	−61.4	−0.7	9.9	143.0	−0.2	2.6	−63.3	3.9	21.4	36.4	−60.0	37.1	17.2	−8.9
125	33.6	26.0	1.0	40.5	−61.4	−0.7	9.9	143.0	−0.2	2.6	−63.3	1.8	23.5	35.0	−55.2	37.1	17.2	−8.9
120	0.0	0.0	0.0	40.5	−61.4	−0.7	9.9	143.0	−0.2	0.0	0.0	0.0	24.0	32.0	−53.1	37.1	17.2	−8.9
115				40.5	−61.4	−0.6	9.9	143.0	−0.2				23.3	31.1	−54.0	36.9	17.8	−8.8
110				40.5	−61.4	−0.5	9.9	143.0	−0.2				22.6	30.3	−54.9	36.6	18.4	−8.8
105				40.5	−61.4	−0.4	9.9	143.0	−0.2				21.9	29.6	−55.9	36.4	19.0	−8.7
100				40.5	−61.4	−0.3	9.9	143.0	−0.2				21.3	28.8	−56.8	36.1	19.6	−8.7
95				40.6	−61.4	−0.2	9.9	143.0	−0.2				20.7	28.1	−57.8	35.9	20.2	−8.6
90				39.5	−61.4	−0.1	9.9	143.0	−0.2				20.0	27.5	−58.8	35.6	20.8	−8.6
85				27.7	−61.4	0.0	9.9	143.0	−0.2				22.2	22.5	−53.9	35.4	21.3	−8.5
80				0.0	0.0	0.0	9.9	143.0	−0.2				21.1	21.2	−51.2	35.3	21.6	−8.5
75							9.9	143.0	−0.2				19.9	22.0	−48.8	35.3	21.6	−8.5
70							9.9	143.0	−0.2				19.1	23.0	−45.6	35.3	21.6	−8.5
65							9.9	143.0	−0.2				16.2	27.3	−42.7	35.3	21.6	−8.5
60							9.9	143.0	−0.2				16.1	31.5	−37.2	35.3	21.6	−8.5
55							9.9	143.0	−0.2				18.5	33.8	−30.8	35.3	21.6	−8.5
50							9.9	143.0	−0.2				20.3	39.9	−24.8	35.3	21.6	−8.5
45							9.9	143.0	−0.2				21.1	43.9	−21.5	35.3	21.6	−8.5
40							9.9	143.0	−0.2				20.7	45.1	−19.5	35.3	21.6	−8.5
35							9.9	143.0	−0.2				20.7	43.9	−17.0	35.3	21.6	−8.5
30							9.9	143.0	−0.2				21.7	41.8	−14.2	35.6	20.8	−7.4
25							9.9	143.0	−0.2				23.6	38.2	−11.2	36.3	18.6	−5.6
20							9.9	143.0	−0.2				26.5	32.2	−8.3	36.5	18.0	−4.7
15							9.9	143.0	−0.2				25.4	31.3	−5.9	36.5	18.0	−4.0
10							14.9	150.2	−0.2				25.0	33.0	−3.9	36.5	18.0	−3.3
5							34.9	−165.7	−0.3				28.1	32.9	−2.0	36.5	18.0	−1.7

(continued on next page)

Table 6 (*continued*)

b. Relative fits for Gondwana (South Africa is fixed) continued (fits at 190 Ma is used back to 550 Ma).

	Australia			East Antarctica			Amazonia (SAM)			Parana (SAM)			Colorado (SAM)			Patagonia (SAM)		
AGE	Lat	Long	Angle	Lat	Long	Angle	Lat	Long	Angle	Lat	Long	Angle	Lat	Long	Angle	Lat	Long	Angle
190	19.6	117.9	−56.4	10.4	148.7	−58.4	50.0	−32.5	55.1	47.5	−33.3	56.2	47.5	−33.3	57.3	47.5	−33.3	63.0
185	19.6	117.9	−56.4	10.4	148.7	−58.4	50.0	−32.5	55.1	47.5	−33.3	56.2	47.5	−33.3	57.3	47.5	−33.3	62.2
180	19.6	117.9	−56.4	10.4	148.7	−58.4	50.0	−32.5	55.1	47.5	−33.3	56.2	47.5	−33.3	57.3	47.5	−33.3	61.3
175	19.6	117.9	−56.4	10.4	148.7	−58.4	50.0	−32.5	55.1	47.5	−33.3	56.2	47.5	−33.3	57.3	47.5	−33.3	60.5
170	19.6	117.9	−56.4	10.4	148.7	−58.4	50.0	−32.5	55.1	47.5	−33.3	56.2	47.5	−33.3	57.3	47.5	−33.3	59.7
165	19.6	117.9	−56.4	10.4	148.7	−58.4	50.0	−32.5	55.1	47.5	−33.3	56.2	47.5	−33.3	57.3	47.5	−33.3	58.8
160	19.6	117.9	−56.4	10.4	148.7	−58.4	50.0	−32.5	55.1	47.5	−33.3	56.2	47.5	−33.3	57.3	47.5	−33.3	58.0
155	17.6	115.8	−54.5	9.0	148.0	−55.6	50.0	−32.5	55.1	47.5	−33.3	56.2	47.5	−33.3	57.3	47.5	−33.3	58.0
150	15.5	113.6	−52.7	7.4	147.1	−52.8	50.0	−32.5	55.1	47.5	−33.3	56.2	47.5	−33.3	57.3	47.5	−33.3	58.0
145	15.1	113.2	−50.7	7.3	148.0	−50.9	50.0	−32.5	55.1	47.5	−33.3	56.1	47.5	−33.3	57.2	47.5	−33.3	57.7
140	15.7	113.8	−48.5	8.0	150.1	−49.5	50.0	−32.5	55.1	47.5	−33.3	56.1	47.5	−33.3	57.1	47.5	−33.3	57.5
135	16.0	113.2	−46.7	8.6	150.9	−47.8	50.0	−32.5	55.1	47.5	−33.3	56.0	47.5	−33.3	57.1	47.5	−33.3	57.2
130	15.9	111.7	−44.6	9.0	151.5	−45.5	50.1	−32.8	54.8	48.5	−33.4	55.4	48.5	−33.4	56.1	48.5	−33.4	56.1
125	15.8	110.4	−42.4	9.4	152.4	−43.2	50.8	−33.9	54.0	50.8	−33.9	54.0	50.8	−33.9	54.0	50.8	−33.9	54.0
120	16.4	109.5	−40.5	10.2	153.5	−41.5	51.7	−35.0	52.8	51.7	−35.0	52.8	51.7	−35.0	52.8	51.7	−35.0	52.8
115	16.9	105.8	−37.6	9.0	152.2	−37.8	52.1	−35.0	51.9	52.1	−35.0	51.9	52.1	−35.0	51.9	52.1	−35.0	51.9
110	17.4	101.3	−35.0	7.4	150.7	−34.1	52.9	−35.0	50.0	52.9	−35.0	50.0	52.9	−35.0	50.0	52.9	−35.0	50.0
105	17.9	95.9	−32.7	5.5	148.8	−30.5	54.1	−34.9	46.8	54.1	−34.9	46.8	54.1	−34.9	46.8	54.1	−34.9	46.8
100	18.5	89.7	−30.9	3.1	146.5	−27.0	55.5	−34.8	43.7	55.5	−34.8	43.7	55.5	−34.8	43.7	55.5	−34.8	43.7
95	16.0	86.5	−31.2	2.7	−38.3	26.0	57.1	−34.7	40.6	57.1	−34.7	40.6	57.1	−34.7	40.6	57.1	−34.7	40.6
90	17.8	81.3	−29.0	1.3	−37.1	22.5	59.0	−34.5	37.5	59.0	−34.5	37.5	59.0	−34.5	37.5	59.0	−34.5	37.5
85	19.9	75.1	−27.0	0.7	144.6	−19.0	61.2	−34.3	34.4	61.2	−34.3	34.4	61.2	−34.3	34.4	61.2	−34.3	34.4
80	20.6	69.0	−26.6	2.8	142.7	−16.3	62.7	−34.3	31.5	62.7	−34.3	31.5	62.7	−34.3	31.5	62.7	−34.3	31.5
75	20.0	63.8	−26.7	3.8	139.0	−14.1	63.2	−33.9	28.6	63.2	−33.9	28.6	63.2	−33.9	28.6	63.2	−33.9	28.6
70	17.8	60.9	−26.3	0.4	137.2	−12.5	63.5	−33.4	26.1	63.5	−33.4	26.1	63.5	−33.4	26.1	63.5	−33.4	26.1
65	15.6	60.2	−26.1	4.3	−45.3	11.9	63.7	−33.5	24.6	63.7	−33.5	24.6	63.7	−33.5	24.6	63.7	−33.5	24.6
60	14.2	58.9	−25.7	7.7	−46.1	11.2	62.5	−32.8	23.3	62.5	−32.8	23.3	62.5	−32.8	23.3	62.5	−32.8	23.3
55	13.8	57.7	−24.9	9.5	−44.5	10.5	60.7	−31.9	22.0	60.7	−31.9	22.0	60.7	−31.9	22.0	60.7	−31.9	22.0
50	14.8	56.1	−23.6	8.8	−40.7	9.5	58.2	−31.2	20.5	58.2	−31.2	20.5	58.2	−31.2	20.5	58.2	−31.2	20.5
45	14.3	54.3	−23.0	11.0	−41.8	8.4	57.0	−31.4	18.6	57.0	−31.4	18.6	57.0	−31.4	18.6	57.0	−31.4	18.6
40	14.1	52.1	−22.4	13.1	−43.6	7.2	57.1	−32.6	16.6	57.1	−32.6	16.6	57.1	−32.6	16.6	57.1	−32.6	16.6
35	13.7	51.4	−20.7	12.2	−44.2	6.2	56.5	−33.4	14.3	56.5	−33.4	14.3	56.5	−33.4	14.3	56.5	−33.4	14.3
30	13.0	50.9	−17.8	11.4	−44.8	5.1	56.7	−34.5	11.9	56.7	−34.5	11.9	56.7	−34.5	11.9	56.7	−34.5	11.9
25	13.2	49.4	−14.9	10.6	−45.7	4.0	57.7	−36.4	9.6	57.7	−36.4	9.6	57.7	−36.4	9.6	57.7	−36.4	9.6
20	12.7	49.0	−11.8	9.2	−47.1	3.0	58.5	−37.1	7.5	58.5	−37.1	7.5	58.5	−37.1	7.5	58.5	−37.1	7.5
15	11.8	51.2	−9.0	8.0	−47.4	2.4	59.6	−38.1	5.4	59.6	−38.1	5.4	59.6	−38.1	5.4	59.6	−38.1	5.4
10	11.0	54.6	−6.2	5.5	−47.1	1.7	61.8	−40.3	3.3	61.8	−40.3	3.3	61.8	−40.3	3.3	61.8	−40.3	3.3
5	12.8	56.7	−3.2	2.2	142.7	−0.9	62.1	−40.2	1.6	62.1	−40.2	1.6	62.1	−40.2	1.6	62.1	−40.2	1.6

Table 7
Gondwana APWP in South African co-ordinates. The recommended APWP are shown with **bold** numbers. See Table 3 for more information.

		RM			RM f = 0.6			Spline 500 Q f = 0.6		
Age	N	A95	Plat	Plon	A95	Plat	Plon	Plat	Plon	GCD
0	15	2.5	−87.1	11.9	2.5	−87.1	11.9	**−87.9**	**65.6**	**2.4**
10	26	2.6	−85.6	3.6	2.6	−86.5	3.4	**−85.1**	**5.1**	**1.5**
20	16	3.9	−82.8	7.2	4.3	−85.0	5.1	**−84.6**	**1.9**	**0.5**
30	8	4.9	−80.0	2.2	6.0	−82.6	353.6	**−83.1**	**346.5**	**1.1**
40	8	5.6	−75.8	356.8	6.0	−77.9	351.4	**−79.1**	**338.3**	**2.8**
50	5	7.9	−75.0	2.5	8.4	−76.7	359.5	**−77.6**	**6.4**	**1.8**
60	10	3.0	−71.0	44.9	3.0	−71.0	44.9	**−73.9**	**35.2**	**4.2**
70	11	1.7	−69.7	46.3	1.7	−69.7	46.3	**−69.7**	**47.0**	**0.2**
80	14	2.9	−70.5	53.2	2.9	−70.5	53.2	**−70.1**	**50.6**	**1.0**
90	20	2.6	−70.3	58.0	2.6	−70.3	58.0	**−69.7**	**58.7**	**0.6**
100	9	4.2	−68.9	63.9	4.2	−68.9	63.9	**−66.1**	**73.0**	**4.5**
110	13	3.2	−56.6	83.7	4.0	−56.7	82.2	**−59.9**	**81.7**	**3.2**
120	18	3.1	−54.1	82.4	3.6	−54.1	81.3	**−52.8**	**82.3**	**1.4**
130	10	4.4	−48.9	79.1	4.4	−48.9	79.1	**−49.5**	**81.1**	**1.5**
140	5	8.1	−49.9	77.4	8.1	−49.9	77.4	**−54.5**	**72.8**	**5.4**
150	4	14.5	−62.8	63.6	14.5	−62.8	63.6	**−61.0**	**64.0**	**1.8**
160	6	10.7	−61.1	74.5	10.7	−61.1	74.5	**−60.5**	**73.0**	**0.9**
170	9	6.0	−55.8	76.7	6.0	−55.7	76.7	**−52.8**	**79.3**	**3.3**
180	22	4.5	−60.6	82.5	4.5	−60.6	82.5	**−56.8**	**83.6**	**3.9**
190	26	4.4	−66.3	82.2	4.4	−66.3	82.2	**−70.3**	**82.9**	**4.1**
200	14	5.0	−72.1	65.0	6.4	−70.8	64.1	**−71.4**	**65.6**	**0.7**
210	9	5.7	−66.6	64.0	8.0	−64.6	63.0	**−62.9**	**60.1**	**2.1**
220	3	15.9	−59.0	53.6	18.0	−56.8	44.9	**−58.1**	**50.8**	**3.6**
230	7	7.2	−55.9	56.4	5.9	−54.7	47.1	**−55.0**	**48.9**	**2.5**
240	9	7.7	−51.1	65.8	9.1	−48.3	56.0	**−47.8**	**57.7**	**1.2**
250	13	6.5	−48.1	71.7	7.8	−42.6	59.7	**−43.2**	**63.5**	**2.8**
260	10	8.0	−47.8	69.4	8.4	−42.6	62.0	**−42.3**	**62.5**	**0.5**
270	11	6.0	−38.5	63.5	7.4	−38.1	59.6	**−37.5**	**59.0**	**1.6**
280	17	6.5	−37.5	59.6	7.4	−36.4	53.1	**−35.6**	**48.8**	**3.6**
290	14	7.3	−40.4	57.4	8.3	−38.7	48.8	**−36.9**	**48.1**	**1.9**
300	14	5.9	−33.3	55.7	6.8	−29.5	48.4	**−30.8**	**48.7**	**1.7**
310	14	3.9	−28.7	55.7	4.4	−24.3	48.0	**−24.3**	**47.9**	**3.1**
320	9	4.9	−26.4	53.5	5.4	−24.4	46.2	**−23.3**	**44.2**	**2.2**
330	2	16.4	−29.7	47.2	41.1	−25.3	42.5	**−23.0**	**40.3**	**3.0**
340			−18.6	33.2		−22.0	37.7	**−21.7**	**36.3**	**1.6**
350	1	5.9	−18.6	33.2	5.9	−18.6	33.2	**−19.4**	**31.4**	**1.5**
360	5	11.9	−10.2	16.5	11.8	−10.8	18.3	**−15.2**	**24.4**	**7.3**
370	7	13.0	−5.7	15.6	13.1	−6.2	16.9	**−7.8**	**16.6**	**1.3**
380	4	21.4	−0.3	12.3	21.4	−0.3	12.3	**−4.3**	**13.2**	**4.3**
390			10.0	15.0	0.0	−12.0	13.2	**−9.1**	**13.3**	**3.2**
400	2	180.0	−17.0	13.6	105.8	−23.6	14.2	**−19.8**	**13.4**	**4.4**
410	1	6.6	−43.9	11.7	6.6	−43.9	11.7	**−31.0**	**9.8**	**13.0**
420			−21.3	0.0		−23.9	2.3	**−28.9**	**2.7**	**5.3**
430			1.9	351.6		−3.5	355.5	**−14.7**	**355.3**	**11.5**
440	1	18.0	25.0	343.0	18.0	17.0	349.0	**3.1**	**350.4**	**14.0**
450	1	18.0	25.0	343.0	18.0	17.0	349.0	**20.5**	**347.8**	**4.1**
460	2	95.6	32.7	351.5	151.4	31.8	358.2	**30.5**	**349.5**	**8.6**
470	5	14.3	34.0	356.0	17.0	33.6	358.6	**33.2**	**358.6**	**0.6**
480	5	7.2	33.5	3.4	11.0	30.7	3.6	**31.1**	**6.8**	**3.3**
490	7	4.2	32.8	7.8	13.4	30.8	7.9	**34.3**	**12.9**	**5.5**
500	10	10.7	25.2	6.5	10.7	25.2	6.5	**30.7**	**10.7**	**6.7**
510	9	7.8	16.9	4.4	7.9	17.0	4.2	**19.9**	**4.0**	**2.9**
520	11	9.2	13.6	357.8	9.4	13.8	357.1	**9.3**	**351.0**	**7.5**
530	7	13.5	7.7	347.0	13.8	8.5	344.7	**4.2**	**339.8**	**6.5**
540	4	30.9	−6.9	332.1	32.4	−3.9	326.8	**−1.3**	**328.6**	**3.2**
550	2	44.7	−18.6	320.7	66.3	−14.7	315.2	**−7.5**	**313.4**	**7.4**

Table 8
Updated Siberian APWP (see Cocks and Torsvik, 2007 for pole entries and text for changes). Spline path (Q-weighted; smoothing, 300). Clastics corrected for potential I-error ($f = 0.6$). See Table 3 for more information.

Age	Plat	Plon
250	−56.1	326.2
260	−54.2	336.2
270	−51.1	343.7
280	−47.1	348.6
290	−42.8	351.2
300	−38.2	352.1
310	−34.0	351.4
320	−29.4	349.2
330	−24.7	346.0
340	−20.1	341.6
350	−15.6	336.1
360	−11.1	329.4
370	−6.8	321.5
380	−2.6	313.2
390	1.3	305.3
400	4.7	298.4
410	7.4	294.1
420	10.0	292.3
430	12.1	294.3
440	13.9	300.9
450	16.5	312.9
460	21.8	328.0
470	31.1	332.1
480	38.0	323.3
490	38.9	317.3
500	39.0	314.4
510	42.3	318.4
520	43.6	322.8
530	45.8	327.8
537	49.1	340.7

Kodama, 2009). We use a benchmark flattening (f) value of 0.6, which leads to much smoother APWPs and elimination of Pangaea reconstruction artefacts (see also Domeier et al., 2011a, 2012).

Our new I-error corrected GAPWaP is based on five hundred Laurussia/Laurasia and Gondwana poles, and owing to the large number of poles and absence (mostly) of large age gaps, running mean and spline paths are almost identical. We employ the running mean GAPWaP for palaeogeographic reconstructions and dynamic calculations because it is more easily reproduced. On the other hand, when data-coverage is poorer (i.e. before 320 Ma) we use spline-derived APWPs for all our reconstructions. With the exception of a few intervals where data are truly scarce (e.g., Mid-Devonian to Early Carboniferous) or where palaeomagnetic misfits still exist (e.g., between Jurassic Europe and North America), the palaeomagnetic data are robust. As examples, we have constructed ten palaeogeographic reconstructions from the Late Cambrian to the Palaeogene in 50 M.y. intervals. The Palaeozoic maps mainly address the location of Gondwana and peri-Gondwana terranes (e.g. Avalonia), Baltica and Laurentia, and they portray the complex evolution of large oceans such as Iapetus, Rheic Ocean, and the Palaeotethys. Maps for the times after Pangaea assembly are more global in nature and demonstrate that Pangaea was drifting systematically northward until break-up occurred in the Central Atlantic (shortly after 200 Ma and eruption of the CAMP), causing Laurasia to separate from Gondwana.

We devise two new GAPWaP's, (1) one without correction of TPW to be used in classic palaeogeographic reconstructions (Figs. 17–19 and 21–22) where the relations to the spin axis or climate zones are of importance, and (2) one with TPW correction in order to link plate reconstructions to mantle geodynamic models. The latter should always be employed when attempting to correlate surface volcanism (e.g., LIPs) with heterogeneities in the deepest mantle (e.g. LLSVPs) because the latter are kept fixed in these exercises. Net-rotation calculations must also be carried out in a TPW-corrected reference frame to avoid toroidal spikes in the analysis. We have identified four important episodes of TPW since Pangaea assembly. These episodes are recognised between 250 and 100 Ma and comprise 37% of the GAPWaP in this time interval. TPW rates vary between 0.45 and 0.8°/M.y. but cumulative TPW is nearly zero since the Late Carboniferous due to both clockwise and counterclockwise episodes of TPW centred on 0°N and 11°E. The latter observations are 'good' news because errors in linking plate reconstructions with (for instance) the eruption location of LIPs and with

Table 9
Relative fits for North America vs. NW Africa (fixed). Fits at 210 Ma are used back to 320 Ma.

AGE	Lat	Long	Angle
210	64.3	−14.7	78.0
205	64.3	−14.9	77.7
200	64.3	−15.0	77.4
195	64.3	−15.2	77.1
190	64.8	−15.0	75.8
185	65.4	−14.7	74.5
180	65.9	−14.5	73.1
175	66.5	−14.2	71.8
170	67.1	−13.9	70.6
165	67.1	−14.4	68.6
160	67.1	−15.1	66.6
155	67.1	−15.7	64.6
150	66.4	−17.8	63.2
145	66.1	−18.6	61.8
140	66.4	−18.2	60.1
135	66.4	−18.5	58.7
130	66.0	−19.2	57.7
125	65.9	−19.8	56.0
120	66.0	−20.6	54.2
115	66.7	−21.4	51.0
110	67.5	−22.1	47.5
105	68.4	−22.9	44.0
100	69.4	−23.5	40.5
95	71.6	−24.2	37.1
90	74.3	−22.7	33.9
85	76.2	−21.2	30.5
80	78.2	−18.8	27.5
75	80.4	−13.1	24.6
70	81.6	−6.5	22.4
65	82.6	3.2	20.7
60	81.6	5.1	19.1
55	79.8	4.1	17.6
50	75.9	−3.5	16.2
45	74.3	−4.3	14.6
40	74.5	−1.1	12.6
35	75.4	3.5	10.5
30	77.4	12.5	8.6
25	79.5	28.1	6.8
20	80.6	24.4	5.5
15	80.9	23.2	4.1
10	80.9	22.9	2.6
5	80.9	22.8	1.3

Table 10
Global APWP in South African co-ordinates. The recommended APWP is shown with **bold** numbers. See Table 3 for more information.

		RM no correction			RM f = 0.6			Spline 300 Q f = 0.6		
Age	N	A95	Plat	Plon	A95	Plat	Plon	Plat	Plon	GCD
0–5	24	1.9	−88.6	325.9	**1.9**	**−88.5**	**353.9**	−89.4	299.4	1.3
10	49	1.8	−86.3	342.1	**1.8**	**−86.6**	**350.0**	−84.2	349.9	2.4
20	31	2.5	−83.2	354.5	**2.6**	**−84.2**	**355.6**	−84.3	354.7	0.1
30	24	2.5	−82.0	3.2	**2.6**	**−82.9**	**0.3**	−83.3	0.1	0.4
40	24	2.7	−79.8	6.9	**2.9**	**−80.5**	**9.0**	−80.9	359.9	1.5
50	33	2.8	−75.3	20.2	**2.8**	**−75.5**	**25.6**	−77.5	23.9	2.0
60	44	2.1	−73.1	30.9	**2.1**	**−72.9**	**35.3**	−72.7	34.5	0.3
70	32	2.4	−72.0	39.7	**2.5**	**−71.7**	**43.3**	−71.5	44.0	0.3
80	25	2.7	−70.6	47.7	**2.9**	**−70.6**	**49.2**	−71.3	51.5	1.1
90	28	2.5	−69.4	55.6	**2.5**	**−69.4**	**55.6**	−68.9	55.3	0.5
100	14	3.3	−67.0	63.2	**3.3**	**−67.0**	**63.2**	−65.0	65.6	2.2
110	21	3.0	−58.2	79.7	**3.3**	**−58.2**	**78.7**	−59.7	77.8	1.5
120	28	2.4	−53.6	82.0	**2.6**	**−53.6**	**81.3**	−52.9	81.7	0.7
130	18	2.8	−49.3	80.9	**2.8**	**−49.3**	**80.9**	−47.3	84.1	3.0
140	9	5.9	−47.1	77.8	**6.0**	**−45.8**	**82.1**	−44.2	83.1	1.8
150	15	6.1	−54.0	72.7	**6.4**	**−53.1**	**77.2**	−50.2	75.3	3.2
160	19	5.0	−56.5	70.4	**5.1**	**−55.4**	**75.9**	−54.2	76.7	1.3
170	18	4.6	−56.6	70.6	**4.6**	**−55.9**	**73.9**	−53.8	72.4	2.3
180	33	3.6	−62.3	77.6	**3.4**	**−62.1**	**78.5**	−59.6	79.8	2.6
190	46	3.0	−67.0	75.5	**2.9**	**−66.8**	**76.6**	−69.6	77.7	2.8
200	39	2.6	−69.2	60.8	**2.8**	**−69.0**	**62.2**	−70.0	60.1	1.2
210	41	2.1	−64.5	53.2	**2.2**	**−64.6**	**56.3**	−65.1	55.7	0.6
220	35	2.2	−58.0	47.6	**2.3**	**−58.4**	**50.4**	−58.1	49.4	0.6
230	33	2.7	−52.9	49.3	**2.5**	**−53.0**	**50.0**	−52.1	49.8	0.9
240	31	3.8	−48.5	56.1	**3.6**	**−48.3**	**56.1**	−48.4	55.4	0.5
250	34	3.7	−45.7	64.0	**3.6**	**−44.7**	**60.7**	−44.6	63.5	2.0
260	35	2.9	−44.4	62.0	**2.6**	**−44.3**	**61.8**	−44.2	60.8	0.7
270	34	2.7	−39.0	60.2	**2.9**	**−39.8**	**60.1**	−39.6	61.0	0.7
280	56	2.6	−34.5	58.5	**2.8**	**−34.4**	**57.1**	−33.4	54.7	2.2
290	74	2.2	−32.6	56.3	**2.4**	**−32.9**	**55.4**	−32.6	56.2	0.8
300	54	2.6	−31.6	54.8	**2.8**	**−31.3**	**53.5**	−32.4	55.0	1.7
310	28	3.7	−30.2	52.2	**3.9**	**−28.0**	**48.5**	−26.4	47.1	2.0
320	15	5.7	−26.8	46.4	**4.9**	**−25.1**	**41.8**	−24.7	36.3	4.9

LLSVPs in the deep mantle are 'minimised' with low cumulative TPW. This is why palaeomagnetic reference frames corrected or not corrected for TPW both show a striking correlation between surface LIPs and the LLSVPs (e.g., compare Torsvik et al., 2006, 2010a).

Quantifying TPW back to the dawn of the Phanerozoic is much more difficult because relative (and absolute!) longitudes are unknown, except between the major Gondwana continents. After Pangaea times, we used Africa as a plate that was quasi-stable in longitude, in order to derive semi-absolute longitudes but this approach cannot be used for the Palaeozoic. We are therefore limited to identify periods of rapid APW rates and/or major cusps in the APWPs for the major continental players. APW rates for the past 320 M.y. (Fig. 25b) average to ~0.4°/M.y. with a maximum value of 1.12°/M.y. for the GAPWaP. These values are considerable lower than Palaeozoic rates for only Gondwana, Laurussia or Laurentia, which can be as high as 2°/M.y. (Fig. 26). Thus at face value there could be considerable TPW in the available data-sets. Of course, it can also be a factor that the quality of the APWPs may be degraded with increasing age.

A Siluro-Devonian cusp in the APWPs is an obvious candidate for TPW (Van der Voo, 1993; see also Evans, 2003), and is prominent in the Laurussian path (Fig. 9), and to a lesser extent in the Gondwanan path (Fig. 11); however, note the unfortunate over-reliance on only a single 410 Ma pole in the Gondwana path, whereas in the Siberian APWP (Fig. 12) the Devonian segment is heavily interpolated. We note, however, that the Rheic Ocean, once separating Laurussia and Gondwana, was narrowing dramatically during Silurian and Early Devonian times (see Figs. 17 and 18) and thus there must also have been a *significant* component of 'continental drift' in the APWPs between 430 and 400 Ma. Van der Voo (1993) estimated a cumulative TPW of 75° from the Late Ordovician to Late Devonian times (~75 M.y.) which on average amounts to 1°/M.y. For Laurussia we now consider that TPW may have occurred between 430 and 410 Ma. Total APW is ~40° (Figs. 9a and 26; 2°/M.y.) but a substantial part must include 'continental drift' as ~2500 km of the Rheic Ocean was subducted at an average rate of 12 cm/yr in this important Mid Silurian–Early Devonian interval. After 410 Ma there is no need to appeal for TPW as APW rates are as low as 0.5°/M.y. on average (Fig. 26). Conversely, Piper (2006) argues for 90° Inertial Interchange TPW between 410 and 390 Ma (4.5°/M.y.); this captivating claim is not justified by palaeomagnetic data.

To explore TPW in detail for times before Pangaea, we need to establish a semi-absolute longitude model. The plume generation zone (PGZ) method (Torsvik et al., 2008b, 2010b) may provide the much needed longitude information. However, this approach assumes that the Earth has remained in degree-two mode for the entire Phanerozoic, and that the African and Pacific LLSVPs have remained the same throughout the Phanerozoic (see Zhong et al., 2007; Torsvik et al., 2008b). The stability of the LLSVPs before Pangaea (Torsvik et al., 2010a) is currently being tested and refined by restoring continents longitudinally based on their contained LIPs and kimberlites. Satisfying the PGZ method, LIP and kimberlite occurrences should coincide with the edges of the African and/or Pacific LLSVPs. If the resulting reconstructed continents and plate

Table 11
GAPWaP (as running mean path in Table 10) but here listed in six other co-ordinate frames.

			North America		Europe		India		Amazonia		Australia		East Antarctica	
Age	N	A95	Plat	Plon	Plat	Plon	Plat	Plon	Plat	Plon	Plat	Plon	Plat	Plon
0	24	1.9	−88.5	353.9	−88.5	353.9	−88.5	353.9	−88.5	353.9	−88.5	353.9	−88.5	353.9
10	49	1.8	−86.4	342.2	−86.7	330.0	−87.2	60.4	−87.0	319.8	−86.6	119.3	−87.3	319.7
20	31	2.6	−83.7	343.2	−84.4	332.1	−83.7	74.7	−84.8	308.3	−82.2	113.0	−85.6	325.9
30	24	2.6	−82.1	338.7	−83.1	326.5	−79.7	101.7	−83.2	294.7	−77.1	121.4	−84.9	314.9
40	24	2.9	−80.1	337.2	−81.1	324.3	−74.7	106.8	−81.4	296.2	−72.9	119.5	−84.1	320.0
50	33	2.8	−76.4	354.5	−78.9	344.7	−65.1	98.4	−80.3	320.9	−69.6	109.6	−82.9	351.7
60	44	2.1	−73.6	7.5	−78.2	352.6	−48.5	100.8	−80.2	340.0	−65.5	110.3	−83.6	17.8
70	32	2.5	−73.5	12.6	−79.2	355.7	−36.4	100.7	−80.8	348.7	−63.1	112.6	−84.1	35.4
80	25	2.9	−74.7	10.5	−79.7	357.9	−29.0	103.5	−82.2	342.2	−63.1	118.5	−86.7	34.6
90	28	2.5	−76.8	4.8	−80.4	347.2	−20.9	111.4	−84.4	317.2	−62.7	130.2	−87.9	209.0
100	14	3.3	−78.7	358.4	−80.8	332.3	−19.7	113.0	−85.7	284.7	−60.8	136.4	−84.9	202.0
110	21	3.3	−75.2	21.7	−81.2	13.1	−11.1	115.9	−87.3	73.0	−52.7	140.5	−78.9	172.1
120	28	2.6	−73.7	15.5	−79.0	10.1	−8.6	116.4	−84.8	68.7	−50.2	146.4	−75.9	183.6
130	18	2.8	−70.9	5.4	−75.0	3.4	1.0	117.1	−83.6	47.4	−47.7	146.4	−73.7	178.7
140	9	6.0	−67.9	5.7	−72.4	7.9	5.3	117.9	−80.3	47.4	−44.8	147.6	−70.8	176.8
150	15	6.4	−72.6	339.4	−72.9	334.2	−2.9	122.3	−87.4	6.6	−47.0	160.8	−67.5	201.7
160	19	5.1	−72.0	325.9	−70.5	323.4	−9.7	126.6	−88.0	305.7	−47.4	172.7	−62.3	216.3
170	18	4.6	−70.1	314.8	−67.3	316.4	−10.7	125.8	−86.8	297.0	−48.6	173.3	−62.8	218.9
180	33	3.4	−74.1	290.0	−68.3	293.9	−14.8	131.3	−83.4	219.4	−45.7	182.3	−56.4	223.2
190	46	2.9	−71.6	266.4	−64.1	278.8	−19.3	133.1	−78.5	221.4	−45.9	189.2	−53.1	229.4
200	39	2.8	−64.9	259.9	−57.9	279.3	−24.4	130.0	−74.4	238.7	−50.1	195.1	−53.3	239.0
210	41	2.2	−62.0	269.0	−56.1	290.8	−23.0	124.8	−75.4	257.5	−54.3	190.8	−58.0	241.9
220	35	2.3	−57.4	279.2	−52.8	304.1	−21.0	117.7	−74.1	283.2	−60.0	183.6	−64.2	247.7
230	33	2.5	−54.8	287.6	−50.7	312.1	−17.6	113.2	−72.8	301.7	−62.6	173.8	−69.6	249.6
240	31	3.6	−55.5	298.1	−52.2	321.5	−11.6	112.5	−74.2	322.6	−60.0	162.4	−74.1	236.8
250	34	3.6	−55.8	306.6	−53.4	329.2	−6.8	112.5	−74.1	340.2	−57.0	155.2	−76.5	220.3
260	35	2.6	−56.1	308.0	−53.8	330.5	−6.0	112.7	−74.2	343.3	−56.3	154.4	−76.5	216.5
270	34	2.9	−52.2	312.4	−50.4	335.6	−3.4	108.9	−69.9	348.6	−57.0	146.1	−80.8	207.7
280	56	2.8	−46.6	315.5	−45.1	339.8	−0.9	103.5	−64.0	350.4	−58.2	135.2	−86.2	182.5
290	74	2.4	−44.6	315.4	−43.1	340.2	−0.8	101.4	−62.0	349.4	−59.1	131.6	−88.0	161.4
300	54	2.8	−42.3	315.2	−40.8	340.4	−0.7	99.2	−59.8	348.1	−60.0	127.6	−88.5	83.6
310	28	3.9	−37.0	313.4	−35.4	339.6	−1.5	93.8	−54.8	344.1	−62.7	117.6	−84.0	23.4
320	15	5.0	−31.0	309.9	−29.1	337.0	−4.1	87.6	−49.2	338.2	−66.3	104.6	−77.7	9.2

motion histories are consistent with geological records, the stability of LLSVPs for the entire Phanerozoic and perhaps longer may become a viable model — this will have profound implications for determining ancient longitude and to better quantify Palaeozoic TPW.

Acknowledgements

This paper stems from a palaeomagnetic workshop in Luleå (2009), locally organised by Sten-Åke Elming, and building upon numerous Scandinavian workshops that first started in Helsinki (1986) under the excellent leadership of Lauri Pesonen. Compilations and analysis were further developed at the Center for Advanced Study of the Norwegian Academy of Science and Letters (2010–2011). RVdV and MD were supported by a grant from the U.S. National Science Foundation, Division of Earth Sciences (Tectonics Program), and NSF's Office of International Science and Engineering (Americas Program), grant EAR-0634807. We also acknowledge funding from Statoil (Akademiavtalen), the Norwegian Research Council (Mantle Forcing: grant number 195911), Estonian Science Foundation (grant number 8701), and the European Research Council under the European Union's Seventh Framework Programme (FP7/2007–2013)/ERC advanced grant agreement number 267631 (Beyond Plate Tectonics).

Table 12
True Polar Wander correction for the past 250 Myr in Southern Africa co-ordinates (finite reconstruction rotation for the entire Earth relative to spin axis).

	Euler pole		
Age	Lat	Long	Angle
0	0	0	0
100	0	0	0
110	0	11	−8
140	0	11	−8
150	0	11	0
200	0	11	22.5
250	0	11	0

Appendix 1. Computing TPW in the absence of hotspot tracks

Finite and stage rotations for all plates, which are required to determine the motion of continents, are computed in 1 M.y. intervals. These plates are South Africa, Northwest Africa, North America, Eurasia, Greenland, South America, Antarctica, Australia, Central Indian Basin, Madagascar, India, Somalia, Northeast Africa, and Arabia. We determine for each point on a 1° latitude–longitude grid that is located on a continent (here using the −200 m contour line as a proxy for the continent–ocean boundary) whether it is located on one of these plates (except for the "Central Indian Basin"). Points that are inside polygons for Northwest Africa, Greenland, Madagascar, Somalia and Northeast Africa are assigned to these plates. Any remaining points that are inside the present-day plate boundaries for South Africa, North America, Eurasia, South America, Antarctica, Australia, India and Arabia are assigned to those plates.

All continental points are then reconstructed back in time in 1-M.y. intervals. To each point, an area 1 deg^2 cos (latitude) is assigned as its "mass". From these, the centre of mass and the moment of inertia tensor I are determined in 1-M.y. intervals. For each 1-M.y. step, we also calculate the angular momentum L, using differences between consecutive locations of reconstructed points. A mean rotation ω of all continents can thus be found by solving the equation

Table 13
GAPWaP corrected for TPW in South African co-ordinates. As running mean path in Table 10 but with added rotations from Table 12 with opposite sense of rotation.

Age	N	A95	Plat	Plon
0–5	24	1.9	−88.5	353.9
10	49	1.8	−86.6	350.0
20	31	2.6	−84.2	355.6
30	24	2.6	−82.9	0.3
40	24	2.9	−80.5	9.0
50	33	2.8	−75.5	25.6
60	44	2.1	−72.9	35.3
70	32	2.5	−71.7	43.3
80	25	2.9	−70.6	49.2
90	28	2.5	−69.4	55.6
100	14	3.3	−67.0	63.2
110	21	3.3	−65.5	72.2
120	28	2.6	−61.0	76.6
130	18	2.8	−56.8	76.9
140	9	6.0	−53.3	78.8
150	15	6.4	−53.1	77.2
160	19	5.1	−51.3	78.4
170	18	4.6	−47.7	78.7
180	33	3.4	−49.3	85.1
190	46	2.9	−49.8	86.4
200	39	2.8	−49.1	81.0
210	41	2.2	−49.9	73.0
220	35	2.3	−48.6	63.2
230	33	2.5	−46.8	57.9
240	31	3.6	−45.1	59.4
250	34	3.6	−44.7	60.7
260	35	2.6	−44.3	61.8
270	34	2.9	−39.8	60.1
280	56	2.8	−34.4	57.1
290	74	2.4	−32.9	55.4
300	54	2.8	−31.3	53.5
310	28	3.9	−28.0	48.5
320	15	4.9	−25.1	41.8

$L = I\omega$. This mean rotation is decomposed into three components in a coordinate system with one axis along the Earth's spin axis, one in the equatorial plane and passing through the longitude of the centre of mass of all continents, and one in the equatorial plane 90° away. These components are “integrated” (i.e. added up) back in time, which gives the brown and black contiguous lines in the top panel of Fig. 23. Although these “cumulative” rotations are not finite rotations in the true sense, even in a rotating coordinate system in which the zero meridian is fixed to the longitude of the centre of mass, they nevertheless provide a simple qualitative way for examining the changes in the mean continental motion through time and defining episodes of TPW.

References

Abdul Aziz, H., Hilgen, F.J., Krijgsman, W., Sanz, E., Calvo, M., 2000. Astronomical forcing of sedimentary cycles in the middle to late Miocene continental Calatayud Basin (NE Spain). Earth and Planetary Science Letters 177, 9–22.

Abdul Aziz, H., van Dam, J., Hilgen, F.J., Krijgsman, W., 2004. Astronomical forcing in Upper Miocene continental sequences: implications for the Geomagnetic Polarity Time Scale. Earth and Planetary Science Letters 222, 243–258.

Abels, H.A., Hilgen, F.J., Krijgsman, W., Kruk, R., Raffi, I., Turco, E., Zachariasse, W.J., 2005. Long-period orbital control on middle Miocene global cooling: integrated stratigraphy and astronomical tuning of the Blue Clay Formation on Malta. Paleoceanography 20. http://dx.doi.org/10.1029/2004PA001129.

Abels, H.A., Abdul Aziz, H., Ventra, D., Hilgen, F.J., 2009. Orbital climate forcing in mudflat to marginal lacustrine deposits in the Miocene Teruel Basin (northeast Spain). Journal of Sedimentary Research 79, 831–847.

Abou Deeb, J.M., Tarling, D.H., 2005. A palaeomagnetic study of the volcanic rocks of El-Mane mountain, south of Damascus, Syria. Geofisica Internacional 44, 187–195.

Abou Deeb, J.M., Otaki, M.M., Tarling, D.H., Abdeldayem, A.L., 1999. A palaeomagnetic study of Syrian volcanic rocks of Miocene to Holocene age. Geofisica Internacional 38, 17–26.

Abrajevitch, A., Van der Voo, R., Bazhenov, M.L., Levashova, N.M., McCausland, P.J.A., 2008. The role of the Kazakhstan orocline in the late Paleozoic amalgamation of Eurasia. Tectonophysics 455, 61–76.

Alvey, A. 2009. Using crustal thickness and continental lithosphere thinning factors from gravity inversion to refine plate reconstruction models for the Arctic & North Atlantic. Ph.D thesis, University of Liverpool, 189 pp.

Audin, L., Quidelleur, X., Coulié, E., Courtillot, V., Gilder, S., Manighetti, I., Gillot, P.Y., Tapponnier, P., Kidane, T., 2004. Palaeomagnetism and K–Ar and $^{40}Ar/^{39}Ar$ ages in the Ali Sabieh area (Republic of Djibouti and Ethiopia): constraints on the mechanism of Aden ridge propagation into southeastern Afar during the last 10 Myr. Geophysical Journal International 158, 327–345.

Bachtadse, V., Briden, J.C., 1990. Palaeomagnetic constraints on the position of Gondwana during Ordovician to Devonian Times. In: McKerrow, W.S., Scotese, C.R. (Eds.), Palaeozoic Palaeogeography and Biogeography. Geological Society, London, pp. 43–48.

Bazhenov, M.L., Grishanov, A.N., Van der Voo, R., Levashova, N.M., 2008. Late Permian paleomagnetic data east and west of the Urals. Geophysical and geological implications, Geophysical Journal International 173, 395–408.

Becker, T.W., Boschi, L., 2002. A comparison of tomographic and geodynamic mantle models. Geochemistry, Geophysics, Geosystems 3, 1003. http://dx.doi.org/10.1029/2001GC000168.

Besse, J., Courtillot, V., 2002. Apparent and True Polar Wander and the geometry of the geomagnetic field over the last 200 Myr. Journal of Geophysical Research 107. http://dx.doi.org/10.1029/2000JB000050.

Bilardello, D., Kodama, K.P., 2010a. Paleomagnetism and magnetic anisotropy of Carboniferous red beds from the Maritime Provinces of Canada: evidence for shallow paleomagnetic inclinations and implications for North American Apparent Polar Wander. Geophysical Journal International 180, 1013–1029.

Bilardello, D., Kodama, K.P., 2010b. Rock magnetic evidence for inclination shallowing in the early Carboniferous Deer Lake Group red beds of western Newfoundland. Geophysical Journal International 181, 275–289.

Boyden, J.A., Müller, R.D., Gurnis, M., Torsvik, T.H., Clark, J.A., Turner, M., Ivey-Law, H., Watson, R.J., Cannon, J.S., 2011. Next-generation plate-tectonic reconstructions using GPlates. In: Keller, G.R., Baru, C. (Eds.), Geoinformatics: Cyberinfrastructure for the Solid Earth Sciences. Cambridge University Press, pp. 95–113.

Brandt, D., Ernesto, M., Rocha-Campos, A.C., Dos Santos, R., 2009. Paleomagnetism of the Santa Fé Group, central Brazil: implications for the late Paleozoic Apparent Polar Wander path for South America. Journal of Geophysical Research 114 (B02101) http://dx.doi.org/10.1029/2008JB005735.

Brown, L.L., Singer, B.S., Gorring, M.L., 2004. Paleomagnetism and $^{40}Ar/^{39}Ar$ chronology of lavas from Meseta del Lago Buenos Aires, Patagonia. Geochemistry, Geophysics, Geosystems 5, Q01H04. http://dx.doi.org/10.1029/2003GC000526.

Bryan, P., Gordon, R.G., 1990. Rotation of the Colorado Plateau: an updated analysis of paleomagnetic data. Geophysical Research Letters 17, 1501–1504. http://dx.doi.org/10.1029/GL017i010p01501.

Buiter, S.J.H., Torsvik, T.H., 2007. Horizontal movements in the eastern Barents Sea constrained by numerical models and plate reconstructions. Geophysical Journal International 171, 1376–1389.

Bullard, E., Everett, J.E., Smith, A.G., 1965. The fit of continents around the Atlantic. Philosophical Transactions of the Royal Society of London, Series A: Mathematical and Physical Sciences 258 (1088), 41–51.

Burke, K., Torsvik, T.H., 2004. Derivation of large igneous provinces of the past 200 million years from long-term heterogeneities in the deep mantle. Earth and Planetary Science Letters 227, 531–538.

Burke, K., Steinberger, B., Torsvik, T.H., Smethurst, M.A., 2008. Plume generation zones at the margins of large low shear velocity provinces on the core–mantle boundary. Earth and Planetary Sciences 265, 49–60.

Camps, P., Henry, B., Nicolaysen, K., Plenier, G., 2007. Statistical properties of paleomagnetic directions in Kerguelen lava flows: implications for the late Oligocene paleomagnetic field. Journal of Geophysical Research — Solid Earth 112, B06102. http://dx.doi.org/10.1029/2006JB004648.

Cande, S.C., Stegman, D.R., 2011. Indian and African Plate motions driven by the push force of the Reunion plume head. Nature 475, 47–52.

Cande, S.C., Patriat, P., Dyment, J., 2010. Motion between the Indian, Antarctica and African plates in the early Cenozoic. Geophysical Journal International 183, 127–149.

Ceja, M.R., Goguitchaichvili, A., Calvo-Rathert, M., Morales-Contreras, J., Alva-Valdivia, L., Elguera, J.R., Urrutia-Fucugauchi, J., Granados, H.D., 2006. Paleomagnetism of the Pleistocene Tequila volcanic field (Western Mexico). Earth, Planets and Space 58, 1349–1358.

Chalmers, J.A., Laursen, K.H., 1995. Labrador Sea: the extent of continental and oceanic crust and the timing of the onset of seafloor spreading. Marine and Petroleum Geology 12, 205–217. http://dx.doi.org/10.1016/0264-8172(95)92840-S.

Chen, Z., Li, Z.-X., Powell, C.M., Balme, B.E., 1994. An early Carboniferous pole for Gondwanaland: new results from the Mount Eclipse Sandstone in the Ngalia Basin, central Australia. Journal of Geophysical Research 99, 2909–2924.

Clyde, W.C., Hamzi, W., Finarelli, J.A., Wing, S.L., Schankler, D., Chew, A., 2007. Basin-wide magnetostratigraphic framework for the Bighorn Basin, Wyoming. Geological Society of America Bulletin 119, 848–859.

Cocks, L.R.M., Torsvik, T.H., 2002. Earth geography from 500 to 400 million years ago: a faunal and palaeomagnetic review. Journal of the Geological Society of London 159, 631–644.

Cocks, L.R.M., Torsvik, T.H., 2005. Baltica from the late Precambrian to mid Palaeozoic: the gain and loss of a terranes's identity. Earth-Science Reviews 72, 39–66.

Cocks, L.R.M., Torsvik, T.H., 2007. Siberia, the wandering northern terrane and its changing geography through the Palaeozoic. Earth-Science Reviews 82, 29–74.

Cocks, L.R.M., Fortey, R.A., 2009. Avalonia: a long-lived terrane in the Lower Palaeozoic? Geological Society, London. Special Publications 325, 141–155.

Cocks, L.R.M., Torsvik, T.H., 2011. The Palaeozoic geography of Laurentia and western Laurussia: a stable craton with mobile margins. Earth-Science Reviews 106, 1–51. http://dx.doi.org/10.1016/j.earscirev.2011.01.007.
Cojan, I., Moreau, M.G., 2006. Correlation of terrestrial climatic fluctuations with global signals during the Upper Cretaceous–Danian in a compressive setting (Provence, France). Journal of Sedimentary Research 76, 589–604.
Cottrell, R.D., Tarduno, J.A., 2003. A late Cretaceous pole for the Pacific plate: implications for Apparent and True Polar Wander and the drift of hotspots. Tectonophysics 362, 321–333.
Courtillot, C., Besse, J., Théveniaut, H., 1994. North American Jurassic Apparent Polar Wander: the answer from other continents? Physics of the Earth and Planetary Interiors 82, 87–104.
Creer, K.M., Irving, E., Runcorn, S.K., 1954. The direction of the geomagnetic field in remote epochs in Great Britain. Journal of Geomagnetism and Geoelectricity 250, 164–168.
Dawes, P.R., 2009. Precambrian–Palaeozoic geology of Smith Sound, Canada and Greenland: key constraint to palaeogeographical reconstructions of northern Laurentia and the North Atlantic region. Terra Nova 21, 1–13.
De Kock, M.O., Kirschvink, J.L., 2004. Paleomagnetic constraints on the Permian–Triassic Boundary in terrestrial strata of the Karoo Supergroup, South Africa: implications for causes of the end-Permian extinction event. Gondwana Research 7, 175–183.
Deenen, M.H.L., Ruhl, M., Bonis, N.R., Krijgsman, W., Kuerschner, W., Reitsma, M., van Bergen, M.J., 2010. A new chronology for the end-Triassic mass extinction. Earth and Planetary Science Letters 291, 113–125.
Derder, M.E.M., Henry, B., Bayou, B., Ouabadi, A., Bellon, H., Djellit, H., Khaldi, A., Amenna, M., Baziz, K., Hemmi, A., Guemache, M.A., 2006. New African Lower Carboniferous paleomagnetic pole from intrusive rocks of the Tin Serririne basin (southern border of the Hoggar, Algeria). Tectonophysics 418, 189–203.
Derder, M.E.M., Henry, B., Amenna, M., Bayou, B., Djellit, H., Guemache, M.A., Hemmi, A., 2009. New structural implications for the central Sahara (Algeria), from the revisited Upper Carboniferous "Hassi Bachir" formation: paleomagnetic constraints. Tectonophysics 463, 69–76.
Domeier, M., Van der Voo, R., Denny, F.B., 2011a. Widespread inclination shallowing in Permian and Triassic paleomagnetic data from Laurentia: support from new paleomagnetic data from Middle Permian shallow intrusions in southern Illinois (USA) and virtual geomagnetic pole distributions. Tectonophysics 511, 38–52.
Domeier, M., Van der Voo, R., Tohver, E., Tomezzoli, R.N., Vizan, H., Torsvik, T.H., Kirshner, J., 2011b. New Late Permian paleomagnetic data from Argentina: refinement of the Apparent Polar Wander path of Gondwana. Geochemistry, Geophysics, Geosystems 12, Q07002. http://dx.doi.org/10.1029/2011GC003616.
Domeier, M., Van der Voo, R., Tomezzoli, R.N., Tohver, E., Hendriks, B.W.H., Torsvik, T.H., Vizan, H., Dominguez, A.R., 2011c. Support for an "A-type" Pangea reconstruction from high-fidelity Late Permian and Early–Middle Triassic paleomagnetic results from Argentina. Journal of Geophysical Research 116, B12114. http://dx.doi.org/10.1029/2011JB008495.
Domeier, M., Van der Voo, R., Torsvik, T.H., 2012. Paleomagnetism and Pangea: the road to reconciliation. Tectonophysics 514–517, 14–43. http://dx.doi.org/10.1016/j.tecto.2011.10.021.
Dominguez, A.R., Van der Voo, R., Torsvik, T.H., Hendriks, B.W.H., Abrajevitch, A., Domeier, M., Larsen, B.T., Rousse, S., 2011. The 270 Ma paleolatitude of Baltica and its significance for Pangea models. Geophysical Journal International 186, 529–550.
Donohoo-Hurley, L.L., Geissman, J.W., Lucas, S.G., 2010. Magnetostratigraphy of the uppermost Triassic and lowermost Jurassic Moenave Formation, western United States: correlation with strata in the United Kingdom, Morocco, Turkey, Italy and the eastern United States. Geological Society of America Bulletin 122, 1936–1950.
Doubrovine, P.V., Tarduno, J.A., 2008a. A revised kinematic model for the relative motion between Pacific oceanic plates and North America since the Late Cretaceous. Journal of Geophysical Research 113, B121011. http://dx.doi.org/10.1029/2008JB005585.
Doubrovine, P.V., Tarduno, J.A., 2008b. Linking the Late Cretaceous to Palaeogene Pacific plate and the Atlantic bordering continents using plate circuits and paleomagnetic data. Journal of Geophysical Research 113, B07104. http://dx.doi.org/10.1029/2008JB005584.
Dupont-Nivet, G., Sier, M., Campisano, C.J., Arrowsmith, J.R., DiMaggio, E., Reed, K., Lockwood, C., Franke, C., Hüsing, S., 2008. Magnetostratigraphy of the eastern Hadar Basin (Ledi-Geraru research area, Ethiopia) and implications for hominin paleoenvironments. In: Quade, J., Wynn, J.G. (Eds.), The Geology of Early Humans in the Horn of Africa: Geological Society of America Special Paper, 446, pp. 67–85.
Eagles, G., König, M., 2008. A model of plate kinematics in Gondwana breakup. Geophysical Journal International 173, 703–717.
Evans, D.A.D., 2003. True Polar Wander and supercontinents. Tectonophysics 362, 303–320.
Font, E., Ernesto, M., Silva, F., Correia, B., Nascimento, M.A.L., 2009. Paleomagnetism, rock magnetism and AMS of the Cabo Magmatic Province, NE Brazil, and the opening of the South Atlantic. Geophysical Journal International 179, 905–922.
Gaina, C., Roest, W., Mueller, R.D., 2002. Late Cretaceous–Cenozoic deformation of Northeast Asia. Earth and Planetary Science Letters 197, 273–286.
Gaina, C., Müller, R.D., Brown, B., Ishihara, T., Ivanov, K.S., 2007. Breakup and early seafloor spreading between India and Antarctica. Geophysical Journal International. http://dx.doi.org/10.1111/j.1365-246X.2007.03450.x.
Gaina, C., Gernigon, L., Ball, P., 2009. Palaeocene–Recent plate boundaries in the NE Atlantic and the formation of the Jan Mayen microcontinent. Journal of the Geological Society 166, 601–616.
Gallet, Y., Pavlov, V., 1996. Magnetostratigraphy of the Moyero River Section (North-Western Siberia): constraints on geomagnetic reversal frequency during the early Palaeozoic. Geophysical Journal International 125, 95–105.
Ganerød, M., Smethurst, M.A., Rousse, S., Torsvik, T.H., Prestvik, T., 2008. Reassembling the Paleogene–Eocene North Atlantic igneous province: new paleomagnetic constraints from the Isle of Mull, Scotland. Earth and Planetary Science Letters 272, 464–475.
Ganerød, M., Smethurst, M.A., Torsvik, T.H., Prestvik, T., Rousse, S., McKenna, C., van Hinsbergen, D.J.J., Hendriks, B.W.H., 2010. The North Atlantic Igneous Province reconstructed and its relation to the Plume Generation Zone: the Antrim Lava Group revisited. Geophysical Journal International 182, 183–202.
Ganerød, M., Torsvik, T.H., van Hinsbergen, D., Gaina, C., Corfu, F., Werner, S., Owen-Smith, T.M., Ashwal, L.D., Webb, S.J., Hendriks, B.W.H., 2011. Palaeoposition of the Seychelles microcontinent in relation to the Deccan Traps and the Plume Generation Zone in Late Cretaceous–Early Palaeogene time. In: Van Hinsbergen, D.J.J., Buiter, S.J.H., Torsvik, T.H., Gaina, C., Webb, S.J. (Eds.), The Formation and Evolution of Africa: A Synopsis of 3.8 Ga of Earth History: Geological Society, London, Special Publications, 357, pp. 229–252. http://dx.doi.org/10.1144/SP357.12.
Geuna, S.E., Escosteguy, L.D., 2004. Paleomagnetism of the Upper Carboniferous–Lower Permian transition from Paganzo basin, Argentina. Geophysical Journal International 157, 1071–1089.
Geuna, S.E., Somoza, R., Vizán, H., Figari, E.G., Rinaldi, C.A., 2000. Paleomagnetism of Jurassic and Cretaceous rocks in central Patagonia: a key to constrain the timing of rotations during the breakup of southwestern Gondwana? Earth and Planetary Science Letters 181, 145–160.
Goguitchaichvili, A., Petronille, M., Henry, B., Valdivia, L.A., Morales, J., Urrutia-Fucugauchi, J., 2007. Paleomagnetism of the Eastern Alkaline Province (Mexico): contribution to the time-averaged field global database and geomagnetic instability time scale. Earth, Planets and Space 59, 775–783.
Goldreich, P., Toomre, A., 1969. Some remarks on polar wandering. Journal of Geophysical Research 74, 2555–2569.
Gradstein, F.M., Ogg, J.G., Smith, A.G. (Eds.), 2004. A Geologic Time Scale 2004. Cambridge University Press, Cambridge. 589 pp.
Gripp, A., Gordon, R.G., 2002. Young tracks of hotspots and current plate velocities. Geophysical Journal International 150, 321–361.
Gurevitch, E.L., Heunemann, C., Radko, V., Westphal, M., Bachtadse, V., Pozzi, J.P., Feinberg, H., 2004. Palaeomagnetism and magnetostratigraphy of the Permian–Triassic northwest central Siberian Trap Basalts. Tectonophysics 379, 211–226.
Gurnis, M., Torsvik, T.H., 1994. Rapid drift of large continents during the late Precambrian and Palaeozoic: palaeomagnetic constraints and dynamic models. Geology 22, 1023–1026.
Hager, B.H., 1984. Subducted slabs and the geoid: constraints on mantle rheology and flow. Journal of Geophysical Research 89, 6003–6015.
Harlan, S.S., Morgan, L.A., 2010. Paleomagnetic results from Tertiary volcanic strata and intrusions, Absaroka Volcanic Supergroup, Yellowstone National Part and vicinity: contributions to the North American Apparent Polar Wander path. Tectonophysics 485, 245–259.
Harlan, S.S., Geissman, J.W., Whisner, S.C., Schmidt, C.J., 2008. Paleomagnetism and geochronology of sills of the Doherty Mountain area, southwestern Montana; implications for the timing of fold-and-thrust belt deformation and vertical-axis rotations along the southern margin of the Helena Salient. Geological Society of America Bulletin 120, 1091–1104.
Harland, W.B., Gayer, R.A., 1972. The Arctic Caledonides and earlier oceans. Geological Magazine 109, 289–314.
Heine, C., Müller, R.D., Gaina, C., 2004. Reconstructing the Lost Eastern Tethys Ocean Basin: convergence history of the SE Asian margin and marine gateways. In *Continent–Ocean Interactions in Southeast Asia*, eds. P. Clift, D. Hayes, W. Kuhnt, and P. Wang. American Geophysical Union Geophysical Monograph 149, 37–54.
Horner-Johnson, B.C., Gordon, R.G., Argus, D.F., 2007. Plate kinematic evidence for the existence of a distinct plate between the Nubian and Somalian plates along the Southwest Indian Ridge. Journal of Geophysical Research 112, BO5418. http://dx.doi.org/10.1029/2006JB004519.
Hospers, J., Van Andel, S.I., 1968. Palaeomagnetic data from Europe and North America and their bearing on the origin of the North Atlantic Ocean. Tectonophysics 6, 475–490.
Hurley, N., Van der Voo, R., 1987. Paleomagnetism of Upper Devonian reefal limestones, Canning basin, western Australia. Geological Society of America Bulletin 98, 138146.
Iglesia-Llanos, M.P., Riccardi, A.C., Singer, S.E., 2006. Paleomagnetic study of Lower Jurassic marine strata from the Neuquén Basin, Argentina: a new Jurassic Apparent Polar Wander path for South America. Earth and Planetary Science Letters 252, 379–397.
Iosifidi, A.G., Mac Niocaill, C., Khramov, A.N., Dekkers, M.J., Popov, V., 2010. Palaeogeographic implications of differential inclination shallowing in Permo-Carboniferous sediments from the Donets Basin, Ukraine. Tectonophysics 490, 229–240.
Irving, E., 1964. Paleomagnetism and Its Application to Geological and Geophysical Problems. Wiley and Sons, New York. 399 pp.
Irving, E., 1977. Drift of the major continental blocks since the Devonian. Nature 270, 304–674.
Irving, E., 1979. Paleopoles and paleolatitudes of North America and speculations about displaced terrains. Canadian Journal of Earth Sciences 16, 669–694.
Irving, E., 2004. The case for Pangea B, and the intra-Pangean megashear. In: Channell, J.E.T., Kent, D.V., Lowrie, W., Meert, J.G. (Eds.), Timescales of the paleomagnetic field: AGU Geophys. Monogr., 145, pp. 13–27.
Irving, E., Irving, G.A., 1982. Apparent Polar Wander paths Carboniferous through Cenozoic and the assembly of Gondwana. Geophysical Surveys 5, 141–188.

Irving, E., Baker, J., Wynne, P.J., Hamilton, T.S., Wingate, M.T.D., 2000. Evolution of the Queen Charlotte Basin; further paleomagnetic evidence of Tertiary extension and tilting. Tectonophysics 326, 1–22.
Jay, A.E., Mac Niocaill, C., Widdowson, M., Self, S., Turner, W., 2009. New palaeomagnetic data from the Mahabaleshwar Plateau, Deccan flood basalt province, India., implications for the volcanostratigraphic architecture of continental flood basalt provinces. Journal of the Geological Society of London 166.
Jelenska, M., Bakhmutov, V., Konstantinienko, L., 2005. Paleomagnetic and rock magnetic data from the Silurian succession of the Dniester basin, Ukraine. Physics of Earth and Planetary Interiors 149, 307–320.
Johnson, A.H., Nairn, A.E.M., 1972. Jurassic paleomagnetism. Nature 240, 551–552.
Jones, D.L., Duncan, R.A., Briden, J.C., Randall, D.E., MacNiocaill, C., 2001. Age of the Batoka basalts, northern Zimbabwe, and the duration of Karoo large igneous province magmatism. Geochemistry, Geophysics, Geosystems 2 (paper no. 2000GC000110).
Jupp, P.E., Kent, J.T., 1987. Fitting smooth paths to spherical data. Applied Statistics 36, 34–36.
Kent, D.V., Irving, E., 2010. Influence of inclination error in sedimentary rocks on the Triassic and Jurassic Apparent Pole Wander path for North America and implications for Cordilleran tectonics. Journal of Geophysical Research 115, B10103. http://dx.doi.org/10.1029/2009JB007205.
Kent, D.V., Olsen, E., 2008. Early Jurassic magnetostratigraphy and paleolatitudes from the Hartford continental rift basin (eastern North America); testing for polarity bias and abrupt polar wander in association with the Central Atlantic magmatic province. Journal of Geophysical Research 113 (B6), B06105. http://dx.doi.org/10.1029/2007JB005407.
Kent, D.V., Tauxe, L., 2005. Corrected Late Triassic latitudes for continents adjacent to the North Atlantic. Science 307, 240–244.
Kent, D.V., Van der Voo, R., 1990. Paleozoic paleogeography from paleomagnetism of the Atlantic-bordering continents. In: McKerrow, S., Scotese, C.R. (Eds.), Paleozoic Biogeography: Geological Society of London Memoir, 12, p. 4956.
Kent, J.T., Briden, J.C., Mardia, K.V., 1983. Linear and planar structure in ordered multivariate data as applied to progressive demagnetisation of palaeomagnetic remanence. Geophysical Journal of the Royal Astronomical Society 81, 75–87.
Khramov, A.N., Iosifidi, A.G., 2009. Paleomagnetism of the Lower Ordovician and Cambrian sedimentary rocks in the section of the Narva River right bank, for the construction of the Baltica kinematic model in the early Paleozoic. Izvestiya Physics Solid Earth 45, 465–481.
Kidane, T., Platzman, E., Ebinger, C.J., Abebe, B., Rochette, P., 2006. Palaeomagnetic constraints on continental break-up processes: observations from the Main Ethiopian Rift. In: Yirgu, G., Ebinger, C.J., Maguire, P.K.H. (Eds.), The Afar Volcanic Province within the East African Rift System: Geological Society London, Special Publication, 259.
King, R.F., 1955. The remanent magnetism of artificially deposited sediments. Monthly Notices Royal Astronomical Society Geophysics Supplement 7, 115–134.
Kirschvink, J.L., 1980. The least-squares line and plane and the analysis of paleomagnetic data. Geophysical Journal of the Royal Astrological Society 62, 699–718.
Klootwijk, C.T., 1996. Phanerozoic configurations of greater Australia: evolution of the north west shelf. Part two: palaeomagnetic and geological constraints on reconstructions. Australian Geol. Surv. Org. Rec., 52 (85 pp.).
Kluger-Cohen, K., Anderson, T.H., Schmidt, A., 1986. A paleomagnetic test of the proposed Mojave–Sonora megashear in northwestern Mexico. Tectonophysics 131, 23–51.
Knight, K.B., Nomade, S., Renne, R., Marzoli, A., Bertrand, H., Youbi, N., 2004. The Central Atlantic magmatic province at the Triassic–Jurassic boundary; paleomagnetic and (super 40) Ar/(super 39) Ar evidence from Morocco for brief, episodic volcanism. Earth and Planetary Science Letters 228, 143–160.
Kodama, K.P., 2009. Simplification of the anisotropy-based inclination correction technique for magnetite- and hematite bearing rocks: a case study for the Carboniferous Glenshaw and Mauch Chunk formations, North America. Geophysical Journal International 176, 467–477.
König, M., Jokat, W., 2010. Advanced insights into magmatism and volcanism of the Mozambique Ridge and Mozambique Basin in the view of new potential field data. Geophysical Journal International 180, 158–180.
Kravchinsky, A., Konstantinov, K.M., Courtillot, V., Savrasov, J.I., Valet, J.P., Cherniy, S.D., Mishenin, S.G., Parasotka, B.S., 2002. Palaeomagnetism of East Siberian traps and kimberlites: two new poles and palaeogeographic reconstructions at about 360 and 250 Ma. Geophysical Journal International 148, 1–33.
Kristjánsson, L., Gudmundsson, M.T., Smellie, J.L., McIntosh, W.C., Esser, R., 2005. Palaeomagnetic, 40Ar/39Ar, and stratigraphical correlation of Miocene–Pliocene basalts in the Brandy Bay area, James Ross Island, Antarctica. Antarctic Science 17, 409–417.
Labails, C., Torsvik, T.H., Gaina, C., Cocks, L.R.M., 2009. Global Plate Polygons 2009. SPlates Model (version 2.0). NGU Report 2009.047. 270 pp. (confidential).
Labails, C., Olivet, J.L., Aslanian, D., Roest, W.R., 2010. An alternative early opening scenario for the Central Atlantic Ocean. Earth and Planetary Science Letters 297, 355–368.
Lange, U., Bröcker, M., Armstrong, R., Żelaźniewicz, A., Trapp, E., Mezger, K., 2005. Orthogneisses of the Orlica–Śnieżnik complex (West Sudetes, Poland): geochemical characteristics, the importance of pre-Variscan migmatization and constraints on the cooling history. Journal of the Geological Society of London 162, 973–984.
Larochelle, A., 1971. Note on the paleomagnetism of two diabase dikes, Anticosti Island, Québec. Geological Association of Canada Proceedings 23, 73–76.
Liss, D., Owens, W.H., Hutton, D.H.W., 2004. New palaeomagnetic results from the Whin Sill Complex: evidence for a multiple intrusion event and revised virtual geomagnetic poles for the Late Carboniferous for the British Isles. Journal of the Geological Society of London 161, 927–938.
Lotfy, H., Van der Voo, R., 2007. Tropical northeast Africa in the middle–late Eocene: paleomagnetism of the marine-mammals sites and basalts in the Fayum province, Egypt. Journal of African Earth Science 47, 135–152.
Løvlie, R., Torsvik, T.H., 1984. Magnetic remanence and fabric properties of laboratory-deposited hematite bearing red sandstone. Geophysical Research Letters 11, 221–224.
Mac Niocaill, C., Smethurst, M.A., 1994. Palaeozoic palaeogeography of Laurentia and its margins: a reassessment of palaeomagnetic data. Geophysical Journal International 116, 715–725.
Maciel Peña, R., Goguitchaichvili, A., Garduño Monroy, V.H., Ruiz Martinez, V.C., Aguilar Reyes, B., Morales, J., Alva-Valdivia, L., Caballero Miranda, C., Urrutia-Fucugauchi, J., 2009. Paleomagnetic and rock-magnetic survey of Brunhes lava flows from Tancitaro volcano, Mexico. Geofisica Internacional 48, 375–384.
Mankinen, E.A., 2008. Paleomagnetic study of late Miocene through Pleistocene igneous rocks from the southwestern USA: results from the historic collections of the U.S. Geological Survey Menlo Park laboratory. Geochemistry, Geophysics, Geosystems 9 (5), Q05017. http://dx.doi.org/10.1029/2008GC001957.
Marcano, M.C., Van der Voo, R., Mac Niocaill, C., 1999. True Polar Wander during the Permo-Triassic. Journal of Geodynamics 28, 75–95.
Matte, P., 2001. The Variscan collage and orogeny (480–290 Ma) and the tectonic definition of the Armorica Microplate; a review. Terra Nova 13, 122–128.
McCausland, J.A., Van der Voo, R., Hall, C.M., 2007. Circum-Iapetus paleogeography of the Precambrian–Cambrian transition with a new paleomagnetic constraint from Laurentia. Precambrian Research 156, 125–152.
McElhinny, M.W., 1973. Paleomagnetism and Plate Tectonics. Cambridge University Press, Cambridge. 358 pp.
McKerrow, W.S., Mac Niocaill, C., Alberg, P., Clayton, G., Cleal, C., Eagar, M., 2000a. The Late Palaeozoic relations between Gondwana and Laurussia. In: Franke, W., Haak, V., Oncken, O., Tanner, D. (Eds.), Orogenic Processes: Quantification and Modelling in the Variscan Belt of Central Europe: Geological Society of London Special Publication, 179, pp. 9–20.
McKerrow, W.S., Mac Niocaill, C., Dewey, J.F., 2000b. The Caledonian orogeny redefined. Journal of the Geological Society of London 157, 1149–1154.
Meert, J.G., Tamrat, E., 2006. Paleomagnetic evidence for a stationary Marion hotspot: additional paleomagnetic data from Madagascar. Gondwana Research 10, 340–348.
Meert, J.G., Van der Voo, R., 1997. The assembly of Gondwana 800–550 Ma. Journal of Geodynamics 23, 223–235.
Meert, J.G., Nédélec, A., Hall, C.M., 2003. The stratoid granites of central Madagascar: paleomagnetism and further age constraints on Neoproterozoic deformation. Precambrian Research 120, 101–129.
Meijers, M.J.M., Hamers, M.F., van Hinsbergen, D.J.J., van der Meer, D.G., Kitchka, A., Langereis, C.G., Stephenson, R.A., 2010. New late Paleozoic paleopoles from the Donbas Foldbelt (Ukraine): implications for the Pangea A vs. B Controversy. Earth and Planetary Science Letters 297, 18–33.
Mejia, V., Böhnel, H., Opdyke, N.D., Ortega-Rivera, M.A., Lee, J.K.W., Aranda-Gomez, J.J., 2005. Paleosecular variation and time-averaged field recorded in late Pliocene–Holocene lava flows from Mexico. Geochemistry, Geophysics, Geosystems 6, Q07H19. http://dx.doi.org/10.1029/2004GC000871.
Mihut, D., Müller, R.D., 1998. Volcanic margin formation and Mesozoic rift propagators in the Cuvier abyssal plain off Western Australia. Journal of Geophysical Research 103, 27135–27150.
Mitchell, R.N., Evans, D.A.D., Kilian, T.M., 2010. Rapid Early Cambrian rotation of Gondwana. Geology 38, 755–758.
Molina-Garza, R.S., Ortega-Rivera, A., 2006. Chronostratigraphy and paleomagnetism of the Balsas Group in the Tuzantlán–Copalillo basin, northern Guerrero state, Mexico. Revista Mexicana de Ciencias Geologicas 23 (2), 215–232.
Morel, P., Irving, E., 1978. Tentative paleocontinental maps for the early Phanerozoic and Proterozoic. Journal of Geology 86, 535–561.
Mosar, J., Lewis, G., Torsvik, T.H., 2002. North Atlantic sea-floor spreading rates: implications for the Tertiary development of inversion structures of the Norwegian–Greenland Sea. Journal of the Geological Society of London 159, 503–515.
Muttoni, G., Kent, D.V., Garzanti, E., Bracke, P., Abrahamsen, N., Gaetani, M., 2003. Early Permian Pangea B′ to Late Permian Pangea A′. Earth and Planetary Science Letters 215, 379–394.
Nawrocki, J., Fanning, M., Lewandowska, A., Polechonska, O., Werner, T., 2008. Palaeomagnetism and the age of the Krakow volcanic rocks (S Poland). Geophysical Journal International 174, 475–488.
O'Connell, R.J., Gable, C.W., Hager, B.H., 1991. Toroidal–poloidal partitioning of lithospheric plate motions. In: Sabadini, R. (Ed.), Glacial Isostasy, Sea-Level and Mantle Rheology. Kluwer Acad, Dordrecht, Netherlands, pp. 535–551.
O'Neill, C., Müller, R.D., Steinberger, B., 2005. On the uncertainties in hot spot reconstructions and the significance of moving hot spot reference frames. Geochemistry, Geophysics, Geosystems 6, Q04003. http://dx.doi.org/10.1029/2004GC000784.
Oakey, G.N., Damaske, D., 2006. Continuity of basement structures and dyke swarms in the Kane Basin region of central Nares Strait constrained by aeromagnetic data. Polarforschung 74, 51–62.
Palencia-Ortas, A., Ruiz-Martínez, V.C., Villalaín, J.J., Osete, M.L., Vegas, R., Touil, A., Hafid, A., McIntosh, G., van Hinsbergen, D.J.J., Torsvik, T.H., 2011. A new 200 Ma paleomagnetic pole for Africa, and paleo-secular variation scatter from Central Atlantic Magmatic Province (CAMP) intrusives in Morocco (Ighrem and Foum Zguid dykes). Geophysical Journal International 185, 1220–1234.
Pavlov, E., Courtillot, V., Bazhenov, M.L., Veselovsky, R.V., 2007. Paleomagnetism of the Siberian Traps; new data and a new overall 250 Ma pole for Siberia. Tectonophysics 443, 72–92.
Pavlov, V., Bachtadse, V., Mikhailov, V., 2008. New Middle Cambrian and Middle Ordovician palaeomagnetic data from Siberia; Llandelian magnetostratigraphy and

relative rotation between the Aldan and Anabar-Angara blocks. Earth and Planetary Science Letters 276, 229–242.
Pavoni, N., 1985. Pacific/anti-Pacific bipolarity in the structure of the Earth's mantle. Eos Transactions, American Geophysical Union 66, 497.
Petronis, M.S., Hacker, D.B., Holm, D.K., Geissman, J.W., Harlan, S., 2004. Magmatic flow paths and palaeomagnetism of the Miocene Stoddard Mountain laccolith, Iron Axis region, Southwestern Utah, USA. In: Martin-Hernandez, F., Luneberg, C.M., Aubourg, C., Jackson, M. (Eds.), Magnetic Fabric: Methods and Applications: Geological Society London, Special Publications, 238, pp. 251–283.
Piper, J.D.A., 2006. A 90° Late Silurian–Early Devonian Apparent Polar Wander loop: the latest inertial interchange of planet earth? Earth and Planetary Science Letters 250, 345–357.
Plado, J., Preeden, U., Pesonen, L.J., Mertanen, S., Puura, V., 2010. Magnetic history of Early and Middle Ordovician sedimentary sequence, northern Estonia. Geophysical Journal International 180, 147–157.
Rakotosolofo, N.A., Tait, J.A., Carlotto, V., Cárdenas, J., 2006. Palaeomagnetic results from the Early Permian Copacabana Group, southern Peru: implication for Pangea palaeogeography. Tectonophysics 413, 287–299.
Rapalini, A.E., Fazzito, S., Orue, D., 2006. A new Late Permian paleomagnetic pole for stable South America; the Independencia Group, eastern Paraguay. Earth, Planets and Space 58, 1247–1253.
Rehnström, E.F., Torsvik, T.H., 2003. Cambrian sediments and Proterozoic granites in the Dividalen–Torneträsk area, northern Scandinavia; palaeomagnetism and U–Pb geochronology. Geologiska Föreningens i Stockholm Förhandlingar 125, 131–138.
Reynolds, R.L., Goldhaber, M.B., Snee, L.W., 1997. Paleomagnetic and $^{40}Ar/^{39}Ar$ results from the Grant intrusive breccia and comparison to the Permian Downeys Bluff sill — evidence for Permian igneous activity at Hicks Dome, southern Illinois Basin. U.S. Geological Survey Bulletin, 2094-G (16 pp.).
Ricard, Y., Doglioni, C., Sabbadini, R., 1991. Differential rotation between lithosphere and mantle; a consequence of lateral mantle viscosity. Journal of Geophysical Research 96 (B5), 8407–8415.
Riisager, J., Riisager, P., Pedersen, A.K., 2003a. The C27n–C26r geomagnetic polarity reversal recorded in the West Greenland flood basalt province: how complex is the transitional field? Journal of Geophysical Research 108, 2155. http://dx.doi.org/10.1029/2002JB002124.
Riisager, J., Riisager, P., Pedersen, A.K., 2003b. Paleomagnetism of large igneous provinces: case-study from West Greenland, North Atlantic igneous province. Earth and Planetary Science Letters 214, 409–425.
Riisager, P., Knight, K.B., Baker, J.A., Ukstins Peate, I., Al-Kadasi, M., Al-Subbary, A., Renne, P.R., 2005. Paleomagnetism and $^{40}Ar/^{39}Ar$ Geochronology of Yemeni Oligocene volcanics: implications for timing and duration of Afro-Arabian traps and geometry of the Oligocene paleomagnetic field. Earth and Planetary Science Letters 237, 647–672.
Rochette, P., Vandamme, D., 2001. Pangea B: an artifact of incorrect paleomagnetic assumptions? Annali Geofisicae 44, 649–658.
Ruiz-Martínez, V.C., Urrutia-Fucugauchi, J., Osete, M.L., 2010. Palaeomagnetism of the western and central sectors of the Trans-Mexican volcanic belt; implications for tectonic rotations and palaeosecular variation in the past 11 Ma. Geophysical Journal International 180, 577–595.
Ruiz-Martinez, V.C., Torsvik, T.H., van Hinsbergen, D.J.J., Gaina, C., 2012. Earth at 200 Ma: global palaeogeography refined from CAMP palaeomagnetic data. Earth and Planetary Science Letters 331–332, 67–79.
Runcorn, S.K., 1956. Palaeomagnetic comparisons between Europe and North America. Proceedings of the Geological Association of Canada 8, 77–85.
Runcorn, S.K., 1965. Palaeomagnetic comparisons between Europe and North America. Philosophical Transactions of the Royal Society of London, Series A, Mathematical and Physical Sciences 258 (1088), 1–11.
Schmidt, P.W., Embleton, B.J.J., 1990. The palaeomagnetism of the Tumblagooda Sandstone, Western Australia; Gondwana Palaeozoic apparent polar wandering. Physics of the Earth and Planetary Interiors 64, 303–313.
Schmidt, A.G., Riisager, P., Abrahamsen, N., Riisager, J., Pedersen, A.K., Van der Voo, R., 2005. Palaeomagnetism of Eocene Talerua Member lavas on Hareøen, West Greenland. Bulletin of the Geological Society of Denmark 52, 27–38.
Seguin, M.-K., Singh, A., Fyffe, L., 1985. New paleomagnetic data from Carboniferous volcanics and red beds from central New Brunswick. Geophysical Research Letters 12, 81–84.
Şengör, A.M.C., Yilmaz, Y., Sungurlu, O., 1984. Tectonics of the Mediterranean Cimmerides: nature and evolution of the western termination of Paleo-Tethys. Geological Society London Special Publication 17, 77–112.
Shatsillo, A.V., Paverman, V.I., Pavlov, V.E., 2007. Middle Paleozoic segment of the Apparent Polar Wander path from the Siberian platform: new palaeomagnetic evidence for the Silurian of the Nyuya–Berezovskii facial province. Izvestiya Physics of the Solid Earth 43, 880–889.
Shive, N., Frerichs, W.E., 1974. Paleomagnetism of the Niobrara Formation in Wyoming, Colorado, and Kansas. Journal of Geophysical Research 79, 3001–3007.
Smith, W.H.F., Sandwell, D.T., 1997. Global Sea Floor Topography from Satellite Altimetry and Ship Depth Soundings. Science 277, 1956–1962.
Somoza, R., 2007. Eocene paleomagnetic pole for South America: northward continental motion in the Cenozoic, opening of Drake Passage and Caribbean convergence. Journal of Geophysical Research B Solid Earth 112, B03104. http://dx.doi.org/10.1029/2006JB004610.
Somoza, R., Zaffarana, C.B., 2008. Mid-Cretaceous polar standstill of South America, motion of the Atlantic hotspots and the birth of the Andean Cordillera. Earth and Planetary Science Letters 271, 267–277.
Steinberger, B., Sutherland, R., O'Connell, R.J., 2004. Prediction of Emperor-Hawaii seamount locations from a revised model of global plate motion and mantle flow. Nature 430, 167–173.
Steinberger, B., Torsvik, T.H., 2008. Absolute plate motions and True Polar Wander in the absence of hotspot tracks. Nature 452, 620–623.
Steinberger, B., Torsvik, T.H., 2010. Toward an explanation for the present and past locations of the poles. Geochemistry, Geophysics, Geosystems 11. http://dx.doi.org/10.1029/2009GC002889.
Steiner, M.B., 2003. A cratonic Middle Jurassic paleopole; Callovian–Oxfordian stillstand (J-2 cusp), rotation of the Colorado Plateau, and Jurassic North American Apparent Polar Wander. Tectonics 22, 1020. http://dx.doi.org/10.1029/2001TC001284.
Steiner, M.B., Helsley, C.E., 1974. Magnetic polarity sequence of the Upper Triassic Kayenta Formation. Geology 2, 191–194.
Storey, M., Mahoney, J.J., Saunders, A.D., Duncan, R.A., Kelley, S.P., Coffin, M.F., 1995. Timing of hot spot-related volcanism and the break-up of Madagascar and India. Science 267, 852–855.
Symons, D.T.A., Bormann, R.E., Jans, R.P., 1989. Paleomagnetism of the Triassic red beds of the lower Fundy Group and Mesozoic tectonism of the Nova Scotia Platform, Canada. Tectonophysics 164, 13–24.
Symons, D.T.A., Erdmer, P., McCausland, P.J.A., 2003. A new cratonic North American paleomagnetic pole from the Yukon shows post-Eocene mobility of the Canadian Cordilleran terranes. Canadian Journal of Earth Science 40, 1321–1334.
Symons, D.T.A., Kawasaki, K., McCausland, J.A., 2009. The Yukon–Tanana terrane: part of North America at 215 Ma from paleomagnetism of the Taylor Mountain batholith, Alaska. Tectonophysics 465, 60–74.
Szurlies, M., 2004. Magnetostratigraphy; the key to a global correlation of the classic Germanic Trias; case study Volpriehausen Formation (middle Buntsandstein), central Germany. Earth and Planetary Science Letters 227, 395–410.
Szurlies, M., Bachmann, G.H., Menning, M., Nowaczyk, N.R., Kaeding, K.C., 2003. Magnetostratigraphy and high-resolution lithostratigraphy of the Permian–Triassic boundary interval in central Germany. Earth and Planetary Science Letters 212, 263–278.
Tan, X.D., Kodama, K.P., Gilder, S., Courtillot, V., 2007. Rock magnetic evidence for inclination shallowing in the Passaic Formation red beds from the Newark basin and a systematic bias of the Late Triassic Apparent Polar Wander path for North America. Earth and Planetary Science Letters 254, 345–357.
Tarduno, J.A., 2007. On the motion of Hawaii and other mantle plumes. Chemical Geology 241, 234–247.
Tarduno, J.A., Cottrell, R.D., Smirnov, A.V., 2001. High geomagnetic intensity during the Mid-Cretaceous from Thellier analysis of single plagioclase crystals. Science 291, 1779–1783.
Tauxe, L., 2005. Inclination flattening and the geocentric axial dipole hypothesis. Earth and Planetary Science Letters 233, 247–261.
Tauxe, L., 2009. Essentials of Paleomagnetism: Web Edition 1.0. , http://magician.ucsd.edu/Essentials/.
Tauxe, L., Kent, D.V., 1984. Properties of a detrital remanence carried by haematite from study of modern river deposits and laboratory redepositiomn sediments. Geophysical Journal of the Royal Astronomical Society 76, 543–561.
Tauxe, L., Kent, D.V., 2004. A simplified statistical model for the geomagnetic field and the detection of shallow bias in paleomagnetic inclinations: was the ancient magnetic field dipolar? In: Channell, J.E.T., Kent, D., Lowrie, W., Meert, J.G. (Eds.), Timescales of the paleomagnetic field. : Geophysical Monograph, 145. AGU, Washington, DC, pp. 101–117.
Tauxe, L., Gans, P., Mankinen, E.A., 2004. Paleomagnetism and $^{40}Ar/^{39}Ar$ ages from volcanics extruded during the Matuyama and Brunhes Chrons near McMurdo Sound, Antarctica. Geochemistry, Geophysics, Geosystems 5, Q06H12. http://dx.doi.org/10.1029/2003GC000656.
Tohver, E., D'Agrella Filho, M., Trindade, R.I.F., 2006. Paleomagnetic record of Africa and South America for the 1200–500 Ma interval, and evaluation of Rodinia and Gondwana assemblies. Precambrian Research 147, 193–222.
Tohver, E., Trindade, R.I.F., Solum, J.G., Hall, C.M., Riccomini, C., Nogueira, A.C., 2010. Closing the Clymene Ocean and Bending a Brasiliano belt, evidence for the Cambrian formation of Gondwana from SE Amazon craton. Geology 38, 267–270.
Tohver, E., Cawood, P.A., Rossello, E.A., Jourdan, F., 2012. Closure of the Clymene Ocean and formation of West Gondwana in the Cambrian: evidence from the Sierras Australes of the southernmost Rio de la Plata craton, Argentina. Gondwana Research 21, 394–405. http://dx.doi.org/10.1016/j.gr.2011.04.001.
Torsvik, T.H., 1998. Palaeozoic palaeogeography: a North Atlantic viewpoint. Geologiska Föreningens Förhandlingar 120, 109–118.
Torsvik, T.H., Cocks, L.R.M., 2004. Earth geography from 400 to 250 million years: a palaeomagnetic, faunal and facies review. Journal Geological Socity London 161, 555–572.
Torsvik, T.H., Cocks, L.R.M., 2009. The Lower Palaeozoic palaeogeographical evolution of the northeastern and eastern peri-Gondwanan margin from Turkey to New Zealand. In: Bassett, M.G. (Ed.), Early Palaeozoic Peri-Gondwana Terranes: New Insights from Tectonics and Biogeography: Geological Society, London, Special Publications, 325.
Torsvik, T.H., Cocks, L.R.M., 2011. The Palaeozoic palaeogeography of central Gondwana. In: Van Hinsbergen, D.J.J., Buiter, S.J.H., Torsvik, T.H., Gaina, C., Webb, S.J. (Eds.), The Formation and Evolution of Africa: A Synopsis of 3.8 Ga of Earth History: Geological Society, London, Special Publications, 357, pp. 137–166. http://dx.doi.org/10.1144/SP357.8.
Torsvik, T.H., Cocks, L.R.M., in press. New global palaeogeographical reconstructions for the Lower Palaeozoic and their generation. Memoirs of the Geological Society London.
Torsvik, T.H., Rehnström, E.F., 2003. The Tornquist Sea and Baltica–Avalonia docking. Tectonophysics 362, 67–82.
Torsvik, T.H., Smethurst, M.A., 1999. Plate tectonic modeling: virtual reality with GMAP. Computer & Geosciences 25, 395–402.

Torsvik, T.H., Van der Voo, R., 2002. Refining the paleogeography of Gondwana and Pangea: estimates of Phanerozoic non-dipole (octupole) fields. Geophysical Journal International 151, 771–794.
Torsvik, T.H., Smethurst, M.A., Van der Voo, R., Trench, A., Abrahamsen, N., Halvorsen, E., 1992. Baltica — a synopsis of Vendian–Permian palaeomagnetic data and their palaeotectonic implications. Earth-Science Reviews 33, 133–152.
Torsvik, T.H., Trench, A., Svensson, I., Walderhaug, H.J., 1993. Silurian palaeomagnetic results from Southern Britain: palaeogeographic significance and major revision of the Apparent Polar Wander Path for Eastern Avalonia. Geophysical Journal International 113, 651–668.
Torsvik, T.H., Smethurst, M.A., Meert, J.G., Van der Voo, R., McKerrow, W.S., Sturt, B.A., Brasier, M.D., Walderhaug, H.J., 1996. Continental break-up and collision in the Neoproterozoic and Palaeozoic — a tale of Baltica and Laurentia. Earth-Science Reviews 40, 229–258.
Torsvik, T.H., Tucker, R.D., Ashwal, L.D., Carter, L.M., Jamtveit, B., Vidyadharan, K.T., Venkataramana, P., 2000. Late Cretaceous India–Madagascar fit and timing of break-up related magmatism. Terra Nova 12, 220–224.
Torsvik, T.H., Van der Voo, R., Meert, J.G., Mosar, J., Walderhaug, H.J., 2001. Reconstructions of the continents around the North Atlantic at about the 60th parallell. Earth and Planetary Science Letters 187, 55–69.
Torsvik, T.H., Van der Voo, R., Redfield, T.F., 2002. Frontier — relative hotspot motions versus True Polar Wander. Earth and Planetary Science Letters 202, 185–200.
Torsvik, T.H., Gaina, C., Steinberg, M., Van der Voo, R., 2006. North Atlantic fits with implications for the Barents Sea. Norwegian Geol. Survey Industry Report (confidential).
Torsvik, T.H., Müller, R.D., Van der Voo, R., Steinberger, B., Gaina, C., 2008a. Global plate motion frames: toward a unified model. Reviews of Geophysics 46, RG3004. http://dx.doi.org/10.1029/2007RG000227.
Torsvik, T.H., Steinberger, B., Cocks, L.R.M., Burke, K., 2008b. Longitude: linking Earth's ancient surface to its deep interior. Earth and Planetary Science Letters 276, 273–283.
Torsvik, T.H., Gaina, C., Redfield, T.F., 2008c. Antarctica and global paleogeography: from Rodinia, through Gondwanaland and Pangea, to the birth of the Southern Ocean and the opening of gateways. In: Cooper, A.K., Barrett, P.J., Stagg, H., Storey, B., Stump, E., Wise, W., the 10th ISAES editorial team (Eds.), *Antarctica: A Keystone in a Changing World*. Proceedings of the 10th International Symposium on Antarctic Earth Sciences. The National Academies Press, Washington, D.C., pp. 125–140.
Torsvik, T.H., Rousse, S., Labails, C., Smethurst, M.A., 2009. A new scheme for the opening of the South Atlantic Ocean and dissection of an Aptian Salt Basin. Geophysical Journal International 177, 1315–1333.
Torsvik, T.H., Burke, K., Steinberger, B., Webb, S.C., Ashwal, L.D., 2010a. Diamonds sourced by plumes from the core mantle boundary. Nature 466. http://dx.doi.org/10.1038/nature09216.
Torsvik, T.H., Steinberger, B., Gurnis, M., Gaina, C., 2010b. Plate tectonics and net lithosphere rotation over the past 150 My. Earth and Planetary Science Letters 291, 106–112.
Trindade, R.I.F., D'Agrella Filho, M.S., Epof, I., Neves, B.B.B., 2006. Paleomagnetism of Early Cambrian Itabaiana mafic dikes (NE Brazil) and the final assembly of Gondwana. Earth and Planetary Science Letters 244, 361–377.
Tripati, A., Backman, J., Elderfield, H., Ferretti, P., 2005. Eocene bipolar glaciation associated with global carbon cycle changes. Nature 436, 341–346.
Turner, G.M., Michalk, D.M., Morgans, H.E.G., Walbrecker, J.O., 2007. Early Miocene magnetostratigraphy and a new palaeomagnetic pole position from New Zealand. Earth, Planets and Space 59, 841–851.
van der Meer, D., Spakman, W., van Hinsbergen, D.J.J., Amaru, M.L., Torsvik, T.H., 2010. Absolute plate motions since the Permian interred from lower mantle slab remnants. Nature Geoscience. http://dx.doi.org/10.1038/NGEO708.
Van der Voo, R., 1981. Paleomagnetism of North America: a brief review. In: McElhinny, M.W., Valencio, D.A. (Eds.), Paleoreconstruction of the Continents. : Geodynamics Series, vol. 2. AGU, Washington, D.C., pp. 159–176.
Van der Voo, R., 1990. Phanerozoic paleomagnetic poles from Europe and North America and comparisons with continental reconstructions. Reviews of Geophysics 28, 167–206.
Van der Voo, R., 1992. Jurassic paleopole controversy: contributions from the Atlantic-bordering continents. Geology 20, 975–978.
Van der Voo, R., 1993. Paleomagnetism of the Atlantic, Tethys and Iapetus Oceans. Cambridge University Press. 411 pp.
Van der Voo, R., 1994. True Polar Wander during the middle Paleozoic? Earth and Planetary Science Letters 122, 239–243.
Van der Voo, R., French, R.B., 1974. Apparent Polar Wander for the Atlantic-bordering continents: Late Carboniferous to Eocene. Earth-Science Reviews 10, 99119.
Van der Voo, R., Torsvik, T.H., 2004. The quality of the European Permo-Triassic paleopoles and its impact on Pangea reconstructions, AGU Monograph on Timescales of the paleomagnetic field. In: Channell, J.E.T., Kent, D., Lowrie, W., Meert, J.G. (Eds.), pp. 29–42.
Van der Voo, R., Levashova, N.M., Skrinnik, L.I., Kara, T.V., Bazhenov, M.L., 2006. Late orogenic, large-scale rotations in the Tien Shan and adjacent mobile belts in Kyrgyzstan and Kazakhstan. Tectonophysics 426, 335–360.
Van Fossen, M.C., Kent, D.V., 1990. High-latitude paleomagnetic poles from Middle Jurassic plutons and Moat Volcanics in New England and the controversy regarding Jurassic Apparent Polar Wander for North America. Journal of Geophysical Research 95, 17,503–17,516.
van Hinsbergen, D.J.J., Straathof, G.B., Kuiper, K.F., Cunningham, W.D., Wijbrans, J., 2008. No vertical axis rotations during Neogene transpressional orogeny in the NE Gobi Altai: coinciding Mongolian and Eurasian early Cretaceous Apparent Polar Wander paths. Geophysical Journal International 173, 105–126.
van Hinsbergen, D.J.J., Steinberger, B., Doubrovine, P.V., Gassmöller, R., 2011. Acceleration and deceleration of India–Asia convergence since the Cretaceous: roles of mantle plumes and continental collision. Journal of Geophysical Research 116, B06101. http://dx.doi.org/10.1029/2010JB008051.
van Hinsbergen, D.J.J., Lippert, P.C., Dupont-Nivet, G., McQuarrie, N., Doubrovine, P.V., Spakman, W., Torsvik, T.H., 2012. Greater Indian Basin hypothesis and a two-stage Cenozoic collision between India and Asia. Proceedings of the National Academy of Sciences of the United States of America 109, 7659–7664.
Vizán, H., Ixer, R., Turner, P., Cortes, J.M., Cladera, G., 2004. Paleomagnetism of Upper Triassic rocks in the Los Colorados Hill section, Mendoza Province, Argentina. Journal of South American Earth Science 18, 41–59.
Walderhaug, H., 1993. Rock magnetic and magnetic fabric variations across three thin alkaline dykes from Sunnhordland, western Norway; influence of initial mineralogy and secondary chemical alterations. Geophysical Journal International 115, 97–108.
Walderhaug, H.J., Eide, E.A., Scott, R.A., Inger, S., Golionko, E.G., 2005. Paleomagnetism and $^{40}Ar/^{39}Ar$ geochronology from the South Taimyr igneous complex, Arctic Russia; a Middle–Late Triassic magmatic pulse after Siberian flood-basalt volcanism. Geophysical Journal International 163, 501–517.
Wegener, A., 1912. Die Entstehung der Kontinente. Petermanns Geographische Mitteilungen 58 (I), 1–309.
Weil, A.B., Yonkee, A., Sussman, A., 2010. Reconstructing the kinematic evolution of curved mountain belts: a paleomagnetic study of Triassic red beds from the Wyoming salient, Sevier thrust belt, USA. Geological Society of America Bulletin 122, 3–23.
Wessel, P., Smith, W.H.F., 1991. Free software helps map and display data. Eos 72, 441.
Yan, M.D., Van der Voo, R., Tauxe, L., Fang, X.M., Parés, J.M., 2005. Shallow bias in Neogene paleomagnetic directions from the Guide Basin, NE Tibet, caused by inclination error. Geophysical Journal International 163, 944–948.
Yuan, K., Van der Voo, R., Bazhenov, M.L., Bakhmutov, V., Alekhin, V., Hendriks, B.W.H., 2011. Permian and Triassic Paleolatitudes of the Ukrainian Shield with Implications for Pangea Reconstructions. Geophysical Journal International 184, 595–610.
Zhong, S., Zhang, N., Li, Z.-X., Roberts, J.H., 2007. Supercontinent cycles, True Polar Wander, and very long-wavelength mantle convection. Earth and Planetary Science Letters 261, 551–564.
Zijderveld, J.D.A., 1975. Paleomagnetism of the Estérel rocks. PhD Thesis, University of Utrecht, 199 pp.